NAVAL POSTGRADUATE SCHOOL

Monterey, California

HYDRODYNAMIC INTERACTION OF WAVES WITH

A LARGE DISPLACEMENT FLOATING BODY

BY

C. J. GARRISON

NAVAL POSTGRADUATE SCHOOL
Monterey, California

Rear Admiral Isham Linder
Superintendent

J. R. Borsting
Provost

The work reported herein was supported by the Energy Research and Development Administration, OTEC Program, Washington, D.C. 20545.

This report was prepared by:

HYDRODYNAMIC INTERACTION OF WAVES WITH A LARGE DISPLACEMENT FLOATING BODY

by

C. J. Garrison
Associate Professor
Department of Mechanical Engineering
Naval Postgraduate School
Monterey, California

Supported by

U. S. Energy Research and Development Administration
OTEC Program
Washington, D. C. 20545

September 1977

Contract No.
Interim Report

SECURITY CLASSIFICATION OF THIS PAGE (When Data Entered)

REPORT DOCUMENTATION PAGE

READ INSTRUCTIONS BEFORE COMPLETING FORM

1. REPORT NUMBER: NPS-69Gm77091	2. GOVT ACCESSION NO.
3. RECIPIENT'S CATALOG NUMBER	
4. TITLE (and Subtitle): HYDRODYNAMIC INTERACTION OF WAVES WITH A LARGE DISPLACEMENT FLOATING BODY	5. TYPE OF REPORT & PERIOD COVERED: Interim report; April 76 to Aug. 77
	6. PERFORMING ORG. REPORT NUMBER
7. AUTHOR(s): C. J. Garrison	8. CONTRACT OR GRANT NUMBER(s)
9. PERFORMING ORGANIZATION NAME AND ADDRESS: Naval Postgraduate School, Monterey, CA 93940, Code 69Gm	10. PROGRAM ELEMENT, PROJECT, TASK AREA & WORK UNIT NUMBERS: Interagency Agreement E(49-26)-1044
11. CONTROLLING OFFICE NAME AND ADDRESS: Energy Research & Development Administration, OTEC Program, Washington, D.C. 20545	12. REPORT DATE: September 15, 1977
	13. NUMBER OF PAGES: 159
14. MONITORING AGENCY NAME & ADDRESS (if different from Controlling Office)	15. SECURITY CLASS. (of this report): Unclassified
	15a. DECLASSIFICATION/DOWNGRADING SCHEDULE

16. DISTRIBUTION STATEMENT (of this Report)

Approved for public release; distribution unlimited.

17. DISTRIBUTION STATEMENT (of the abstract entered in Block 20, if different from Report)

18. SUPPLEMENTARY NOTES

19. KEY WORDS (Continue on reverse side if necessary and identify by block number)

dynamic response
mooring
wave forces
added mass - floating bodies

20. ABSTRACT (Continue on reverse side if necessary and identify by block number)

This report describes the analytical method and numerical procedure for the calculation of the wave pressure distribution and resulting induced forces and moments acting on large displacement bodies in the sea. The added mass and damping coefficients for the structure oscillating in all six degrees of freedom is computed. Then, the hydrodynamic coefficients associated with both the wave/structure interaction and the oscillation of the structure are determined by use of a Green's function method using quadralateral

DD FORM 1 JAN 73 1473 EDITION OF 1 NOV 65 IS OBSOLETE
S/N 0102-014-6601

SECURITY CLASSIFICATION OF THIS PAGE (When Data Entered)

elements of constant source strength which applies to large structures of rather general shape. The analysis is based on linear theory and viscous effects are neglected on the basis that the size of the structure is large in relation to the amplitude of the incident wave. Also, the equations of motion for a free-floating body are developed which yields the dynamic response of a floating body with linear mooring line forces. Finally, the computer program capable of carrying out the numerical calculations is outlined and the input/output is discussed in some detail.

ABSTRACT

This report describes the analytical method and numerical procedure for the calculation of the wave pressure distribution and resulting induced forces and moments acting on large displacement bodies in the sea. The added mass and damping coefficients for the structure oscillating in all six degrees of freedom are computed. Then, the hydrodynamic coefficients associated with both the wave/structure interaction and the oscillation of the structure are determined by use of a Green's function method using quadralateral elements of constant source strength which applies to large structures of rather general shape. The analysis is based on linear theory and viscous effects are neglected on the basis that the size of the structure is large in relation to the amplitude of the incident wave. Also, the equations of motion for a free-floating body are developed which yields the dynamic response of a floating body with linear mooring line forces. Finally, the computer program capable of carrying out the numerical calculations is outlined and the input/output is discussed in some detail.

TABLE OF CONTENTS

TABLE OF CONTENTS(cont'd)

I. INTRODUCTION

Ocean Thermal Energy Conversion (OTEC) plants will be either moored or dynamically positioned in the ocean and, accordingly, will be subject to wind, wave and current loading. This report deals with the motion of a floating body of arbitrary shape subject to wave motion. The interaction of the waves with the floating body is based on the inviscid (potential flow) theory. This assumption appears to be valid as long as the body involved is large compared to the amplitude of the relative fluid motion.

This report describes the first phase of a project to analytically determine the dynamic response of large floating OTEC plants to ocean waves. The long range goal of the project is to develop analysis and computer code for computation of the dynamic response and structural loading of OTEC structures of rather general configuration. Such configurations are considered to be composed of a large displacement parts where diffraction theory will be required and/or small appendages or members which can be dealt with by use of a Morison equation type analysis. This phase of the work deals with the analysis of large displacement bodies of arbitrary shape. The analysis is based on the use of a surface distribution of sources using quadralateral source patches or panels. The source strengths over each

panel is assumed constant in this phase of the project. The next phase of the work will investigate the use of triangular panels where the source strength varies linearly between the values at the corner node points. A comparison of the triangular patch method will be made with the quadralateral source patch method with constant source strengths over the patch. The better of the two methods will be used in the future phases of this work.

In particular, this report deals with the analytical evaluation of the wave forces and overturning moment acting on a large body of arbitrary shape without appendages in water of finite depth. The same structure is also considered to oscillate in surge, heave, sway, roll, yaw and pitch and for such motion the added mass and damping coefficients are determined. Then, the equations of motion for a free-floating body are developed, and using the computed wave excitation forces and moments and added mass and damping coefficients the response of the floating structure is evaluated.

Although the problems of wave interaction with a fixed body and the oscillation of the same body in otherwise still fluid appear to be physically distinct, they are mathematically similar and as a result are dealt with simultaneously herein. The primary mathematical difference in these problems is the kinematic boundary condition which is applied on the immersed surface. In all cases, however,

the velocity of the fluid in the normal direction relative to the immersed surface must be zero but this statement takes a different form in each case.

The method used to describe the fluid motion involves the use of a Green's function or source distribution. The rigid, immersed surface of the structure is represented by a surface distribution of sources which is assumed to be constant over quadralateral panels and the zero relative normal velocity condition is applied in order to determine the strengths of the sources. Once the source strength distribution is, known the velocity potential at some point in the fluid region is determined by summing the effect of all of the sources at the point in question.

Several authors have computed hydrodynamic coefficients associated with specific shapes. The added mass and damping coefficients for a semi-immersed floating sphere undergoing heaving motion has been obtained by Havelock (2). The vertical wave excitation force was not calculated by Havelock but using the Haskind's Relations [Ref.3] this quantity may be determined from the damping coefficient. Kim (4) determined the added-mass and damping coefficients for this same configuration to wave excitation in heave and surge. Although calculated for the infinite depth case, these results provide an important comparison for establishing confidence in the mathematical validity of the response calculations based on the present analysis.

Several authors have also considered the wave interaction with large displacement fixed and floating bodies. In the case of large North Sea Gravity platform [Refs. 10 and 20] the agreement between the theory and experiment is almost exact. In such structures the caisson was well-submerged and the superstructure only pierced the free-surface. Thus, nonlinear effects which tend to be most pronounced near the free surface were absent. Additional experimental data and comparisons with the linear theory for the case of fixed bodies which are considered to be significant include those presented by Garrison and Seetharama Rao (6) for the case of a bottom mounted hemisphere. Unfortunately, the wave amplitudes were rather small. Also, Garrison and Chow (7) have presented a comparison of the theoretical results based on the distributed source theory similar to that developed herein with two slightly different submerged oil storage tank models. Unfortunately, the vertical force part of this data was rather poor because the vertical model supports had very low spring rates making the natural frequency of the model support system too close to the wave excitation frequency. It is significant, however, that these tests represented North Sea design conditions and in the case of the horizontal force quite good agreement was obtained between the linear theory and experimental results. A third experimental study involving a short vertical circular cylinder (1.16 cylinder radii water depth) extending from the

bottom through the free surface should be noted. Chakrabarti (8) has made measurements of the horizontal force and overturning moment for this configuration and found the results to compare well with MacCamy and Fuch's (1) corresponding theoretical results. However, Chakrabarti gives no indication of the wave height involved in Ref. (8). It is noted that the MacCamy and Fuchs solution is simply a special case of the present more general method so that agreement with this solution implies agreement with the present method.

A series of tests have been conducted by Hogben and Standing (9) of the National Physical Laboratory, London, England with fixed vertical cylinders of square and circular cross-section. They also made calculations using a computer program based on diffraction theory similar to the one presented here and good agreement between theory and experiment has been observed.

Only limited experimental data has been presented in the literature for the dynamic response of three-dimensional floating structures to waves. Among these the results of Faltinsen and Michelsen (11) are the most complete. They compared calculations of diffraction theory with the heave response of a floating box and the agreement obtained was quite good. Also Garrison (12) showed excellent agreement between the results of diffraction theory and the heave and pitch response of a disc buoy. However, as a general assessment of the experimental data available in the literature,

for the hydrodynamic coefficients and dynamic response of floating bodies, it appears that the amount is very small and the understanding of viscous effects and differences or similarities of the experimental results with the theory is nonexistent. This is an area where additional work is needed.

2. FORMULATION OF PROBLEM

Consider a rigid object of arbitrary shape and having characteristic lineal dimension $\bar{a}$ with center of gravity submerged to a depth $\bar{d}$ beneath the free surface in water of depth $\bar{h}$ as shown in Fig. 1. The structure is considered to be smooth to the extent that its unit normal vector is a continuous function and it may or may not intersect the bottom or free surface. Two coordinate systems are identified, $\bar{x},\bar{y},\bar{z}$ coordinates with origin fixed at the free surface and the body coordinates $\bar{x}',\bar{y}',\bar{z}'$ coordinates located at depth $\bar{y} = -\bar{d}$. The bars over the symbols denote dimensional quantities.

The mathematical problem which is now established is that associated with the fluid motion, pressures and resulting forces induced by the small amplitude oscillation of the object in its six degrees of freedom as well as the fluid motion associated with the interaction of the fixed object with a train of regular waves. The small amplitude oscillatory motion of the structure about its equilibrium position with frequency σ is described by the relationship,

$$\bar{X}_i(t) = \bar{X}_i^{\circ} R_e[e^{-i\sigma t}], \quad i = 1,2,3 \qquad (2.1a)$$

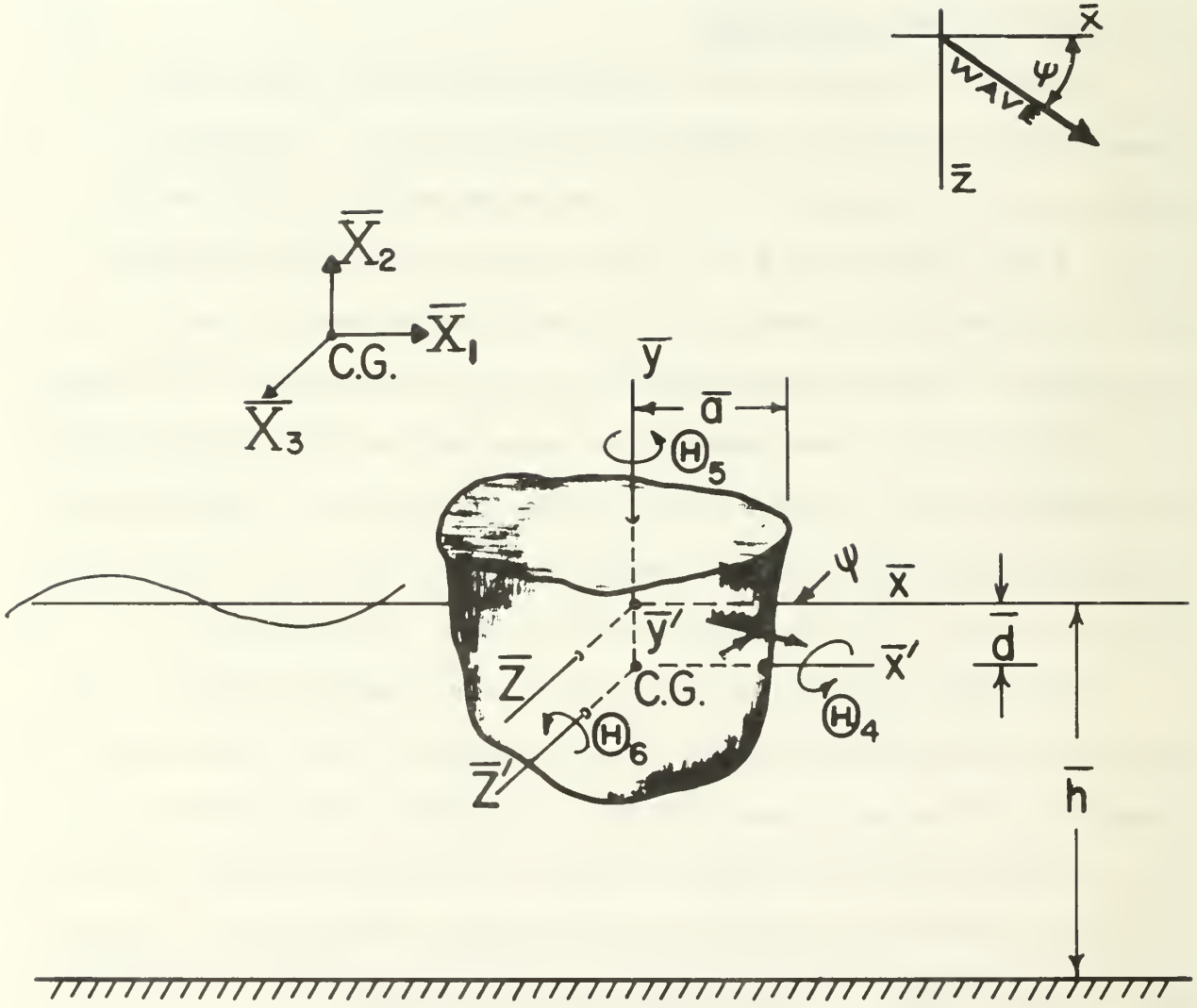

FIGURE 1 DEFINITIONS

$$\theta_i(t) = \theta_i^o \, R_e[e^{-i\sigma t}], \quad i = 4,5,6 \tag{2.1b}$$

where the subscript i = 1,2,3 denotes lineal oscillation in the $\bar{x}',\bar{y}',\bar{z}'$ directions, respectively, and i = 4,5,6 denote angular oscillation about the $\bar{x}',\bar{y}',\bar{z}'$ axes, respectively. The real numbers $\bar{X}_i^o$ and θ_i^o denote the amplitudes of the motion. The displacements, $\bar{X}_1$, $\bar{X}_2$ and $\bar{X}_3$ are normally referred to as surge, heave and sway, respectively, while the angular components θ_4, θ_5 and θ_6 are called roll, yaw and pitch, respectively. The second problem dealt with simultaneously is the interaction of a train of regular surface waves with the object fixed in space. The regular incident waves of wave height $2\bar{\eta}_*^o = \bar{H}$ and wave length $\bar{L}$ are assumed to progress in the positive x-direction and interact with the fixed structure.

The fluid is assumed to be incompressible, and the motion irrotational and harmonic with time dependence $e^{-i\sigma t}$ in all cases. It follows, therefore, that a velocity potential exists such that the fluid velocity vector may be defined as

$$\vec{\bar{q}}_j = R_e[\vec{\bar{\nabla}}\phi_j(\bar{x},\bar{y},\bar{z})e^{-i\sigma t}], \quad j = 1,2,..6 \tag{2.2}$$

where $R_e[\phi_j e^{-i\sigma t}]$ denotes the velocity potential associated with the motion induced by oscillations in the six degrees of freedom and $\vec{\bar{\nabla}} = \vec{i}\frac{\partial}{\partial\bar{x}} + \vec{j}\frac{\partial}{\partial\bar{y}} + \vec{k}\frac{\partial}{\partial\bar{z}}$, the symbols $\vec{i},\vec{j},\vec{k}$ denoting the unit vectors in the $\bar{x},\bar{y},\bar{z}$ directions, respectively.

For the case of regular wave interaction with the fixed structure, the velocity potential may be written as the sum

$$\phi' = \phi_o + \phi_7 \tag{2.3}$$

where ϕ_o denotes the potential associated with the incident wave in the absence of the structure and ϕ_7 denotes the scattering potential which results from the presence of the structure in the wave train. In this case, the fluid velocity vector is given by

$$\vec{\bar{q}}' = R_e[\vec{\bar{\nabla}}(\phi_o + \phi_7)e^{-i\sigma t}] \tag{2.4}$$

The continuity equation shows that ϕ_j, (j = 0,1,2,...7) must satisfy the Laplace equation

$$\bar{\nabla}^2\phi_j(\bar{x},\bar{y},\bar{z}) = 0 \tag{2.5}$$

and from the linearized form of Bernoulli's equation, which is applied throughout, the dynamic fluid pressure is given by,

$$P_j = R_e[i\ \rho\sigma\ \phi_j\ e^{-i\sigma t}], \quad j = 1,2,...6 \tag{2.6}$$

For the second problem involving wave interaction with the fixed object, the pressure is given by

$$P' = R_e[i\ \rho\sigma(\phi_o + \phi_7)\ e^{-i\sigma t}] \tag{2.7}$$

The velocity potentials must satisfy certain boundary conditions in addition to Eq. (2.5). These include the linearized free surface boundary condition,

$$\frac{\partial\phi_j(\bar{x},0,\bar{z})}{\partial\bar{y}} - \frac{\sigma^2}{g}\phi_j(\bar{x},0,\bar{z}) = 0, \quad j = 0,1,2,...7 \tag{2.8}$$

Equation (2.8) is familiar from linear wave theory. Also, ϕ_j must satisfy the kinematic boundary condition on the bottom in all cases,

$$\frac{\partial \phi_j}{\partial \bar{y}}(\bar{x},-\bar{h},\bar{z}) = 0, \quad j = 0,1,2,\ldots 7 \tag{2.9}$$

The surface of the structure in its mean position is described by

$$S(\bar{x},\bar{y},\bar{z}) = 0 \tag{2.10}$$

When the structure oscillates, the velocity of the fluid in the direction normal to the immersed surface must equal the velocity of the surface normal to itself. Also, for the case of wave interaction with the fixed body it is necessary that the normal velocity component be zero. These conditions are stated mathematically as

$$\frac{\partial \phi_1}{\partial \bar{n}} = -i\sigma \bar{X}_1^{\circ} n_x \tag{a}$$

$$\frac{\partial \phi_2}{\partial \bar{n}} = -i\sigma \bar{X}_2^{\circ} n_y \tag{b}$$

$$\frac{\partial \phi_3}{\partial \bar{n}} = -i\sigma \bar{X}_3^{\circ} n_z \tag{c}$$

$$\frac{\partial \phi_4}{\partial \bar{n}} = -i\sigma \Theta_4^{\circ}[(\bar{d}+\bar{y})n_z - \bar{z}n_y] \tag{d}$$

$$\frac{\partial \phi_5}{\partial \bar{n}} = -i\sigma \Theta_5^{\circ}[\bar{z}n_x - \bar{x}n_z] \tag{e}$$

$$\frac{\partial \phi_6}{\partial \bar{n}} = -i\sigma \Theta_6^{\circ}[\bar{x}n_y - (\bar{d}+\bar{y})n_x] \tag{f}$$

$$\frac{\partial \phi_7}{\partial \bar{n}} = -\frac{\partial \phi}{\partial \bar{n}}^{\circ} \tag{g}$$

(2.11)

where $\vec{n} = \vec{i}n_x + \vec{j}n_y + \vec{k}n_z$ denotes the unit normal vector on the surface of the object directed outward into the fluid and $\bar{d}$ denotes the depth of submergence of the $\bar{x}$,$\bar{y}$,$\bar{z}$'coordinate origin. Finally, the velocity potentials must satisfy the radiation condition which allows only outgoing waves,

$$\phi_i(\bar{r}_1,\theta,\bar{y}) - \lambda_i(\theta)\bar{r}_1^{-\frac{1}{2}} \frac{\cosh[k(\bar{y}+\bar{h})]e^{ik\bar{r}_1}}{\cosh(k\bar{h})} \to 0, \bar{r}_1 \to \infty, \quad i = 1,2,..7 \tag{2.12}$$

where $\bar{r}_1 = [\bar{x}^2 + \bar{z}^2]^{\frac{1}{2}}$ and $\theta = \tan^{-1}(\bar{z}/\bar{x})$. The wave number is defined as $k = 2\pi/\bar{L}$ where $\bar{L}$ denotes the wave length and is related to the frequency of the motion according to the well-known relationship,

$$\frac{\sigma^2}{g} = k \tanh(k\bar{h}) \tag{2.13}$$

The velocity potential of the incident wave alone progressing in the positive $\bar{x}$ direction which satisfies Eqs. (2.5), (2.8) and (2.9) is given by

$$\phi_0(\bar{x},\bar{y}) = -\frac{ig\bar{\eta}_*^o}{\sigma} \frac{\cosh[k(\bar{h}+\bar{y})]e^{ik(\bar{x}\cos\psi + \bar{z}\sin\psi)}}{\cosh(k\bar{h})} \tag{2.14}$$

where as indicated in Figure 1, ψ denotes the angle of the incident wave measured clockwise from the x-axis and $\bar{\eta}_*^o = \bar{H}/2$ denotes the amplitude of the incident wave, $\bar{H}$ being the wave height. Moreover, from the linearized form of Bernoulli's equation, the free surface of the incident wave alone is evaluated from

$$\bar{\eta}_* = -\frac{1}{g}\frac{\partial}{\partial t}\left\{R_e[\phi_0 e^{-i\sigma t}]\right\}_{\bar{y}=0} \tag{2.15}$$

Using (2.14) this gives,

$$\bar{\eta}_* = \bar{\eta}_*^{\circ} \cos(k\bar{x} \cos \psi + k\bar{z} \sin \psi) \qquad (2.16)$$

Thus, for purposes of reckoning phase angle it is noted that at t = 0 the crest of the incident wave is just passing the coordinate origin.

For convenience in carrying out the solution for the seven potentials, ϕ_j, and to show clearly the dependence of the solution on the parameter, $a = 2\pi\bar{a}/\bar{L} = k\bar{a}$, the relative water depth, $h = \bar{h}/\bar{a}$ and the relative depth of submergence, $d = \bar{d}/\bar{a}$, the space variables and amplitudes are first made dimensionless with the characteristic linear dimension of the object, $\bar{a}$,

$$x = \bar{x}/\bar{a},\ y = \bar{y}/\bar{a},\ z = \bar{z}/\bar{a},\ r = \bar{r}/\bar{a}$$
$$X_i^{\circ} = \bar{X}_i/\bar{a},\ (i = 1,2,3),\ X_i^{\circ} = \Theta_i^{\circ},\ (i = 4,5,6)$$
$$\eta_*^{\circ} = \bar{\eta}^{\circ}/\bar{a} = \bar{H}/2\bar{a},\ r_1 = \bar{r}_1/\bar{a},\ \nu = \sigma^2\bar{a}/g \qquad (2.17)$$

and then the dimensionless potential functions u_j are introduced as,

$$i\sigma\phi_j(\bar{x},\bar{y},\bar{z})/g\bar{a}X_j^{\circ} = a \tanh(ah)\ u_j(x,y,z),\quad j = 1,2,..6 \qquad (2.18a)$$

$$i\sigma\phi_7(\bar{x},\bar{y},\bar{z})/g\bar{a}\,\eta_*^{\circ} = -a\ u_7(x,y,z) \qquad (2.18b)$$

$$i\sigma\phi_o(\bar{x},\bar{y})/g\bar{a}\,\eta_*^{\circ} = -a\ u_o(x,y) \qquad (2.18c)$$

The complex dynamic pressure amplitude can now be written by use of the linearized form of Bernouli's equation (2.6) and (2.7), as

$$p_j = a \tanh(ah)\, u_j(x,y,z), \quad j = 1,2,\ldots 6 \tag{2.19a}$$

$$p' = \frac{\cosh[a(h+y)]e^{ia(x\cos\psi + z\sin\psi)}}{\cosh(ah)} - a\, u_7(x,y,z) \tag{2.19b}$$

where the complex amplitudes of the pressure, p_j, are defined as

$$\frac{p_j}{\rho g a X_j^\circ} = R_e[p_j(x,y,z)e^{-i\sigma t}], \quad j = 1,2,\ldots 6 \tag{2.20a}$$

$$\frac{p'}{\rho g \bar{a} \eta_*^\circ} = R_e[p'(x,y,z)e^{-i\sigma t}] \tag{2.20b}$$

The boundary value problem which describes the fluid motion arising from the oscillation of the rigid object in its six degrees of freedom as well as the scattering of the incident wave may now be written concisely in terms of dimensionless parameters. The potentials $u_i(x,y,z)$, $i = 1,2,\ldots 7$, continuous in the fluid region is sought such that:

$$\nabla^2 u_j(x,y,z) = 0 \tag{2.21a}$$

$$\frac{\partial u_j}{\partial y}(x,o,z) - a \tanh(ah)\, u_j(x,o,z) = 0 \tag{2.21b}$$

$$\frac{\partial u_j}{\partial y}(x,-h,z) = 0 \tag{2.21c}$$

$$\frac{\partial u_j}{\partial n}(x,y,z) = g_j(x,y,z) \text{ on } S(x,y,z) = 0 \tag{2.21d}$$

$$u_j(r,\theta,y) - \lambda_i(\theta) r_1^{-\frac{1}{2}} \frac{\cosh[a(h+y)]e^{iar_1}}{\cosh(ah)} \to o, r_1 \to \infty \tag{2.21e}$$

The $g_i(x,y,z)$ functions represent the prescribed functions which depend on the mode of oscillation ($j = 1,2,...6$), and $j = 7$ corresponds to scattering. These functions represent the dimensionless form of (2.11) and are given by

$$g_1 = n_x, \quad g_2 = n_y, \quad g_3 = n_z \tag{2.21f}$$

$$g_4 = (d+y)n_z - zn_y, \quad g_5 = zn_x - xn_z, \quad g_6 = xn_y - (d+y)n_x$$

$$g_7 = \frac{1}{\cosh(ah)} [n_y \sinh[a(h+y)] + i \cosh[a(h+y)]$$
$$.(n_x \cos \psi + n_z \sin \psi)]e^{ia(x \cos \psi + - \sin \psi)}$$

Equations (2.21) define seven boundary-value problems which correspond to oscillation of the immersed surface in each of the six degrees of freedom and to scattering of the incident wave by the fixed body. The problem statement for each of the potentials is the same; the only difference lies in the form of the boundary condition to be applied on the immersed surface.

3. REPRESENTATION OF THE POTENTIAL

The boundary value problem for oscillation in the six degrees of freedom and scattering of the incident wave is specified in (2.21). The solution, (i.e.), the function $u_j(x,y,z)$, may be represented by use of a Green's function having the physical interpretation of a point wave source of unit strength. These sources are distributed over the surface of the object according to the source strength function,f, so that the potential at

some point (x,y,z) within the fluid region is given by the surface integral

$$u_j(x,y,z) = \frac{1}{4\pi} \iint_S f_j(\xi,\eta,\zeta) \; G(x,y,z;\xi,\eta,\zeta) \; dS \qquad (3.1)$$

where (ξ,η,ζ) represents a point on the surface of the structure, G denotes the Green's function (or source potential) and $dS = d\bar{S}/\bar{a}^2$ denotes the dimensionless surface area element. The Green's function is defined, therefore, as the function which satisfies

$$\nabla^2 G(x,y,z;\xi,\eta,\zeta) = \delta(x-\xi)\;\delta(y-\eta)\;\delta(z-\zeta) \qquad (3.2)$$

as well as the boundary conditions (2.21b, c, and e). Such a function is given by Wehausen and Laitone (13) as

$$G(x,y,z;\xi,\eta,\zeta) = \frac{1}{R} + G^* \qquad (3.3a)$$

where $G^* = \frac{1}{R'}$

$$+ 2P.V. \int_0^\infty \frac{(\mu+\nu)e^{-\mu h}\cosh[\mu(\eta+h)]}{\mu \sinh(\mu h) - \nu \cosh(\mu h)} \cosh[\mu(y+h)] \; J_0(\mu r)\, d\mu \qquad (3.3b)$$

$$+ i \frac{2\pi(a^2-\nu^2)\cosh[a(\eta+h)]\cosh[a(y+h)]\; J_0(ar)}{a^2h - \nu^2 h + \nu}$$

$$R = [(x-\xi)^2 + (y-\eta)^2 + (z-\zeta)^2]^{\frac{1}{2}} \qquad (3.3c)$$

$$R' = [(x-\xi)^2 + (y+2h+\eta)^2 + (z-\zeta)^2]^{\frac{1}{2}} \qquad (3.3d)$$

$$r = [(x-\xi)^2 + (z-\zeta)^2]^{\frac{1}{2}} \qquad (3.3e)$$

$$\nu = \sigma^2\bar{a}/g = a\tanh(ah) \qquad (3.3f)$$

and P.V. indicates principal value of the integral. An alternate series form of the Green's function is also given by Wehausen and Laitone (13) as

$$G(x,y,z;\xi,\eta,\zeta) = \frac{2\pi(\nu^2-a^2)}{a^2h-\nu^2h+\nu}\cosh[a(h+y)]\cosh[a(h+\eta)][Y_o(ar)-iJ_o(ar)]$$

$$+ 4\sum_{k=1}^{\infty}\frac{(\mu_k^2+\nu^2)}{\mu_k^2h+\nu^2h-\nu}\cos[u_k(y+h)]\cos[\mu_k(\eta+h)]K_o(\mu_k r) \qquad (3.4a)$$

where J_o and Y_o denote, respectively, Bessel functions of the first and second kind of order zero and K_o denotes the modified Bessel function of the second kind of order zero. The quantities μ_k are the real positive roots of the equation

$$\mu_k \tan(\mu_k h) + \nu = 0 \qquad (3.4b)$$

The Green's functions specified in (3.3) and (3.4) are equivalent. However, for purposes of numerical evaluation it is found that the series formulation given in (3.4) can be evaluated more accurately and with much less expenditure of computer time than the integral form when (ar) is not too small. On the other hand, for small and zero values of (ar) the integral form given in (3.3) is necessary. The integral form of the Green's function as given in Eq. (3.3) may be integrated directly or, it may be rearranged as in Appendix C so as to be somewhat better conditioned for numerical evaluation. In the

computer program when the integral form of the Green's function is required, the form given in Appendix C is actually used for numerical evaluation. It appears that it is somewhat less time consuming to evaluate than the form given by Eq. (3.3). The potentials u_j are represented by (3.1) and with the introduction of the Green's functions (3.3) and (3.4)(or equivalent form given in Appendix C) the only unknown in (3.1) is the source strength function f_j. To evaluate this it is necessary to take the derivative of (3.1) in the direction normal to the immersed surface and then apply the boundary condition (2.21d). This results in the following integral equation from which f_j is to be determined:

$$\frac{1}{4\pi}\iint_S f_j(\xi,\eta,\zeta)\,\frac{\partial G}{\partial n}(x,y,z;\xi,\eta,\zeta)\,dS = g_j(x,y,z),\quad j = 1,2\ldots7 \qquad (3.5$$

where $\partial G/\partial n$ is obtained using the form $\vec{\nabla}G.\vec{n}$ where $\vec{\nabla}G$ is determined by straightforward differentiation of (3.3) or (3.4).

The normal derivative of (3.3) is

$$\begin{aligned}\frac{\partial G}{\partial n} = &-\frac{1}{R^3}\left[n_x(x-\xi) + n_y(y-\eta) + n_z(z-\zeta)\right]\\ &-\frac{1}{R'^3}\left[n_x(x-\xi) + n_y(y+2h+\eta) + n_z(z-\zeta)\right]\\ &-2\,\text{P.V.}\int_0^\infty \frac{\mu(\mu+\nu)e^{-\mu h}\cosh[\mu(\mu+h)]}{\mu\sinh(\mu h) - \nu\cosh(\mu h)} \qquad (3.6)\\ &\cdot\left[\frac{\cosh[\mu(y+h)]\,J_1(\mu r)}{r}\left[n_x(x-\xi)+n_z(z-\zeta)\right]-n_y\sinh[\mu(y+h)]J_0(\mu r)\right]\end{aligned}$$

$$-i\,\frac{2\pi a(a^2-\nu^2)\cosh[a(\eta+h)]}{a^2h-\nu^2h+\nu}\left[\frac{\cosh[a(h+y)]J_1(ar)}{r}\left(n_x(x-\xi)+n_z(z-\zeta)\right)\right.$$

$$\left.-n_y\sinh[a(h+y)]J_o(ar)\right]$$

and the normal derivative of the alternate rearranged form of Eq. (3.3) is given in Appendix C. The normal derivative of the series form given in (3.4) is

$$\frac{\partial G}{\partial n}=\frac{2\pi(\nu^2-a^2)a\cosh[a(h+\eta)]}{a^2h-\nu^2h+\nu}\left[\sinh[a(h+y)][Y_o(ar)-iJ_o(ar)]n_y\right.$$

$$\left.-[n_x(x-\xi)+n_z(z-\zeta)]\cosh[a(h+y)]\frac{1}{r}[Y_1(ar)-iJ_1(ar)]\right] \qquad (3.7)$$

$$-4\sum_{k=1}^{\infty}\frac{\mu_k(\mu_k^2+\nu^2)\cos[\mu_k(\eta+h)]}{\mu_k^2h+\nu^2h-\nu}\left[\sin[\mu_k(y+h)]K_o(\mu_k r)n_y\right.$$

$$\left.+\cos[\mu_k(y+h)]\frac{K_1(\mu_k r)}{r}[n_x(x-\xi)+n_z(z-\zeta)]\right]$$

where n_x, n_y and n_z denote the components of the outward unit normal vector on the immersed surface.

Returning to the integral equation (3.5), it is evident that the $\partial G/\partial n$ occurring therein as given by (3.6) is singular like $1/R^3$ as the point (ξ,η,ζ) approaches the point (x,y,z). Thus, special care must be taken when integrating this term of (3.6) over the singularity. Moreover, the kernel of (3.1) is singular like $1/R$ at this same point and likewise special attention must be given to this situation. Taking the integral

over the complete surface of the object as the sum of two parts, one part being a small circle of radius r_o about the point (x,y,z), as indicated in Figure 2, and the second part being the remainder, S', of the surface, we may write (3.1) as

$$\frac{1}{4\pi}\iint_{\Sigma} f_j(\xi,\eta,\zeta)\ \frac{\partial G}{\partial n}\ (x,y,z;\xi,\eta,\zeta)\ dS$$

$$+\ \frac{1}{4\pi}\iint_{S'} f_j(\xi,\eta,\zeta)\ \frac{\partial G}{\partial n}\ (x,y,z;\ \xi,\eta,\zeta)\ dS = g_j(x,y,z) \tag{3.8}$$

where Σ denotes the area inside the small circle of radius r_o. Now, using the expression for $\partial G/\partial n$ as obtained from (3.3a) and keeping in mind that $f_j(\xi,\eta,\zeta)$ is a well-behaved function, we may take the limiting case as Σ, or equivalently, r_o tends to zero to obtain

$$\lim_{\Sigma\to 0}\ \frac{1}{4\pi}\ f_j(x,y,z)\iint_{\Sigma}\ \frac{\partial}{\partial n}\ \left(\frac{1}{R}\right)\ dS$$

$$+\ \lim_{\Sigma\to 0}\ \frac{1}{4\pi} f_j(x,y,z)\iint_{\Sigma}\frac{\partial G^*}{\partial n}\ dS \tag{3.9}$$

$$+\ \lim_{\Sigma\to 0}\ \frac{1}{4\pi}\iint_{S'} f_j(\xi,\eta,\zeta)\ \frac{\partial G}{\partial n}\ (x,y,z;\xi,\eta,\zeta)\ dS = g_j(x,y,z)$$

Letting the point (x,y,z) lie along the normal at a distance ε above the surface as indicated in Figure 2, it is evident that the first integral in (3.8) can be expressed as

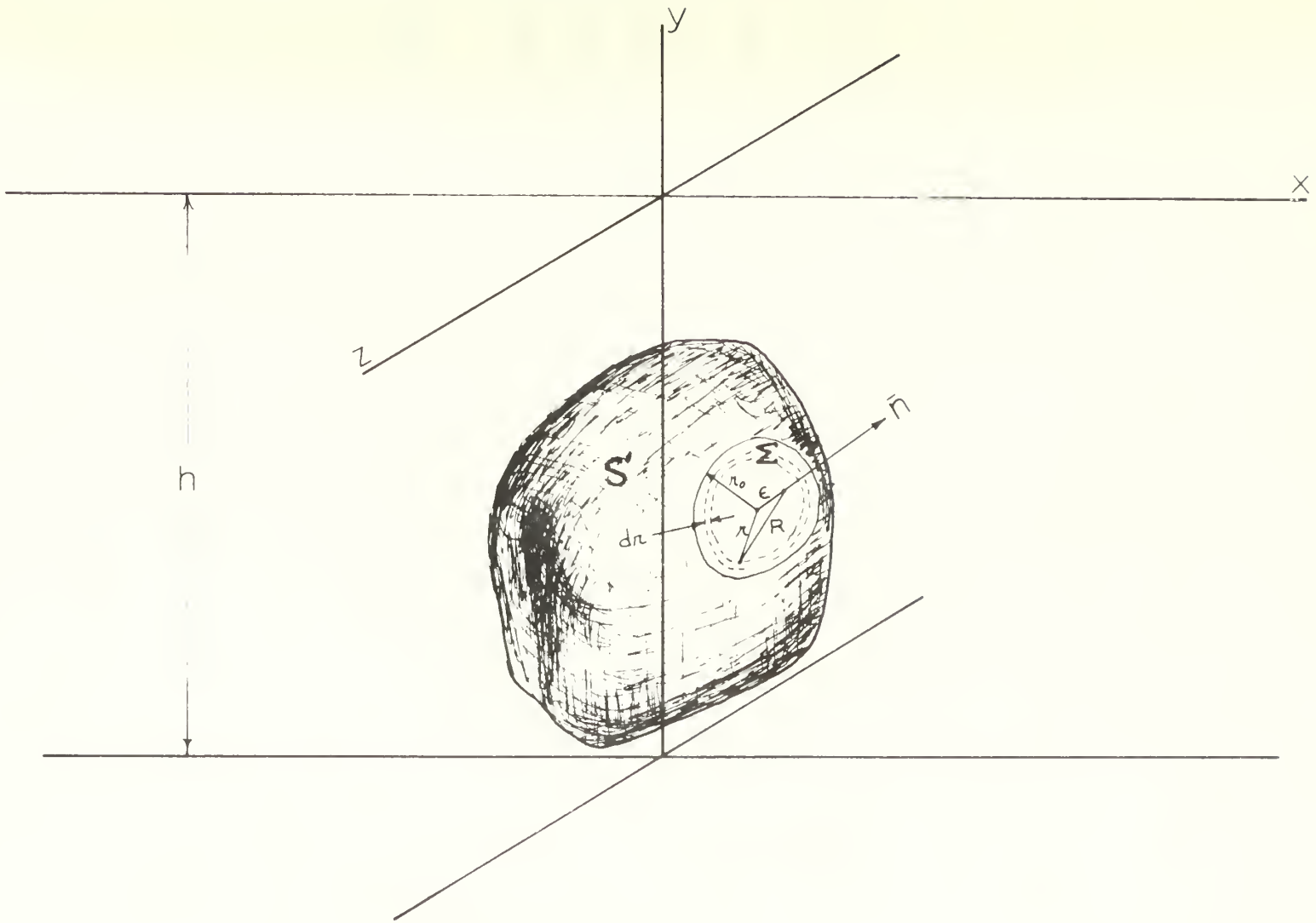

FIG. 2 SINGULAR POINT

$$\lim_{\varepsilon\to 0} \frac{1}{4\pi} f_j(x,y,z)\iint_{\Sigma} \frac{\partial}{\partial n}\left(\frac{1}{R}\right) dS = \lim_{\substack{r_o\to 0 \\ \varepsilon\to 0}} \frac{1}{4\pi} f_j(x,y,z)\frac{\partial}{\partial \varepsilon}\int_{\circ}^{r_o} \frac{2\pi r\,dr}{\sqrt{r^2+\varepsilon^2}}$$

$$= \lim_{\substack{r_o\to 0 \\ \varepsilon\to 0}} \left[\frac{1}{4\pi} f_j(x,y,z)\ 2\pi\ \left(\frac{\varepsilon}{\sqrt{\varepsilon^2+r_o^2}} - 1\right)\right] = -\frac{1}{2} f_j(x,y,z) \qquad (3.10)$$

provided r_o is chosen to be small enough that the surface area inside r_o may be considered to be plane. Moreover, since G* occurring in (3.9) is regular, the second integral vanishes in the limit as $\Sigma\to 0$ giving the integral equation

$$-f_j(x,y,z) + \frac{1}{2\pi}\iint_S f_j(\xi,\eta,\zeta)\ \frac{\partial G}{\partial n}\ (x,y,z;\ \xi,\eta,\zeta)dS = 2\ g_j(x,y,z) \qquad (3.11)$$

In (3.11) the singular point at (x,y,z) is considered to be excluded from the surface S.

As noted, in (3.1) the Green's function is also singular and special consideration is needed. However, using a procedure similar to the above, it can be shown that this 1/R singularity contributes nothing to the surface integral in (3.1). Thus, (3.1) may stand as is without modification and the point (x,y,z) considered to be excluded from the surface S.

However, the integral of 1/R over the facet of area ΔS outside the singular point is not zero. This will be discussed in detail in Appendix B.

4. HYDRODYNAMIC FORCES AND MOMENTS

The forces and moments caused by the dynamic fluid pressure acting upon the immersed surface of the structure may be obtained from the integrals,

$$F_{ij}(t) = -(1.0 \text{ or } \bar{a})\iint_S P_j g_i \, d\bar{S}, \quad i,j = 1,2,\ldots 6 \tag{4.1a}$$

$$F_i(t) = -(1.0 \text{ or } \bar{a})\iint_S P' g_i \, d\bar{S}, \quad i = 1,2,\ldots 6 \tag{4.1b}$$

where $F_{ij}(t)$ denotes the i-th component of load arising from the j-th component of motion and $F_i(t)$ denotes the i-th component of wave force (or moment). The coefficient 1.0 is to be used in the case of a force ($i = 1,2,3$) while $\bar{a}$ is to be used when F denotes a moment ($i = 4,5,6$). The sign convention of the forces, moments, displacements, velocities, etc. follow the right hand rule.

It is convenient and conventional to place the forces and moments in dimensionless coefficient form. Accordingly, the following complex wave force (and moment) coefficients are defined using (4.1b):

$$C_i = \frac{F_{i(max)} e^{i\delta_i}}{\rho g \bar{a}^3 \eta^*_\circ}, \quad i = 1,2,3 \qquad \text{(force)} \tag{4.2a}$$

$$C_i = \frac{F_{i(max)} e^{i\delta_i}}{\rho g \bar{a}^4 \eta^*_\circ}, \quad i = 4,5,6 \qquad \text{(moment)} \tag{4.2b}$$

The symbol $F_i(max)$ denotes the maximum value of the oscillatory force (or moment) and is taken as positive. The wave force may, therefore, be defined by the complex number C_i or by the magnitude of C_i and the phase angle δ_i. Once $|C_i|$ and δ_i are known, the wave force (or moment) is expressed as a function of time as

$$F_i(t) = (1.0 \text{ or } \bar{a})\rho g \bar{a}^3 (\bar{H}/2\bar{a}) |C_i| \cos(\delta_i - \sigma t) \qquad (4.3)$$

where the coefficient (1.0) is applicable in the case of a force ($i = 1,2,3$) and ($\bar{a}$) is applied when ($i = 4,5,6$) and $F_i(t)$ denotes a moment. The dimensionless wave amplitude is defined as $\eta_*^\circ = \bar{H}/2\bar{a}$. It is further recalled that all phase angles are measured in relation to the incident wave; at $t = 0$ the crest of the undisturbed incident wave is located at the coordinate origin.

According to the definitions (4.2), C_i may be expressed, using (4.1b) with (2.20b) and (2.19a), as

$$C_i = \iint_S [a\, u_7(x,y,z) - \frac{\cosh[a(h+y)]}{\cosh(ah)} e^{ia(x\cos\psi + z\sin\psi)}] \qquad (4.4)$$

$$\cdot\, g_i(x,y,z)\, dS, \quad i = 1,2,\ldots 6$$

Thus, once $u_7(x,y,z)$ at all points on the immersed surface is determined, the complex wave force (or moment) coefficient C_i may be evaluated by evaluating the surface integral indicated in (4.4).

Turning now to the force (or moment) produced by oscillations in the various degrees of freedom, (2.19a) and (2.20a) may be used in conjunction with (4.1a) to obtain

$$F_{ij}(t) = -(1.0 \text{ or } \bar{a})\rho g \bar{a}^3 X_j^o \nu R_e\left[e^{-i\sigma t}\iint_S u_j(x,y,z) g_i(x,y,z) dS\right], \quad i,j = 1,2..6 \tag{4.5}$$

where as previously noted (1.0) corresponds to the case of a force ($i = 1,2,3$) and ($\bar{a}$) corresponds to the moment ($i = 4,5,6$). Furthermore, if the two dimensionless real numbers M_{ij} and N_{ij} are defined as

$$M_{ij} = -Re\iint_S u_j(x,y,z) g_i(x,y,z)\, dS \tag{4.6}$$

$$N_{ij} = -Im\iint_S u_j(x,y,z) g_i(x,y,z)\, dS \tag{4.7}$$

where Re and Im denote real part and imaginary part, respectively, then (4.5) may be written as,

$$F_{ij}(t) = (1.0 \text{ or } \bar{a})\, \rho g \bar{a}^3 X_j^o \nu R_e[(M_{ij} + iN_{ij}) e^{-i\sigma t}], \quad i,j = 1,2,..6 \tag{4.8}$$

where, as in (4.5), the coefficient (1.0) corresponds to $i = 1,2,3$ and ($\bar{a}$) corresponds to $i = 4,5,6$.

Equation (4.8) may be further rearranged by defining the dimensionless parameters,

$$C_{ij}(t) = \frac{F_{ij}(t)}{\rho g \bar{a}^3}, \quad i = 1,2,3; \; j = 1,2,...6 \tag{4.9a}$$

and

$$C_{ij}(t) = \frac{F_{ij}(t)}{\rho g \bar{a}^4}, \quad i = 4,5,6; \; j = 1,2,...6 \tag{4.9b}$$

With (4.9) and using the definition $\nu = \sigma^2 \bar{a}/g$, (4.8) may be written,

$$C_{ij}(t) = -\frac{\bar{a}}{g} M_{ij} \ddot{X}_j(t) - \frac{\sigma \bar{a}}{g} N_{ij} \dot{X}_j(t), \quad i,j = 1,2,\ldots 6 \tag{4.10}$$

M_{ij} and N_{ij} $(i,j = 1,2,\ldots 6)$ represent the inertia and damping tensors, respectively, having 36 elements each. The first index denotes the direction of the force or moment and the second index is associated with the component of the motion. It can be shown, moreover, that these tensors are symmetrical so that

$$M_{ij} = M_{ji} \tag{4.11a}$$

and

$$N_{ij} = N_{ji} \tag{4.11b}$$

Except for the diagonal terms it is rather difficult to give simple definitions for the dimensionless added mass and damping tensors, M_{ij} and N_{ij}, respectively. They are best defined by expressing the force (or moment) acting on the immersed surface associated with the dynamic response in terms of these parameters. Equation (4.10) gives:

$$F_{ij} = -\left\{ \begin{matrix} 1.0 \\ \bar{a} \end{matrix} \right\} \left[\rho \bar{a}^4 M_{ij} \ddot{X}_j + \rho\sigma \bar{a}^4 N_{ij} \dot{X}_j \right], \quad \left\{ \begin{matrix} i=1,2,3 \\ i=4,5,6 \end{matrix} \right\}, \quad j=1,2,\ldots 6 \tag{4.12}$$

where when $(i = 1,2,3)$ F_{ij} represents a force and when $(i = 4,5,6)$ F_{ij} represents a moment. The parameters $\dot{X}_j$ and $\ddot{X}_j$ denote the first and second time derivatives of the dimensionless displacements:

$$\ddot{X}_j = \ddot{\bar{X}}_j/\bar{a} \quad \text{and} \quad \dot{X}_j = \dot{\bar{X}}_j/\bar{a}, \quad j = 1,2,3 \qquad (4.13a)$$

$$\ddot{X}_j = \ddot{\theta}_j \quad \text{and} \quad \dot{X}_j = \dot{\theta}_j, \quad j = 4,5,6 \qquad (4.13b)$$

5. NUMERICAL SOLUTION

The primary objective at this juncture is to solve the integral equation (3.11) which has been established for the source strength function, $f_i(\xi,\eta,\zeta)$. Once this function is obtained, u_i can be determined from (3.1) by evaluating the surface integral. Then, all other physical quantities such as pressure and resulting forces and moments may be determined.

A numerical procedure can be devised by approximating the actual immersed surface of the structure by a contour composed of a large but finite number of facets. In the limit as the number of facets increases and the size decreases, the approximate contour approaches the actual contour. Thus, we may assume that in the limit as the number of facets approaches infinity, the numerical scheme converges.

To begin, the immersed surface is subdivided as indicated in Figure 3 and an index is assigned to the nodal point (centroid point) of each of the small facets. It is required that (3.11) be satisfied at each of these nodal points. This is a relaxation of the requirement implicit in (3.11) that the equation be satisfied at every point on the immersed surface.

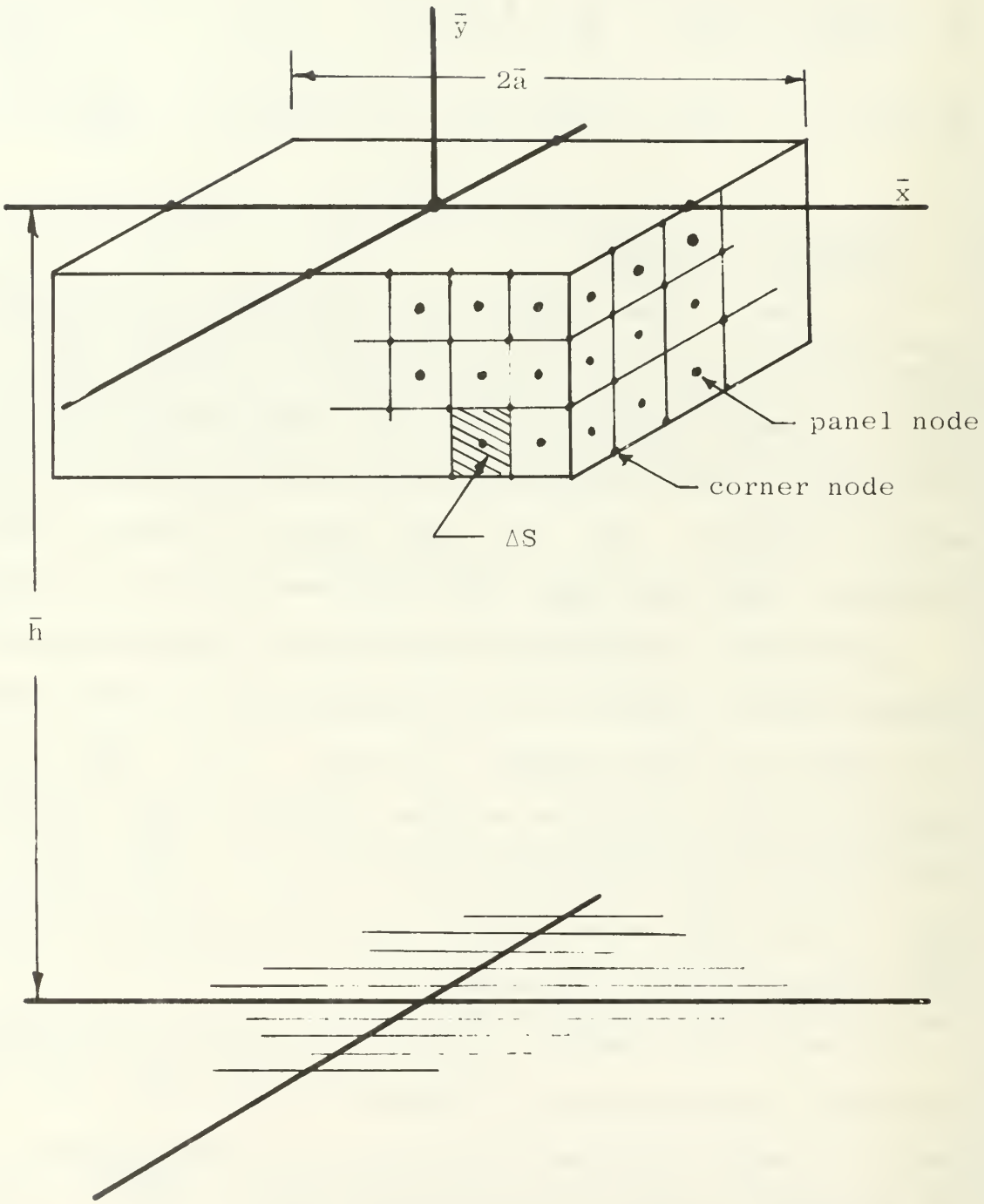

FIGURE 3 NUMERICAL SCHEME

Recognizing that the source strength, $f_j(\xi,\eta,\zeta)$, is a regular well-behaved function, we may approximate (3.11) by

$$-f_n(x_i,y_i,z_i) + \frac{1}{2\pi}\sum_{j=1}^{N} f_n(x_j,y_j,z_j)\iint_{\Delta S_j}\frac{\partial G}{\partial n}(x_i,y_i,z_i;\ x,y,z)\,dS = 2g_n(x_i,y_i,z_i) \qquad (5.1)$$

where ΔS_j denotes the area of the j-th facet and N denotes the total number of facets. In shorthand notation, (5.1) may be written

$$-f_{n_i} + f_{n_j}\,\alpha_{ij} = 2g_{n_i} \qquad (5.2)$$

where n = 1, 2, ...7 corresponds to the six degrees of freedom and scattering, the repeated index indicates summation as usual and α_{ij} is defined as

$$\alpha_{ij} = \frac{1}{2\pi}\iint_{\Delta S_j}\frac{\partial G}{\partial n}(x_i,y_i,z_i;\ x,y,z)\,dS \qquad (5.3)$$

Eq. (5.2) is a complex matrix equation which may be solved using a digital computer to obtain the source strength f_{n_i} once the elements of the square matrix α_{ij} are calculated.

As an approximation, the matrix α_{ij} may be evaluated by using the value of $\partial G/\partial n$ at the nodal point to represent the mean-value over the elemental surface area of the facet and thereby further approximate (5.3) by

$$\alpha_{ij} = \frac{1}{2\pi}\frac{\partial G}{\partial n}(x_i,y_i,z_i;\ x,y,z)\,\Delta S_j \qquad (5.4)$$

where $\partial G/\partial n$ may be evaluated by use of either (3.6) or (3.7). The choice between the two forms depends on the value of r. When r is small, the infinite integral occurring in (3.6) is fairly rapidly convergent while many terms of the series indicated in (3.7) are

required. However, when r is large, the series occurring in (3.7) converged rather rapidly and, consequently, only a few terms are needed.

The potential function u_j may be obtained from (3.1) once the source strength f_j is determined at the nodal points. In a manner similar to that used to solve the integral equation (3.11), the source strength is taken outside the surface integral and (3.1) is written as

$$u_n(x_i,y_i,z_i) = \frac{1}{4\pi} \sum_{j=1}^{N} f_n(x_j,y_j,z_j) \iint_{\Delta S_j} G(x_i,y_i,z_i;\ x,y,z)\ dS \tag{5.5}$$

where as in (5.1) n = 1,2, ...7, and the integer N denotes the total number of nodal points on the immersed surface. In indicial notation (5.5) becomes

$$u_{n_i} = f_{n_j}\ \beta_{ij} \tag{5.6}$$

where the square matrix β_{ij} is defined as the integral over the panel of area ΔS_j as

$$\beta_{ij} = \frac{1}{4\pi} \iint_{\Delta S_j} G(x_i,y_i,z_i;\ x,y,z)\ dS \tag{5.7}$$

Taking the value of G at the nodal point to represent the mean-value over the facet, (5.7) may be approximated for large R as

$$\beta_{ij} = \frac{1}{4\pi}\ G(x_i,y_i,z_i;\ x_j,y_j,z_j)\ \Delta S_j \tag{5.8}$$

where G is evaluated by use of either (3.3) or (3.4), depending on the value of r. When R is not large (5.7) must be used and the integration of 1/R term in G is discussed in Appendix B.

The first step in the numerical solution to the problem is to evaluate the matrices, α_{ij} and β_{ij}. For example, the point (x,y,z)

on the immersed surface is denoted by i and the point where the source is located (ξ,η,ζ) is denoted by j. Thus, using the series form of the Green's function given in (3.4) or its derivative given in (3.7), there is no difficulty in numerical evaluation once the location of the point i and j are specified. However, the integral form of G and its derivatives as specified by (3.3) and (3.6) requires some special consideration. The infinite integral which occurs in both of these expressions poses two difficulties with respect to numerical evaluation; the integral has an infinite upper limit and the integrand is singular at $\mu=\mu_o$ where μ_o is the root of

$$\mu_o \tanh(\mu_o h) - \nu = 0 \qquad (5.9)$$

The root is simply equal to "a" in view of (3.3f). However, these difficulties can be overcome by recognizing that the integrand is singular like $1/(\mu-\mu_o)$, subtracting the singularity out of the integral and carrying out its integration analytically. The remainder of the integral is then carried out numerically and the upper limit is replaced by a suitable large number such that convergence is assured.

For purposes of illustration let the infinite integral in (3.3) be denoted by I so that

$$I = P.V.\int_o^\infty \frac{Q(\mu)\,du}{(\mu-\mu_o)} \qquad (5.10)$$

where

$$Q(\mu) = \frac{P(\mu)\ (\mu-\mu_o)}{\mu\ \tanh\ (\mu h) - \nu} \qquad (5.11)$$

and in the case of (3.3) the function $P(\mu)$ is defined as

$$P(\mu) = \frac{(\mu+\nu)e^{-\mu h}\cosh[\mu(h+\eta)]\cosh[\mu(h+y)]}{\cosh(\mu h)} J_o(\mu r) \qquad (5.12)$$

The integral in (5.10) may be rearranged and written in the form

$$I = \int_o^{2\mu_o} \frac{Q(\mu)-Q(\mu_o)}{(\mu-\mu_o)} d\mu + Q(\mu_o) P.V. \int_o^{2\mu_o} \frac{1}{(\mu-\mu_o)} d\mu \qquad (5.13)$$
$$+ \int_{2\mu_o}^{\infty} \frac{Q(\mu)}{(\mu-\mu_o)} d\mu$$

where the principal value of the second integral can easily be shown to be zero and the other two integrals are proper and easily evaluated by numerical integration. Thus, I may be evaluated by numerical integration of

$$I = \int_o^{2\mu_o} \frac{(Q(\mu)-Q(\mu_o))}{(\mu-\mu_o)} d\mu + \int_{2\mu_o}^{\infty} \frac{Q(\mu)d\mu}{(\mu-\mu_o)} \qquad (5.14)$$

where $Q(\mu_o)$ represents the limit of (5.11) as $\mu \to \mu_o$ where $\mu_o = a$. The result of this limiting process results in the following expression:

$$Q(\mu_o) = \frac{P(\mu_o)}{\tanh(\mu_o h)\left[1-\mu_o h \tanh(\mu_o h)\right]+\mu_o h} \qquad (5.15)$$

or, using (3.3f) and the fact that $\mu_o = a$, (5.15) becomes

$$Q(\mu_o) = \frac{a\, P(a)}{\nu+(a^2-\nu^2)h} \qquad (5.16)$$

For the case of deep water ($h \to \infty$) we find $\nu \to a$ so that

$$Q(\mu_o) = P(a) \qquad (5.17)$$

The same method of integration may be used to evaluate the infinite integral in the derivatives of G as well as in G itself. The only difference is that $P(\mu)$ is defined differently for the other cases but can easily be determined by a comparison of (5.10) and (5.11) with the particular infinite integral to be evaluated.

An alternate method of evaluating the integral form of the Green's function may also be used. This procedure as described in Appendix C involves converting the infinite upper limits and appears to be particularly useful when the wave period is large. The computer program actually uses this form for numerical calculation.

There is one further significant difficulty in evaluating α_{ij}, and β_{ij}. When point i is distant from the source located at point j it is adequate to use approximates such as Eq. (5.4), and (5.8). However, when i = j or point i is near point j the singular term in the Green's function which is of the form 1/R does not vary slowly over the panel of area ΔS_j. Thus, when the node point designated by the index i is rather close to the j-th node point the 1/R term in G and derivatives of 1/R which occurs in α_{ij}, must be integrated over ΔS_j rather than approximated. This integration is described in detail in Appendix B.

Specification of the Subdivision Scheme

The numerical scheme starts with specifying panel corner points on the immersed surface. Each corner node point is assigned an index and then a correspondence table is introduced

which specifies which four corner node points make-up a given panel. Thus, an index is assigned to each panel.

Given the coordinates of the four corners of a given panel it is rather easy to compute its area by breaking it up into two triangular areas. Using the areas and centroids of the two triangular portions of the polygon the centroid of the polygon is computed. Finally, the unit normal vector for the panel is determined by taking the cross-product of vectors running across the two diagonals of the polygon panel. These calculations are described in detail in Appendix A.

6. DYNAMIC RESPONSE FOR A FLOATING BODY

In this section the equations of motion for a floating body in waves are developed. These equations are then applied using hydrodynamic coefficients, which include the wave excitation forces and moments as well as added mass and damping coefficients, in order to compute the dynamic response.

The problem under consideration is represented schematically in Figure 1. In the following, the equations of motion are written with respect to the center of gravity. Thus, the origin of the body coordinates is assumed to be located at the center of gravity of the floating structure and d is defined as the dimensionless depth to that point.

The small amplitude displacement of the body center of mass with respect to its mean position in the inertial reference frame is described by the three coordinates $\bar{X}_1(t)$, $\bar{X}_2(t)$ and $\bar{X}_3(t)$ which are referred to as surge, heave, and sway, respectively. The small angular displacements of the body about the

$\bar{x}'$, $\bar{y}'$ and $\bar{z}'$ axes are denoted by Θ_4, Θ_5, Θ_6 and are referred to as roll, yaw and pitch, respectively.

The equations of motion linearized with respect to the small angular displacements of the body may now be written as follows:

$$F_1^T(t) = \bar{m}\ddot{\bar{X}}_1(t) \tag{6.1a}$$

$$F_2^T(t) = \bar{m}\ddot{\bar{X}}_2(t) \tag{6.1b}$$

$$F_3^T(t) = \bar{m}\ddot{\bar{X}}_3(t) \tag{6.1c}$$

$$F_4^T(t) = \bar{I}_{x'x'}\ddot{\Theta}_4 - \bar{I}_{x'y'}\ddot{\Theta}_5 - \bar{I}_{x'z'}\ddot{\Theta}_6 \tag{6.1d}$$

$$F_5^T(t) = \bar{I}_{y'y'}\ddot{\Theta}_5 - \bar{I}_{y'z'}\ddot{\Theta}_6 - \bar{I}_{y'x'}\ddot{\Theta}_4 \tag{6.1e}$$

$$F_6^T(t) = \bar{I}_{z'z'}\ddot{\Theta}_6 - \bar{I}_{z'x'}\ddot{\Theta}_4 - \bar{I}_{z'y'}\ddot{\Theta}_5 \tag{6.1f}$$

where $F_1^T(t)$, $F_2^T(t)$ and $F_3^T(t)$ denote the three components of the total external force acting on the body and $F_4^T(t)$, $F_5^T(t)$ and $F_6^T(t)$ denote the three components of the total external moment. The symbol $\bar{m}$ denotes the body mass which equals the displaced mass. The moments of inertia are defined, typically, as

$$\bar{I}_{x'y'} = \bar{I}_{y'z'} = \int_{\bar{m}} \bar{x}'\bar{y}'\, d\bar{m} \tag{6.2}$$

where the integration is to be carried out over the complete mass of the body. For bodies having symmetry with respect to the (x'-y') and (y'-z') planes, all of the products of inertia

vanish. Although this type of symmetry is common to most ocean structures, there is no need to apply the limitation at this point since the inclusion of the product of inertia terms do not, in principle, complicate the development.

At this juncture it is convenient to place the equations of motion in dimensionless form and replace the x, y, z subscript system with a less cumbersome indicial system. We may define the following dimensionless parameters for this purpose:

$$m_{11} = m_{22} = m_{33} = \bar{m}/\rho\bar{a}^3, \quad m_{12} = m_{21} = m_{31} = m_{13} = m_{23} = m_{32} = 0$$

$$m_{44} = I_{\bar{x},\bar{x}}/\rho\bar{a}^5, \quad m_{55} = I_{\bar{y},\bar{y}}/\rho\bar{a}^5, \quad m_{66} = I_{\bar{z},\bar{z}}/\rho\bar{a}^5$$

$$m_{45} = m_{54} = -I_{\bar{x},\bar{y}}/\rho\bar{a}^5, \quad m_{46} = m_{64} = -I_{\bar{x},\bar{z}}/\rho\bar{a}^5, \quad m_{65} = m_{56} = -I_{\bar{y},\bar{z}}/\rho\bar{a}^5$$

$$X_1(t) = \bar{X}_1(t)/\bar{a}, \quad X_2(t) = \bar{X}_2(t)/\bar{a}, \quad X_3(t) = \bar{X}_3(t)/\bar{a}$$

$$X_4(t) = \Theta_4(t), \quad X_5(t) = \Theta_5(t), \quad X_6(t) = \Theta_6(t)$$

$$f_1^T(t) = F_1^T(t)/\rho g\bar{a}^3, \quad f_2^T(t) = F_2^T(t)/\rho g\bar{a}^3, \quad f_3^T(t) = F_3^T(t)/\rho g\bar{a}^3$$

$$f_4^T(t) = F_4^T(t)/\rho g\bar{a}^4, \quad f_5^T(t) = F_5^T(t)/\rho g\bar{a}^4, \quad f_6^T(t) = F_6^T(t)/\rho g\bar{a}^4$$

where, as previously given, $\bar{a}$ denotes the characteristic dimension of the body, ρ denotes the fluid density and g denotes the gravitational constant.

Using these definitions, (6.1) may be condensed to the form

$$f_i^T(t) = \frac{\bar{a}}{g} m_{ij} \ddot{X}_j(t) \qquad (6.4)$$

where ij takes on values 1,2,...6, and the repeated index denotes summation as usual.

Equation (6.4) represents the six equations of motion with $f_i^T(t)$ denoting the dimensionless total external force or moment coefficients as defined by (6.3). For free-floating bodies these coefficients represent the contributions from the surrounding fluid only and are generally considered to be composed of three parts: (a) the wave excitation forces and moments, (b) the dynamic forces and moments caused by the motion of the body, and (c) the hydrostatic forces and moments caused by the displacement of the body. For moored bodies the forces and moments associated with the mooring lines must be included and for the linear problem these contributions may be determined separately and superimposed.

In accordance with this idea the three contributions to the force (or moment) coefficient $f_i^T(t)$ may be expressed as the linear combination:

$$f_i^T(t) = c_i(t) + \sum_{j=1}^{6} [c_{ij}(t) + k_{ij}(t) + k'_{ij}(t)] \qquad (6.5)$$

where

$c_i(t)$ = force or moment coefficient associated with wave excitation, $F_i(t)/\rho g\bar{a}^3$ (i=1,2,3); $F_i(t)/\rho g\bar{a}^4$ (i=4,5,6)

$c_{ij}(t)$ = force or moment coefficient associated with the dynamic response of the body, see Eqs. (4.8-4.10).

$k_{ij}(t)$ = force or moment coefficient associated with linear or angular displacement which results from hydrostatic pressures.

$k'_{ij}(t)$ = force or moment coefficient associated with linear or angular displacement resulting from elastic constraints (mooring lines).

The force or moment coefficient $c_i(t)$ may be expressed as

$$c_i(t) = \eta_*^\circ \, R_e[|C_i| e^{i\delta_i} e^{-i\sigma t}], \quad i = 1,2,..6 \qquad (6.6)$$

where i = 1,2,3 refers to the three components of the force and i = 4,5,6 refers to the three components of the moment. The dimensionless coefficients $c_i(t)$ are defined according to the definition of $f_i^T(t)$ as the force made dimensionless with $\rho g\bar{a}^3$ (i = 1,2,3) or the moment made dimensionless with $\rho g\bar{a}^4$ (i = 4,5,6). The frequency of the wave excitation is denoted by σ, and δ_i denotes the phase shift angle of the i-th component of excitation force or moment in relationship to the incident wave. (All phase shift angles are measured as lag positive and in relation to the time that the crest of the undisturbed incident wave is at the coordinate origin.)

The magnitude of the complex excitation force or moment coefficient occurring in (6.6) is defined, as in Section 4, as

$$|C_i| = \frac{F_{i(max)}}{\rho g \bar{a}^3 \eta^\circ_*}, \quad i=1,2,3; \quad |C_i| = \frac{F_{i(max)}}{\rho g \bar{a}^4 \eta^\circ_*}, \quad i=4,5,6 \qquad (6.7)$$

where $\eta^\circ_* = \bar{H}/2\bar{a}$ denotes the dimensionless wave amplitude, $\bar{H}$ being the wave height and $\bar{a}$ the characteristic body dimension. The amplitude of the excitation forces and moments are denoted by $F_{i(max)}$ where i = 1,2,3 refers to the three components of force, and i = 4,5,6 refers to the moment.

As the body responds to the wave excitation, dynamic pressures arise due to the motion which may be resolved into two components of force (or moment), one component in phase and proportional to the acceleration of the body and a second in phase and proportional to the velocity. Equation (4.10) defines this dimensionless force (or moment) which is due to the motion of the body. The dimensionless parameter $c_{ij}(t)$ is defined in (4.10) as the force (i=1,2,3) or moment (i=4,5,6) which is caused by the j-th component of motion. The dimensionless parameters M_{ij} and N_{ij} denote the added mass and damping coefficients which are calculated by use of (4.6) and (4.7).

The final contribution to the force (or moment) resulting from the surrounding fluid comes from the hydrostatic pressure. As the body is displaced from its equilibrium position, forces and moments arise which are proportional to the body displacement.

The hydrostatic pressure increases with depth according to $P = -\rho g\bar{y}$ and, consequently, the i-th component of hydrostatic force or moment resulting from this pressure variation and acting on the body is given by the integral

$$F_i^H = \rho g\bar{a}^3 \iint_S y g_i dS, \quad i = 1,2,3; \quad F_i^H = \rho g\bar{a}^4 \iint_S y g_i dS, \quad i=4,5,6 \qquad (6.8)$$

where $y = \bar{y}/\bar{a}$ denotes the dimensionless y coordinate of a point on the immersed surface, and $dS = d\bar{S}/\bar{a}^2$, $d\bar{S}$ being an elemental surface area. The functions g_i occurring in Eq. (6.8) are defined as follows:

$$\begin{aligned} g_1 &= n_x, & g_2 &= n_y & g_3 &= n_z \\ g_4 &= y'n_z - z'n_y, & g_5 &= z'n_x - x'n_z, & g_6 &= x'n_y - y'n_x \end{aligned} \qquad (6.9)$$

where the dimensionless body coordinates are defined as

$$x' = \bar{x}'/\bar{a}, \qquad y' = \bar{y}'/\bar{a}, \qquad z' = \bar{z}'/\bar{a}, \qquad d = \bar{d}/\bar{a}$$

and the unit normal vector on the immersed surface is defined as $\vec{n}(x',y',z'; X_1,X_2,X_3,X_4,X_5,X_6) = \vec{i}n_x + \vec{j}n_y + \vec{k}n_z$. Eq. (6.9) is the same definition of g_i given in (2.21f), the only difference being that (2.21f) is written in terms of the fixed (x,y,z) coordinate system while (6.9) is expressed in terms of the body axes.

The following linearized relationships exist between the coordinates of the fixed reference frame and the body coordinates for a given point on the immersed surface at x',y',z':

$$\begin{aligned} x &= x' + X_5 z' - X_6 y' + X_1 \\ y &= -d + y' + X_6 x' - X_4 z' + X_2 \\ z &= z' + X_4 y' - X_5 x' + X_3 \end{aligned} \qquad (6.10)$$

Equation (6.7) represents the hydrostatic force (or moment) acting on the immersed surface including the buoyant force which must, of course, just balance the weight. It is desired, however, to determine the i-th component of force associated with a j-th (j = 1,2,...6) component of displacement of the body. j = 1,2,3 denoting linear displacement in the x',y',z' directions, respectively, and j = 4,5,6 denoting angular displacement about x',y',z' axes, respectively. For the linearized problem this force (or moment) may be written, using Eq. (6.8), as

$$F_{ij}^{H} = \frac{\partial F_i^H}{\partial X_j} X_j = (1 \text{ or } \bar{a})\, \rho g \bar{a}^3 X_j \frac{\partial}{\partial X_j} \iint_S y g_i \, dS \qquad (6.11)$$

(The factor 1.0 in brackets in (6.11) is applied when i=1,2,3 and $\bar{a}$ is appropriate when F_{ij} denotes a moment (i.e.), i=4,5,6.) Defining, further, the dimensionless parameter K_{ij} as

$$K_{ij} = -\iint_S \frac{\partial}{\partial X_j} (y g_i) \, dS \qquad (6.12)$$

the dimensionless force (or moment) coefficient $k_{ij}(t)$ may be written, in view of (6.11), as

$$k_{ij}(t) = -K_{ij} X_j(t) \quad \text{(no sum)} \qquad (6.13)$$

Equation (6.13) represents a form appropriate to Eq. (6.5) for the dimensionless force in the i-th direction caused by a displacement in the j-th degree of freedom.

The following expressions are obtained for the hydrostatic force coefficients K_{ij}:

$$K_{22} = -\iint_S n_y \, dS = A_w/\bar{a}^2 \tag{6.14a}$$

$$K_{24} = K_{42} = \iint_S Z' n_y dS \tag{6.14b}$$

$$K_{44} = \iint_S (y'z'n_z - z'^2 n_y) dS \tag{6.14c}$$

$$K_{46} = K_{64} = \iint_S x'z'n_y dS \tag{6.14d}$$

$$K_{26} = K_{62} = -\iint_S x'n_y \, dS \tag{6.14e}$$

$$K_{66} = \iint_S (x'y'n_x - x'^2 n_y) \, dS \tag{6.14f}$$

in which A_w denotes the waterplane area in the equilibrium position. For floating bodies having symmetry with respect to the x'-y' and y'-z' planes the coefficients, $K_{24} = K_{42} = K_{46} = K_{64}$ $K_{26} = K_{62} = 0$.

It is noted here that the expressions, Eqs. (6.14), for the hydrostatic force coefficients are in rather convenient forms for evaluation as a part of the same numerical scheme discussed in Chapter 5 which involves representation of the immersed surface by a large number of nodal points. At each nodal point it is necessary to specify the three coordinates of its location, the three components of the unit vector normal to the surface, and the elemental area of the facet. This information is, therefore, available in convenient forms for use in the evaluation of the integrals in Eq. (6.14) in the computer program.

If the mooring lines can be approximated by linear elastic constraints then the force or moment coefficient may be expressed in terms of a spring constant K'_{ij} and displacement X_j in a form similar to Eq. (6.12) as

$$k'_{ij}(t) = -K'_{ij}X_j(t) \quad \text{(no sum)} \tag{6.15}$$

where

$$k'_{ij}(t) = \begin{cases} i = 1,2,3; \quad j = 1,2,\ldots 6: \text{ force in i-direction}/\rho g\bar{a}^3 \\ i = 4,5,6; \quad j = 1,2,\ldots 6: \text{ moment in i-direction}/\rho g\bar{a}^4 \end{cases}$$

and K'_{ij} denotes a spring constant matrix which depends on the mooring line configuration, stiffness and tension. K'_{ij} is defined as

$$K'_{ij} = -\left[\frac{\partial F_i}{\partial X_j}\right] / \rho g\bar{a}^3, \quad \begin{matrix} i=1,2,3 \\ j=1,2,\ldots 6 \end{matrix} \tag{6.16a}$$

$$K'_{ij} = -\left[\frac{\partial F_i}{\partial X_j}\right] / \rho g\bar{a}^4, \quad \begin{matrix} i=4,5,6 \\ j=1,2,\ldots 6 \end{matrix} \tag{6.16b}$$

in which F_i = the force in the positive i-th direction caused by the mooring lines when i=i,2,3 and F'_i = the moment about the i-th body axis due to the mooring lines when i=4,5,6. The parameters X_j denote dimensionless displacements as defined by Eq. (6.3). That is, when i=1,2,3, X_i denotes dimensionless linear displacements

$$X_i = \bar{X}_i/\bar{a}, \quad i=1,2,3$$

and when i=4,5,6 angular displacements,

$$X_i = \theta_i, \quad i=4,5,6$$

The equations of motion for a free floating body may now be obtained by use of Eqs. (6.4), (6.5), (6.6), (4.10), and (6.13) as follows:

$$\frac{\bar{a}}{g}(m_{ij} + M_{ij})\ddot{X}_j + N_{ij}\frac{\bar{a}\sigma}{g}\dot{X}_j + (K_{ij}+K'_{ij})X_j = \eta^{\circ}_{*} R_e[|C_i|e^{i\delta_i} e^{-i\sigma t}] \tag{6.17}$$

Furthermore, the body response in the j-th degree of freedom may be expressed in the form

$$X_j(t) = X^{\circ}_j R_e[e^{i\psi_j} e^{-i\sigma t}] \tag{6.18}$$

which, when substituted into Eq. (6.17), yields the complex equations of motion,

$$[-(m_{ij}+M_{ij})-iN_{ij}+(K_{ij}+K'_{ij})/\nu]\frac{X_i}{\eta^{\circ}_{*}} e^{i\psi_j} = \left|\frac{C_i}{\nu}\right| e^{i\delta_i} \tag{6.19}$$

where the frequency parameter $\nu = \sigma^2\bar{a}/g$.

Equation (6.19) represents six equations corresponding to i=1,2,3...6. The repeated j index denotes, as usual, the summation over the six degrees of freedom. The amplitude ratio $X^{\circ}_j/\eta^{\circ}_{*}$ denotes the ratio of the amplitude of the motion to the amplitude of the incident wave and ψ_j denotes the phase angle of the motion (displacement) in relation to the reference condition of the crest of the incident wave being located at the coordinate origin.

It will be recalled that for bodies possessing x'-y' and y'-z' plane symmetry, $m_{ij}=0$ for $i\neq j$ in Eq. (6.17). Also, M_{ij} and N_{ij} denote the thirty-six element added mass and damping tensors.

It can be shown, however, that

$$K_{ij} = K_{ji}, \quad M_{ij} = M_{ji}, \quad K_{ij} = K_{ji} \tag{6.20}$$

so that only 21 different values exist in the general six degrees of freedom problem.

To further simplify the notation, we may define the complex matrix,

$$A_{ij} = -(m_{ij}+M_{ij})+(K_{ij}+K'_{ij})/\nu - iN_{ij} \tag{6.21}$$

the complex response vector,

$$\gamma_j = \frac{X^o_j}{\eta^o_*} e^{i\psi_j} \tag{6.22}$$

and, in addition, the vector,

$$B_i = \frac{|C_i|}{\nu} e^{i\delta_i}$$

Then, Eq. (6.19) may be written very simply as

$$A_{ij}\ \gamma_j = B_i, \quad i,j = 1,2,\ldots 6 \tag{6.23}$$

Equation (6.24) may be solved by matrix inversion. Once the solution to Eq. (6.21) for γ_j is obtained, the problem is solved. The amplitude and phase angle of the response can be extracted from the definition of γ_j given in Eq. (6.22).

7. HASKINDS RELATIONS AND ENERGY BALANCE

Even though it may be supposed that the numerical solution proposed here will converge upon increasing the number of partitions, it is important to keep the partition size large (and number of partitions as small) as accuracy considerations will permit in order to reduce computer time and storage requirements. It is, for this reason, important to determine the effect of the partition size on accuracy so that practical limits may be established.

One method of verifying the accuracy is to compare the numerical results with analytical results where closed form solutions exist. Although valid, this approach is limited to a few simple shapes; for more general shapes no such check, of course, exists.

A second method of checking the validity of the numerical results involves the use of an energy balance as well as the use of the so-called Haskind's relations. Conservation of energy requires that a balance must exist between the energy required to oscillate the object, and the wave energy transmitted across some control volume surrounding the object but at a large radial distance. Using the asymptotic form of the Green's function given in (3.4a) for large values of r, along with (3.1) the following relationship for the damping coefficient is so obtained.

$$N_{ii} = \frac{1}{4\pi} \frac{a^2 - \nu^2}{h(a^2-\nu^2)+\nu} \int_0^{2\pi} \left| \iint_S f_i(\xi,\eta,\zeta)\cosh[a(h+\eta)]e^{-ia\rho_1} \cdot \cos(\beta-\theta)\, dS \right|^2 d\theta \qquad (7.1)$$

where $\rho_1 = \sqrt{\xi^2+\eta^2}$ and $\beta = \tan^{-1}(\zeta/\xi)$. This relationship expresses the damping coefficient in terms of the far field behavior of the solution.

A relationship somewhat similar to (7.1) known as Haskind's relations, may be obtained for the wave force (or moment) coefficient. That is, the i-th component wave force (or moment) coefficient is related to the waves produced at infinity by the body oscillating in the i-th mode such that

$$C_i = \frac{1}{\cosh(ah)} \iint_S f_i(\xi,\eta,\zeta)\cosh[a(h+\eta)]\, e^{-ia\rho_1}\cos(\beta-\pi-\psi)\, dS \qquad (7.2)$$

where ψ denotes the incidence angle as indicated in Figure 1. A form of this relationship between the wave force and the waves produced at infinity by the same body oscillating in otherwise still water was first derived by Haskind (14) and later reiterated and discussed by Newman (3). Equation (7.2) may be considered to represent a form of the Haskind's relations as extended to the finite depth case. The details of this extension which involves integration by method of stationary phase are given by Rao and Garrison (15).

Equations (7.1) and (7.2) represent relationships for the damping and wave force (or moment) coefficient based on the behavior of the far field solution. A comparison of these results with N_{ii} and C_i obtained from an integration of the pressure over the immersed surface, i.e., as obtained from (4.2) and (4.7), provides a convenient and valuable self-check on the accuracy of numerical results. These results are not limited to special configurations and may be applied to arbitrary shapes. Equation (7.2) is, however, limited to symmetry with respect to the x-y plane, a condition which is satisfied by most practical shapes.

It may be noted, moreover, that for the special case of the vertical force on an axisymmetric body a very simple relationship between C_2 and N_{22} may be obtained from Eqs. (7.1) and (7.2). That is, in view of the axisymmetry the integrand in Eq. (7.1) must be independent of θ. Accordingly, the integration with θ may be accomplished by evaluating the integrands at any value of θ, say $\theta=\pi$ and multiplying by 2π. The right hand sides of Eqs. (7.1) and (7.2) then become similar and the following relationship may be derived between the wave force and damping coefficient in heave:

$$N_{22} = \frac{a}{2} \frac{\sinh (2\, ah)}{2ah + \sinh (2ah)} |C_2|^2 \qquad (7.3)$$

For the case of infinite depth, Eq. (7.3) reduces to the special case presented by Newman (3)

$$|C_2| = \sqrt{\frac{2N_{22}}{a}} \qquad (7.4)$$

The numerical evaluation of Eqs. (7.1) and (7.2) can be easily carried out using the same numerical scheme outlined in Chapter 5. The numerical integrations over the immersed surfaces are converted to summations and evaluated using the source strength function obtained from solution of (5.2).

8. COMPUTER PROGRAM

The theoretical development outlined in Chapters 1-7 has been coded for digital computer calculations and a description of that program is presented in this chapter. The general arrangement of the numerical procedure, a computational flow-chart and the input-output format are discussed.

The basic requirements established for the program were considered to be as follows:

(a) The program must work for floating bodies of completely arbitrary shape, but when either one or two vertical planes of symmetry exist the program should take advantage of this so as to reduce the input data and calculations.

(b) Run time must be kept as small as possible but without losing accuracy.

(c) Computer core requirements must be kept to a reasonable value even for very complex shapes where a large number of panels are required.

Flow Chart

The flow chart for the computer program is given in Table 1. It should be noted that the total program is divided into two parts, a very small MAIN program which is used only for dimensioning, inputing parameter and calling the first subroutine DYNRES . This arrangement allows all of the subroutines which have variable dimensioning to be placed on files if desired and only the small MAIN program need be altered.

The subroutine OTECPR controls the flow of the calculations and calls essentially all of the other subroutines. It first calls the subroutine GDATA which in turn calls the subroutine CONFIG. This subroutine reads data cards describing the immersed surface and computes the unit normals, areas and centroid locations of each panel. GDATA then calls the subroutine PLT which plots the panels on a calcomp plotter. The CPU time requirement to this point in the program is small, and therefore the program could be terminated at this point so that the plot output could be checked. Once it is determined that the input data is correct a complete run could then be made.

Next the subroutine WAVLIN is called by OTECPR . The purpose of this subroutine is to compute the value of "a"

TABLE I

COMPUTER PROGRAM FLOW CHART - OTECPR1

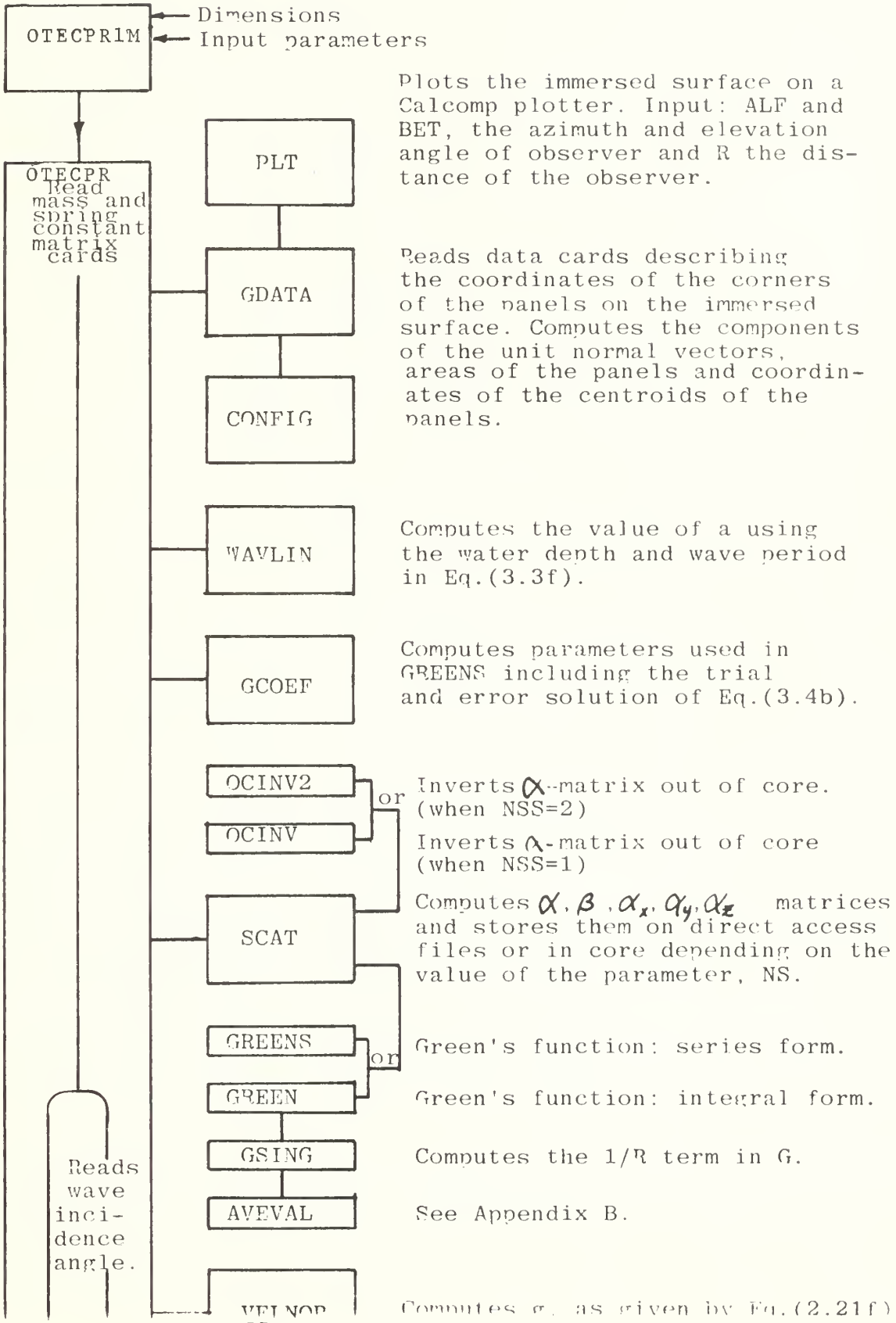

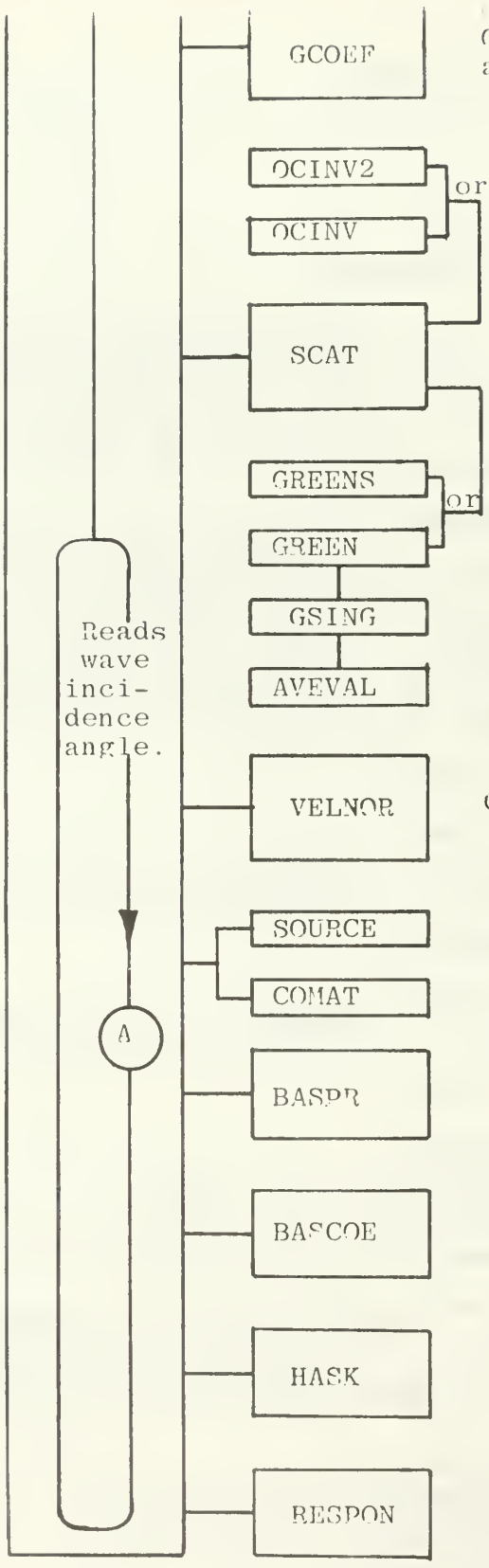

GREENS including the trial and error solution of Eq.(3.4b).

Inverts α-matrix out of core. (when NSS=2)

Inverts α-matrix out of core (when NSS=1)

Computes $\alpha, \beta, \alpha_x, \alpha_y, \alpha_z$ matrices and stores them on direct access files or in core depending on the value of the parameter, NS.

Green's function: series form.

Green's function: integral form.

Computes the 1/R term in G.

See Appendix B.

Computes g_i as given by Eq.(2.21f)

Out of core solution of Eq.(5.2)

In core solution of Eq.(5.2)

Computes the potential at the node points and prints the pressure and velocity dist.

Using the pressure distribution BASCOE computes the excitation forces and moments, added mass and damping coefficients.

Computes the value of the excitation forces and moments and added mass and damping coefficients by use of Haskind's relations and energy balance.

Solves the equations of motion of the floating body,(i.e.), solves Eq.(6.24).

(A) Loops through "NWAVES" times. Each time through the loop a new wave incidence angle is read at the same period and depth.

by trial and error solution of the equation:

$$\nu = a \tanh (ah)$$

The subroutine GCOEF is next called by OTECPR. The function of this subroutine is to compute certain functions which are used repeatedly in the series form of the Green's function. The first fifty values of μ_k given by (3.4b) are computed and these values are used to compute the first fifty values of $\cos[\mu_k(h+y)]$ and $\sin[\mu_k(h+y)]$ for the various different values of y corresponding to the node points at the centroids of the panels on the caisson. The values of these functions are stored and are used by the subroutine GREENS for use in evaluating the series form of the Green's function.

The subroutine SCAT is next called by OTECPR. This subroutine evaluates the elements of the α and β matrices and stores them on FILE #10 and 14, respectively. SCAT calls the subroutine GREEN and GSING or GREENS to evaluate these matrices. GSING calls AVEVAL to evaluate the $1/R$ and $\partial(1/R)/\partial n$ term in the integral form of the Green's function.

The program has, in general, two options for solving the matrix equation (5.2) either by inversion of $(\alpha-I)$ through OCINV or OCINV2 out of core, or by solution through COMAT in core. When the inversion out of core option is selected, SCAT calls OCINV or OCINV2 to invert $(\alpha-I)$ stores $(\alpha-I)^{-1}$ in the file space originally occupied by $(\alpha-I)$.

In addition to the calculation of α and β matrices and the storing of these matrices out of core, SCAT also generates the derivatives of α (i.e., the matrices α_x, α_y and α_z and stores them on Files 11, 12, and 13).

At this juncture in the flow of calculations OTECPR reads the first of a series of data cards which specifies the incidence angle, ψ , of the incident wave relative to the body coordinates. All of the computations made heretofore are dependent on the period and wave height but are independent of the incidence angle. Thus, computations may be made for a series of incidence angles at little additional expenditure of CPU time. The remainder of the program is, therefore, "looped" NWAVES times with different values for the incidence angle.

The next subroutine called by OTECPR is VELNOR. This subroutine computes the velocity induced normal to the caisson by the incident wave. More specifically, VELNOR computes the vector given by (2.21f). This vector represents the right hand side of Equation (5.2) so that the equation can be solved for the source strength.

Depending on the particular option selected for solving (5.2) either SOURCE or COMAT is called next in OTECPR. The function of SOURCE is to multiply $(\alpha-I)^{-1}$ on g in order to evaluate the source strength through (5.2). In the case that $(\alpha-I)^{-1}$ has not been determined through OCINV or OCINV2, the subroutine COMAT is called which solves (5.2) by elimination.

The subroutine BASPR is called next by OTECPR. The purpose of this subroutine is to compute the value of the potentials, $(u_0 + u_7)$, u_1, u_2, u_3, u_4, u_5 and u_6 at the node points on the immersed surface. Using these values of the potentials, BASPR computes the pressure distribution on the immersed surface. This subroutine also reads the FILES #11, 12, and 13 which store α_x, α_y and α_z and with this information computes the three components of velocities in body coordinates at the node points on the immersed surface. It should be noted that the velocities are used only for a check on the solution and are not actually needed in the computation of the loads and response of the floating body. The computation of velocity can be surpressed by simply setting the parameter NBA = 1 in the MAIN program; when NBA = 2 the velocities are computed. When NBA = 1 the FILES #11, 12 and 13 are not used at all.

The subroutine BASCOE is next called by OTECPR. The function of this subroutine is to re-compute the excitation forces and moments by use of the Haskind's relations (Eq. 7.2) and re-compute the damping coefficients, N_{ii}, by use of an energy balance (Eq. 7.1). These results which are computed on the basis of the far-field potential are compared with the same results computed by use of the surface (near-field) pressure distribution as a check on the validity of the solution.

Finally OTECPR calls the subroutine RESPON. This subroutine takes as inputs the excitation forces and moments, added mass and

damping coefficients, mass and spring constant information and then solves Equation (6.24) for the dynamic response of the body.

Input Data

The input data for the program describes the geometry of the immersed surface up to the mean waterline, specifies the water depth and wave conditions as well as the mass and mooring line spring constant parameters. Some of the data is input through data cards and some through constants in the DATA statements in the MAIN program.

The 36 values of mass $\bar{m}$ and mass moments of inertia of the floating body, $I_{\bar{x}}, I_{\bar{y}},$, etc., are input through six data cards, each card containing six values.

The spring constants which account for the effect of the mooring lines are next input. Here again, there are, in general, 36 values which are input through six data cards, each card containing six values.

The immersed surface of the body is described through a set of data cards which give the three coordinates of the corners of the panels. These coordinates are measured with respect to a special coordinate system used for inputing the data only. These special "input axes" allow the user of the program to measure the coordinates of the panel corners in any convenient reference frame and then the subroutines GDATA and CONFIG shift the origin of this special input coordinate system to any desired location by use of the inputs XREF, YREF, ZREF and rotates it by the angle ANGREF.

Another set of data cards following the ones specifying the location of the corner points is used to specify which four corners constitute a given panel. Each data card in this set contains five integers, the first represents the panel number or index and the following four integers specify the indices associated with the corners.

The last set of data cards specify the different values of the incidence angle of the wave. There are "NWAVES" of these cards.

Coordinate Systems

It is important to understand the coordinate systems used in order to input the program properly and, therefore, these are defined in the following. It is convenient to define three coordinate systems:

(x", y", z"): Input axes

(x', y', z'): Body axes

(x, y, z) : Inertial axes

The input axes are used to input the location of the corners of the panels. This set of axes may be located at any convenient point and orientation with respect to the hull but the y"-axis is set vertical with positive y" measured upward. The second two coordinate systems also have their y-axes pointing upwards and the location of their origins and orientation is specified by the five parameters, XREF, YREF, ZREF, ANGREF and ECG.

The inertial axes is located such that the x'-z' plane represents the mean water level. It is located at the point x" = XREF, y" = YREF and z" = ZREF in the input reference frame such that the center of gravity of the body is on a vertical line passing through the origin. The body axes is considered to be aligned with the inertial axes when the body is in its equilibrium position except that it is shifted to the point (0, ECG, 0) in the (x,y,z) reference frame. When the center of gravity lies above the mean waterline ECG represents a positive number and when the center of gravity lies below the mean water level ECG will be negative.

Figure 4 shows the three coordinate systems and their relationship one to another. The reason for the introduction of the input coordinate system is strictly for convenience in inputing data. In the case of certain configuration it may be convenient to measure the location of the corners of the panels in a coordinate system attached to the hull at a reference point which may differ from either the mean waterline or the center of gravity.

Positive values of XREF, YREF, ZREF and ANGREF are shown in Figure 4. The wave incidence angle, ψ, is also shown in the figure and is defined relative to the body and inertial axes as indicated.

Corner Node Point Inputs - No Symmetry:

It would be unusual that a floating structure would possess no symmetry whatsoever but the program has the capability of dealing with such general cases. When no symmetry is present the complete immersed surface of the hull must be covered with panels.

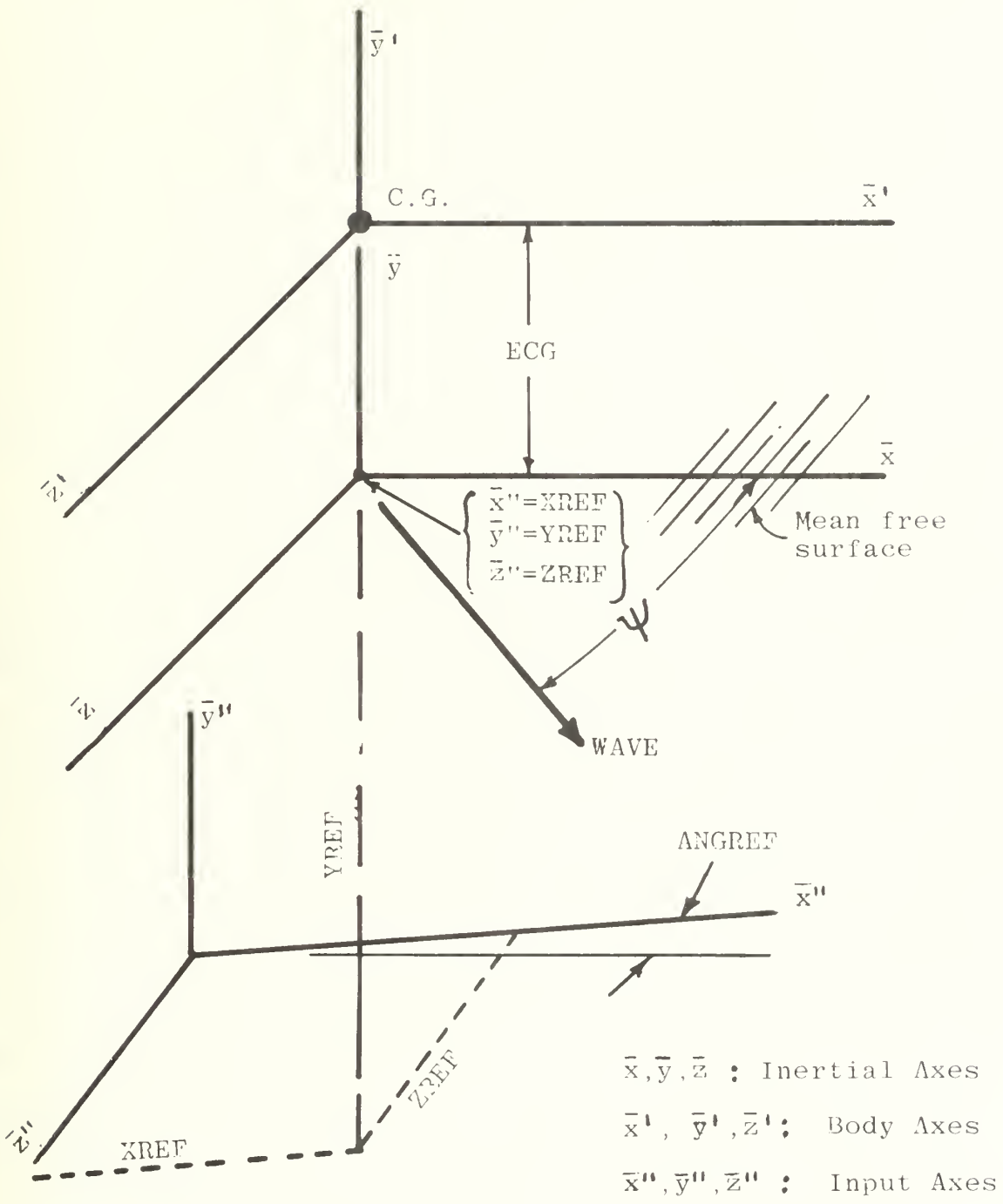

FIGURE 4 DEFINITION OF COORDINATE SYSTEMS

Corner Node Point Input - One Plane of Symmetry:

When the immersed surface has one vertical plane of symmetry and the center of gravity lies in this plane, then only half of surface must be represented by panels. In such a case the input axes may be placed in any desired manner relative to the immersed surface but the parameters XREF, YREF, ZREF and ANGREF must be selected such that the plane of symmetry is coincident with the x' - y' and x - y planes and such that O(x',y',z') is coincident with the center of gravity. The single symmetry case is depicted in Figure 5.

Corner Node Point Inputs - Double Symmetry:

If the hull possesses two planes of symmetry it is necessary to input data cards specifying the panel corners on one quarter of the hull only. Here again the input coordinate system is used to input the coordinates of the corners of the panels and it may be positioned arbitrarily with respect to the hull. However, XREF, YREF, ZREF, ANGREF have to be input such that O(x,y,z) and O(x',y',z') lie on the intersection of the two planes of symmetry and ECG must be such that O(x',y',z') is coincident with the center of gravity. The result is that the (x,y,z) and (x',y',z') are placed relative to the floating body as shown in Figure 6. The portion of the immersed surface input falls in the positive x-z quadrant in the body and inertial axes as indicated in the figure.

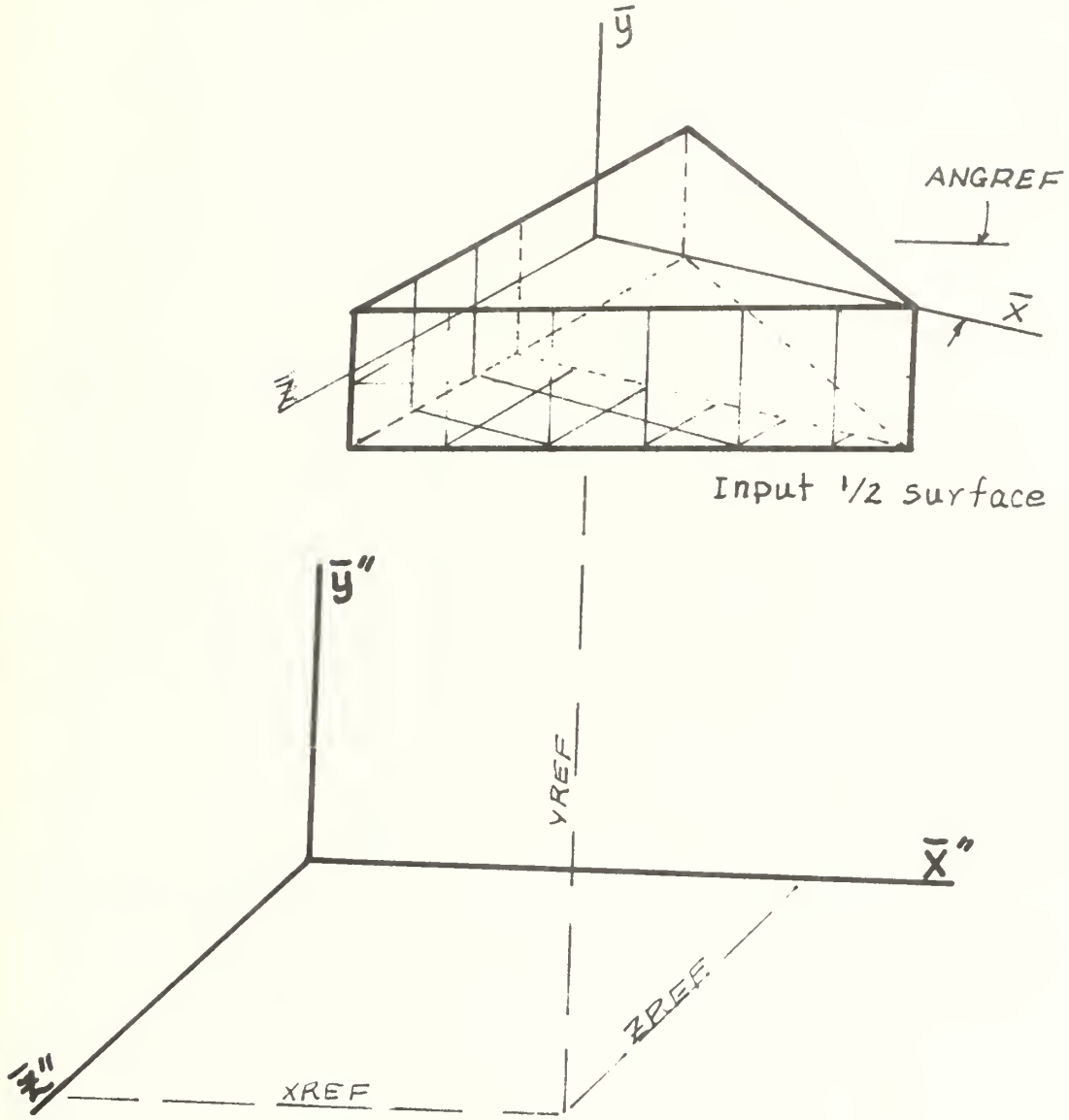

FIGURE 5 SINGLE SYMMETRY

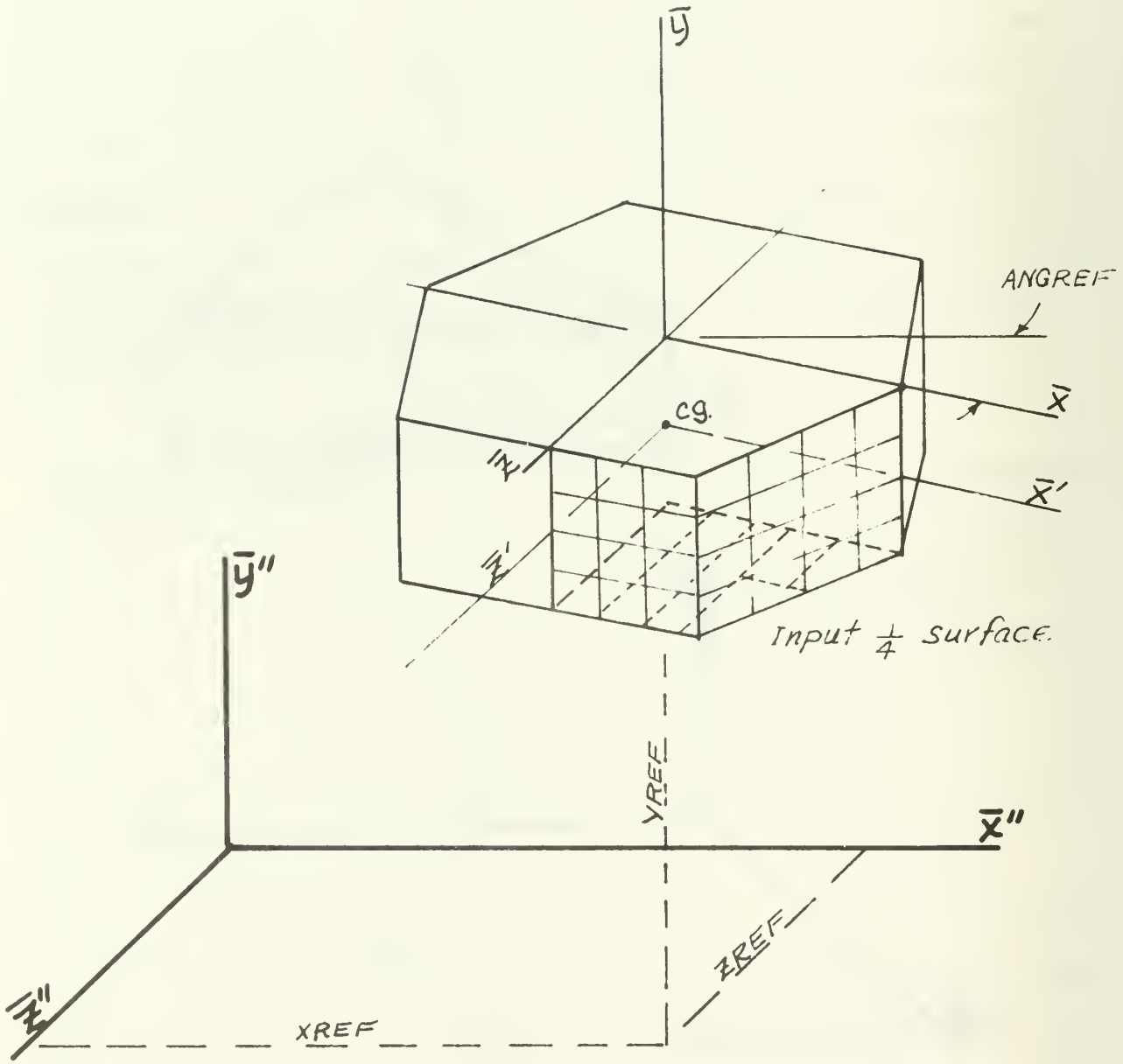

FIGURE 6 DOUBLE SYMMETRY

Although in the above two cases where the body possesses one or two planes of symmetry the input axis was defined such that XREF, YREF, ZREF, and ANGREF were non-zero, the usual case would be to input the data with input coordinate axes aligned with the body and inertial axes. This is generally convenient. However, it is not usually convenient to place the origin of the input axes at either the mean water level or center of gravity. It is generally more convenient to set the origin at the level of the bottom if the hull has a flat bottom so that YREF is normally non-zero.

Input Format

The inputs to the computer program are of three types: (1) specifying certain constants, (2) specifying the dimensions of the arrays, and (3) specifying the geometry of the immersed surface. These inputs and their format are discussed in the following:

Input Constants:

The constants which are input by way of DATA statement cards are defined in terms of both the metric and English system in the following. It is noted, however, that either one system or the other may be selected but no mixing of systems is allowable.

PER.....Wave period and period of the motion of the body(sec.)

H.....Mean water depth (ft. or meters)

ABAR.....Reference dimension of the hull. Any value will do but normally the radius of the hull or the half-length is used (ft. or meters).

RHO.....Density of the water (slugs/ft^3 or kg/m^3).

G.....Acceleration of gravity (32.174 ft/sec^2 or 9.8m/sec^2).

XREF.....x" coordinate of the origin of the body axes (measured in the input axes)(ft. or meters). (See Figure 4).

YREF.....y" coordinate of the origin of the body axes (measured in the input axes)(ft or meters) (See Figure 4).

ZREF.....z" coordinate of the origin of the body axes (measured in the input axes)(ft or meters) (See Figure 4).

ANGREF...Clockwise rotation angle of the body axes (as viewed from above)(Degrees) See Figure 4.

ECG.....Elevation of the center of gravity of the body (y) measured in the inertial axes located with x-z plane on the mean waterline.

ARMIN....Two different forms of the Green's function have been defined, an integral form as given by Equation (3.3) and a series form given by Equation (3.4). The series form requires much less CPU time to evaluate but the modified Bessel function of the second kind $K_0(ar)$ becomes infinite as $(ar)\to 0$. Thus, when (ar) is less than or equal to the value of ARMIN the integral form of the Green's function is used. The parameter (ar) is given by $ar = (2\pi\bar{a}/\bar{L})(\bar{r}/\bar{a})$ where $\bar{L}$ = wave length, $\bar{a}$ = ABAR = characteristic length scale of the hull and $\bar{r}$ denotes the horizontal distance between node points. A value of ARMIN = 0.01 is a reasonable choice. As ARMIN is increased the CPU time increases rapidly.

RMIN.....The value of RMIN is used for two different tests of the distance between panels i and j in computing the values of α_{ij} and β_{ij}. The use of RMIN as well as ARMIN is best demonstrated by the following flow chart:

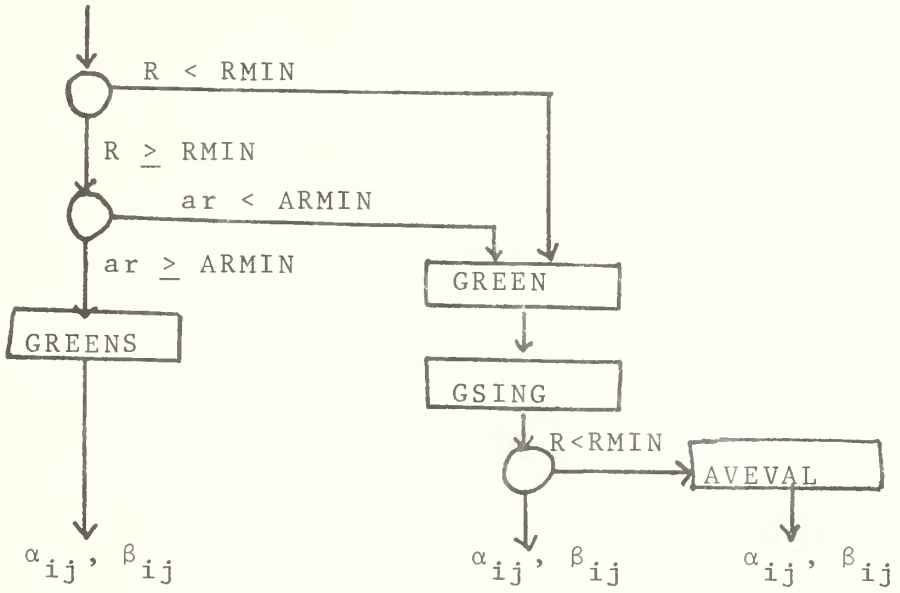

The value of RMIN is used to test R for purposes of selecting GREEN or GREENS. In subroutine GSING it is used to determine whether or not AVEVAL will be called to integrate the 1/R and derivative of 1/R in the integral form of the Green's function.

The value of RMIN should be kept as small as possible consistent with adequate accuracy. Figure B1 in Appendix B indicates that RMIN $\geq 2\sqrt{\Delta S}$ (where ΔS represents the area of a typical panel) represents a reasonable value fo RMIN. (ft or meters).

NC.....Integer denoting the number of panel corner points on the portion of the hull which is input. This integer represents the actual number of data cards read by CONFIG which describe the location of the corner nodes on the hull.

NB.....Integer denoting the <u>total</u> number of panels on the <u>complete</u> hull. The panels are assigned indices running 1 through NB. Figure 7 shows the numbering system when the hull has either single or double symmetry.

NBA.....Integer having the value of either 1 or 2. If NBA = 1 the velocity components at the node points on the hull are <u>not</u> computed and direct access files #11, 12 and 13 are not used. If NBA = 2 the velocity components on the immersed surface are computed. It should be noted that the velocities are not actually used in the calculations of the pressures, excitation forces and moments, added mass and damping coefficients or the resulting dynamic response.

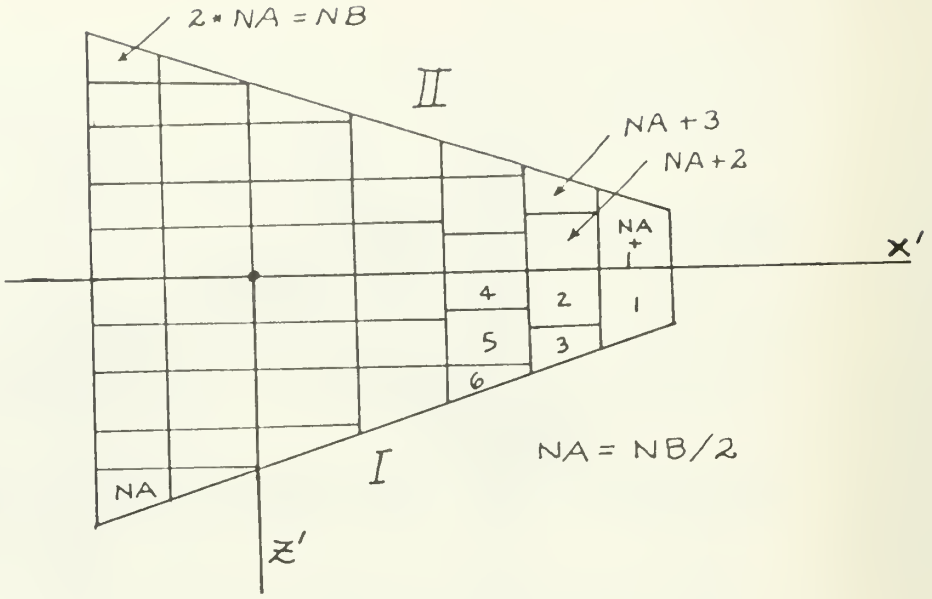

SINGLE SYMMETRY

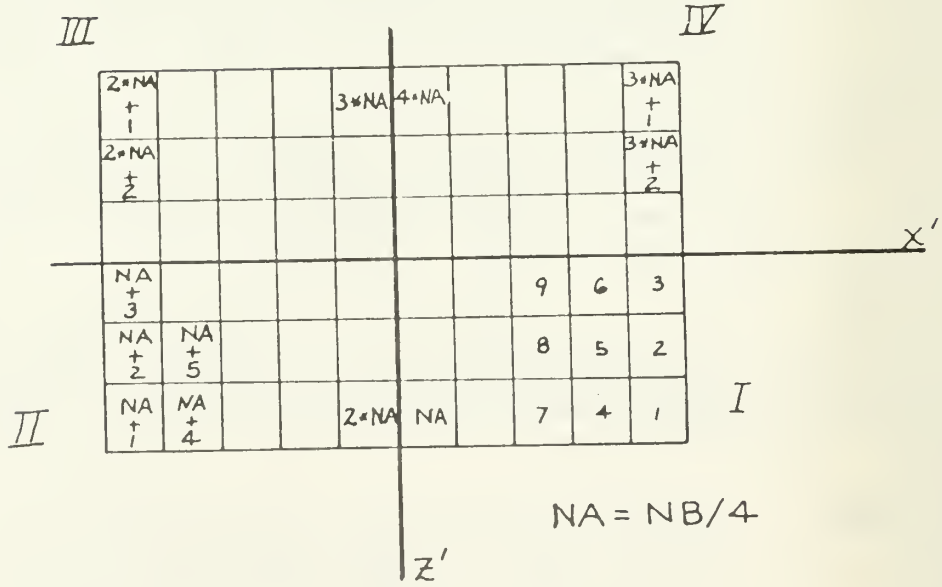

DOUBLE SYMMETRY

FIGURE 7 NUMBERING SYSTEM FOR THE CASE OF SINGLE AND DOUBLE SYMMETRY

NA.....Number of panels defined by the NC corner nodes on: (a) the complete hull for the no symmetry case, (b) half of the hull when the hull has one plane of symmetry, (c) one quarter of the hull when the hull has two planes of symmetry. In the case of (a), (b) and (c) NA will have the values NB, NB/2 and NB/4, respectively.

NEQ.....The $(\alpha-I)$ matrix as indicated in Eq. (5.2) is a square matrix of size NB x NB in all cases except when NSS = 2, in which case it is NB/2 x NB/2.

In all cases, however, the matrix is placed on direct access FILE #14 and is brought into core one piece at a time. The size of the block that is brought in is always NEQ (number of equations) by NB. Thus, it is most efficient to make NEQ as large as possible. However, the block size is limited (about 7200 bytes on an IBM 360) so NEQ may have to be small when NB is large so that the block size remains within the limits for the direct access device used.

In general, NEQ may have any value equal to or greater than unity. The general rule is to make NEQ as large as possible consistent with the maximum block size allowable.

NWAVES...Integer denoting the number of wave directions which will be considered in the run. There must be NWAVES data cards giving the incidence angle (in degrees) of the particular cases to be calculated.

NSS.....Integer having either the value of 1 or 2. The normal value for NSS is 1 but under the special case where the wave direction is aligned with the x'-y' plane (0 or 180 degrees) and this plane represents a plane of symmetry, then NSS may be set to 2. The program will then take advantage of the fact that the source strength function on the positive z'-half of the hull is the same as at the corresponding points on the negative z'-half. Accordingly, the $(\alpha-I)$ matrix will be only (NB/2) x (NB/2) rather than NB x NB and, therefore, a savings in CPU time will be realized during inversion.

NS.....Integer which is normally set to 1. However, under the special case where NSS is set to 2 the $(\alpha-I)$ matrix may be small enough to store in core. If this is the case, NS may be set equal to the integer NB/2. The $(\alpha-I)$ matrix will then be stored in

the ALS matrix and inverted through subroutine COMAT. It is always less time consuming to take the NS = NB/2 option when possible provided the storage requirements do not exceed that available since the in-core inversion is faster than the out-of-core inversion.

Direct Access Files:

The DEFINE FILE statements in the MAIN program specify the block size and number of records on the direct access files #10-14 as follows:

```
DEFINE FILE 10 (a,b,U,LK)
DEFINE FILE 11 (a,b,U,LK)
DEFINE FILE 12 (a,b,U,LK)
DEFINE FILE 13 (a,b,U,LK)
DEFINE FILE 14 (c,d,U,LK)
```

where, for example, in #10, a = number of records and b = number of words in the record. The values of a and b must be input for a given set of data and conditions as follows:

Number of records -

a = NA

c = NB/NEQ (rounded upwards to the nearest integer)

Block size - (in number of words)

b = 2xNB

d = 2xNEQxNB

The factor of 2 accounts for the fact that the words are complex.

For the special case when NSS = 2 :

c = (NB/2)/NEQ (rounded upwards to the nearest integer)

In addition to the DEFINE FILE statements it is necessary to specify adequate and consistent disk space on JCL input.

For efficient operation it is important that the five files #10-14 be placed on separate units when all are being used because these five files are written upon simultaneously in the same DO LOOP.

When NBA = 1 files #11, 12 and 13 are not used. In this special case it is possible to set the file space required for #11-13 to some nominal value.

Summary of Program Options

In view of the fact that the program has several options depending on the incidence angle and symmetry of the immersed surface, these are summarized in the following. The various options are completely independent of the values of NBA and NEQ.

I. Hull has no planes of symmetry:

NA = NB

NS = 1

NSS = 1

The (α-I) matrix stored on file #14 will be NBxNB. The matrix will be inverted by use of an elimination scheme through subroutine OCINV. This option represents the most CPU time consuming method and would be used only if the hull had no planes of symmetry with respect to the body axes. The wave incidence angle may be arbitrary.

II. Hull has either one or two planes of symmetry:

NA = NB/2 (input data for +z' half of the immersed surface when hull has one plane of symmetry.)

NA = NB/4 (input data for +x' and +z' quarter of the hull when the hull has two planes of symmetry).

(a) NS = 1

NSS = 1

The program will take advantage of the symmetry in computing the matrices but the (α-I) matrix will be NB x NB and will be inverted in OCINV. The wave incidence angle may be arbitrary.

(b) NS = 1

NSS = 2

The program will take advantage of the symmetry in computing the large matrices. The incidence angle must be set to either 0 or 180 degrees so that the wave is aligned with the x'-y' plane. The assumption is made that for this case the source strength on the -z' -half of the hull is the same as on the +z' -half. Accordingly, the matrix stored on FILE #14 will be NB/2 x NB/2 and will be inverted out of core by OCINV2.

(c) NS = NB/2

NSS = 2

The (α-I) matrix stored on FILE #14 will be of size NB/2 x NB/2. This matrix is eventually placed in core in the array ALS(NS,NS) which for this option has been dimensioned NS x NS, i.e., the size of the (α-I) matrix. The fact that NS is other than unity signals the computer to solve Eq. (5.2) in core by use of the subroutine COMAT. For this option

(NSS = 2) the incidence angle, ψ , must be 0 and/or 180 degrees so that the wave direction is aligned with the plane of symmetry.

Dimensioning

The general principle to be followed in the dimension statements in the MAIN program is to make the dimensions exactly equal to the size of the array. In the case of two-dimensional arrays it is absolutely necessary that they be dimensioned exactly correctly. The dimensions cannot be either larger or smaller than the actual array. Even in the case of several of the one-dimensional arrays this is essential and, therefore, as a general principle the arrays should always be dimensioned to exactly the size of the array as given in the following with the exception of SH, CH, SINAMU and COSAMU arrays.

The MAIN program contains all of the dimension statements which must be altered. It is unnecessary to make any changes in the subroutines because all arrays are variable dimensioned. The arrays in the MAIN program have the following dimensions:

ALPHA (NEQ,NB)

ALS (NS, NS)

AV(NB), BV(NB), CV(NB), DV(NB), EV(NB)

F(NB,7), HH(NB,7), U(NB,7)

XB(NA), YB(NA), ZB(NA), XNB(NA), YNB(NA), ZNB(NA), DSB(NA)

XC(NC), YC(NC), ZC(NC)

XP(NC), YP(NC), ZP(NC)

NODM(NA,4)

ICOM(NS,3)

SH(a), CH(a), SINAMU(b), COSAMU(b), where

a $\geq$ number of different levels of node points on the immersed surface. That is, "a" should be greater than the largest number printed under the column labeled LEVEL NO. on the output. A value of, say 20, would cover essentially all conceivable cases.

b $\geq$ 50 x a (for example, b = 1000 if a = 20)

(Note: In the case of SH, CH, SINAMU and COSAMU the dimensions may be greater than or equal to the actual array size).

Input Data Cards

Mass Matrix:

The first set of data cards are used to input the mass matrix. There are six cards in this set; each card contains six numbers. The format for each card is 6F10.1 and the units are slugs and slug-ft^2 when the English system is used or kg and kg-m^2 when metric units are used.

The first card contains the values of $\bar{m}_{11}$, $\bar{m}_{12}$, $\bar{m}_{13}$, $\bar{m}_{14}$, $\bar{m}_{15}$ and $\bar{m}_{16}$ the second card contains values of $\bar{m}_{21}$ $\bar{m}_{22}$, $\bar{m}_{23}$, $\bar{m}_{24}$, $\bar{m}_{25}$, $\bar{m}_{26}$, etc. where

$\bar{m}_{11} = \bar{m}_{22} = \bar{m}_{33} = \bar{m}$ = mass of the structure (slugs or kg)

$\bar{m}_{12} = \bar{m}_{21} = \bar{m}_{13} = \bar{m}_{31} = \bar{m}_{23} = \bar{m}_{32} = 0$

$\bar{m}_{44} = I_{\bar{x}',\bar{x}'}$ = moment of inertia about the x' axis (slugs-ft^2 or kg - m^2)

$\bar{m}_{55} = I_{\bar{y}',\bar{y}'}$ = moment of inertia about the y' axis (slugs-ft^2 or kg-m^2)

$\bar{m}_{66} = I_{\bar{z}',\bar{z}'}$ = moment of intertia about the z' axis (slugs - ft^2 or kg - m^2)

(Note, the x', y' and z' axes are centroidal axes by definition)

$\bar{m}_{45} = \bar{m}_{54} = -I_{\bar{x}',\bar{y}'}$ = negative product of inertia (slugs - ft^2 or kg = m^2)

$\bar{m}_{46} = \bar{m}_{64} = -I_{\bar{x}',\bar{z}'}$ = negative product of inertia (slugs - ft^2 or kg - m^2)

$\bar{m}_{56} = \bar{m}_{65} = -I_{\bar{y}',\bar{z}'}$ = negative product of inertia (slugs - ft^2 or kg - m^2)

Spring Constant Matrix:

The second set of data cards are used to describe the elastic constraints of the body due to mooring lines. In the most general case, for displacement in each of the six degrees of freedom a force (i = 1,2,3) and moments (i = 4,5,6) can occur. Thus, in general, there can be 36 elastic coefficients to describe the effect of the mooring lines.

The definition of the elements of the spring constant matrix is as follows:

$$\bar{K}'_{ij} = -\frac{\partial F'_i}{\partial \bar{X}_j}$$

where

F_i' = { Force in the i-direction (i=1,2,3)(lb or N); Moment about i-axis (i=4,5,6)(ft-lb or N-m) }

$\bar{X}_j$ = { Linear displacement in the j-direction(j=1,2,3) (ft or meters); Angular displacement about j-axis (j-4,5,6) (radians) }

Example:

The case of a simple spring restraint is indicated in the following sketch:

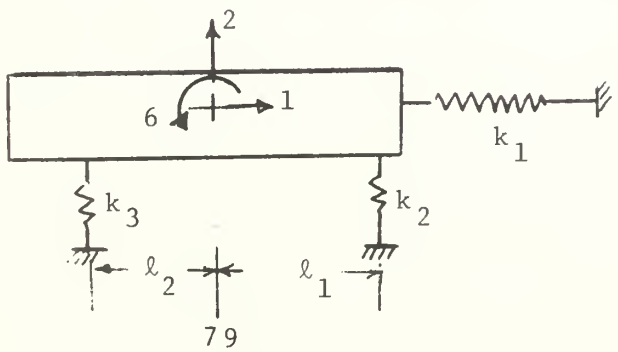

It is possible to derive expressions for the values of $\bar{K}'_{ij}$ by starting with the expressions for the two components of force and moment:

$$F'_1 = -k_1(\bar{X}_1 - \bar{X}_{1_o})$$

$$F'_2 = -k_2(\bar{X}_2 - \bar{X}_{2_o} + \ell_1\bar{X}_6)$$

$$-k_3(\bar{X}_2 - \bar{X}_{2_o} - \ell_2 X_6)$$

$$F'_6 = -k_2\ell_1(\bar{X}_2 - \bar{X}_{2_o} + \ell_1\bar{X}_6)$$

$$+ k_3\,\ell_2(\bar{X}_2 - \bar{X}_{2_o} - \ell_2\bar{X}_6)$$

where the subscript "o" denotes the equilibrium position of the body. By differentiation, the spring constant coefficients $\bar{K}'_{ij}$ are defined as:

$$\bar{K}'_{11} = k_1$$

$$\bar{K}'_{22} = k_2 + k_3$$

$$\bar{K}'_{66} = k_2\ell_1^2 + k_3\,\ell_2^2$$

$$\bar{K}'_{61} = \bar{K}_{16}' = 0$$

$$\bar{K}'_{12} = \bar{K}'_{21} = 0$$

$$\bar{K}'_{26} = \bar{K}'_{62} = k_2\ell_1 - k_3\ell_2$$

where k_1, k_2, and k_3 denote the spring constants of the three springs defined in the usual manner in terms of force/displacement.

Hull Geometry:

The next set of data cards to be read are the ones which describe the immersed surface of the hull. This set of cards gives the coordinates of the four corners of the panels and there will be NC of these cards. When there is no symmetry in the immersed surface, the complete hull must be described; when the hull has a single plane of symmetry (x'-y' plane), then half the surface must be described, and when the immersed surface has two planes of symmetry, one quarter of the hull must be described. When inputing half the immersed surface, the x'-y' plane must represent the plane of symmetry and when inputing one quarter of the hull, the x'-y' plane and y'-z' planes must represent planes of symmetry. In the case of single symmetry the +z' part of the immersed surface is input, and in the case of double symmetry the +x' and +z' quadrant is input.

An example of a subdivided surface with two planes of symmetry is shown in Figure 8. On the quarter of the hull to be described there are 60 corner node points denoted and, therefore, for this example, NC = 60. It should be noted that all panels must have four sides; however, the length of the sides and orientation may be arbitrary, i.e., the panels need not be rectangular or square.

The coordinates of the NC (60 in the example) panel corner points must be input by use of NC data cards punched in the following format:

Cols: 1-10: The corner node index (1-60 in the example) (Integer, right adjusted).

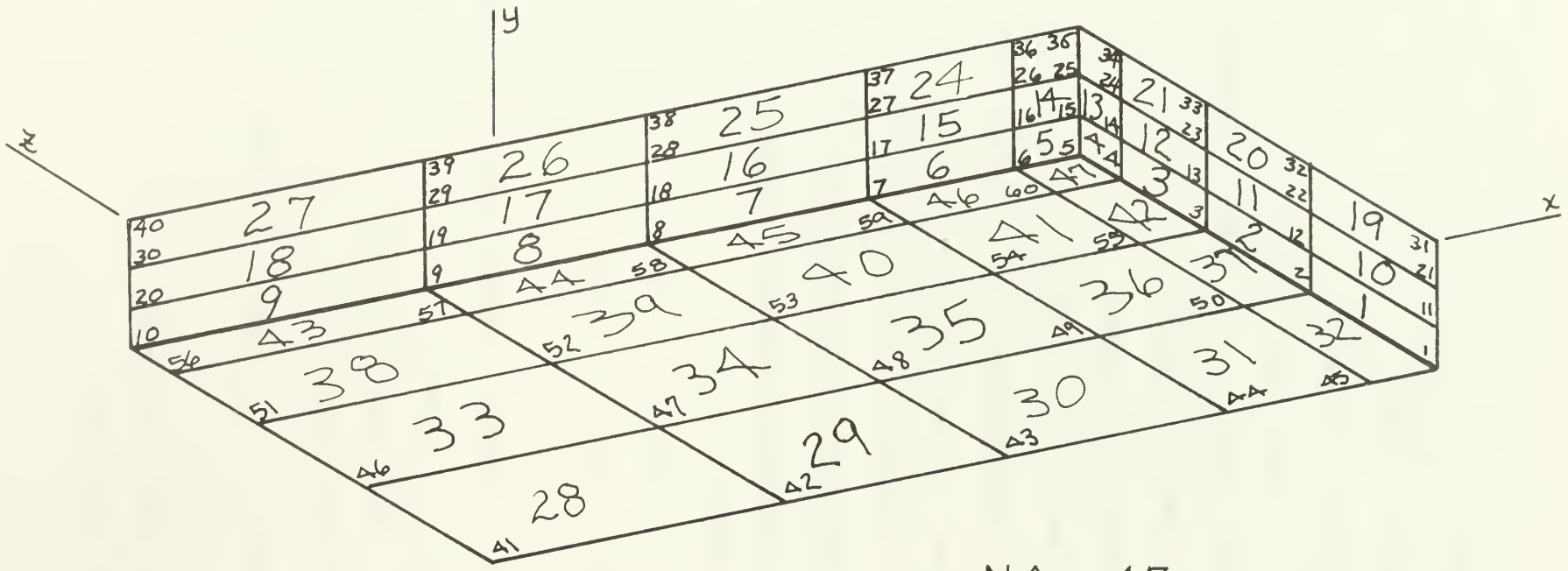

FIGURE 8 EXAMPLE BARGE CONFIGURATION

Cols: 11-20: x" coordinate of the node (ft or m).

Cols: 21-30: y" coordinate of the node (ft or m).

Cols: 31-40: z" coordinate of the node (ft or m).

Correspondence Table:

The next set of data cards will define the sequence of four corner nodes which make up a given panel. There are five integers on each of these data cards, the first represents the panel index and the next four integers correspond to the four corners of the given panel.

There will be NA of these data cards where NA denotes the number of panels on the portion of the immersed surface described by data cards. NA will have the value:

NA = NB (no symmetry)

NA = NB/2 (single symmetry)

NA = NB/4 (double symmetry)

where NB denotes the total number of panels on the complete immersed surface. In the example described in Figure 8:

NC = 60

NB = 188

NA = 47

In this case the hull has double symmetry so NA = NB/4 = 188/4 = 47.

Each of the NA cards will specify which of the four points compose a given panel and are punched according to the following format (all right adjusted integers):

Cols: 1-10: Panel number (1 through 47 in the example)

Cols: 11-20: First corner node index

Cols: 21-30: Second corner node index

Cols: 31-40: Third corner node index

Cols: 41-50: Fourth corner node index

The four corner nodes are specified in sequence as encountered in "walking" around the panel on the water side in such a way that the interior of the panel area remains on the right hand side. Another equivalent way of stating this is to number in sequence moving around the panel clockwise as viewed from the water side of the hull surface. The starting corner point is arbitrary.

Wave Incidence Angle Data Cards:

The final set of data cards are those specifying the different wave directions to be considered in the run. Since the $(\alpha\text{-}I)$ matrix needs to be constructed and inverted only once, it requires little additional CPU time to consider several values of incidence angle in addition to the initial one. It should be remembered, however, that when NSS = 2 the wave must be aligned with the x' axis so the incidence angle can only be 0 and/or 180 degrees only.

The format for the cards are:

Cols: 1-10: Incidence angle, ψ , in degrees.

Computer Print-Out

The computer print-out contains some of the input data as well as the computed results.

The coordinates of the corner nodes are printed as read-in except that they are shifted to the inertial axes (x,y,z) with origin at the mean water level on a vertical passing through the c.g. of the body. The units are the same as input.

The correspondence table is also printed as read in for purposes of double checking.

The centroids (node points) on the panels are computed as well as the components of the unit normal vectors and areas of the NA panels input. These results are printed under the heading, "COORDINATES OF CENTROIDS OF PANELS, COMPONENTS OF N AND PANEL AREAS."

The displacement of the immersed surface is computed by three different methods:

$$\forall = \iint_S x n_x \, dS$$

$$\forall = \iint_S y \, n_y \, dS$$

$$\forall = \iint_S z \, n_z \, dS$$

The results for the volume computed in the three different manners represents a good quick check on the accuracy of the input data. If the input data is correct, the three results should be the same.

In a similar fashion the total surface area as well as the area projected in both the x and z directions are computed as a quick check on the input data.

Next the program goes through the NA panel node points and assigns an index to each different elevation. All of the node points at elevation -10.0, for example, may be assigned the index

1 and all at -5.0 would be assigned 2, etc. The panel node point index and its corresponding "level number" is, therefore, printed. Caution: largest number printed under "LEVEL NO." should not exceed the dimension of the arrays SH and CH. The maximum value would typically be 3 to 10. A dimension of 20 to 30 should include all cases.

The "WAVE NUMBER" is next printed. This is simply an index which indicates that a new wave direction is being considered. The number printed here will range from 1 through "NWAVES."

The next block of information in the print-out is the following:

$a = 2\pi\bar{a}/\bar{L}$ = 2π. hull radius/wave length.

$\nu = (2\pi/T)^2\bar{a}/g$

$\bar{h}$ = water depth (ft or m)

T = wave period (sec)

ψ = wave incidence angle (degrees) See Figure 1

NB = total number of panels on total hull surface.

The next block of data printed represents the pressure distribution associated with the motion of the body in its six degrees of freedom: surge (1), heave (2), sway (3), roll (4), yaw (5), and pitch (6). The subscript (7) denotes wave interaction with the fixed body.

For each mode (six degrees of freedom 1-6 and 7 wave interaction with the fixed hull) the dimensionless pressure amplitude coefficient P1, P2, etc. and pressure phase angle PH1, PH2, etc.

are printed. The definition of the dimensionless amplitude and phase angles are given on the print-out and will be given here also for completeness:

P1 = pressure (half) amplitude in height of water column/(half) amplitude of the motion in surge.

P2 = pressure (half) amplitude in height of water column/(half) amplitude of the motion in heave.

P3 = pressure (half) amplitude in height of water column/(half) amplitude of the motion in sway.

P4 = pressure (half) amplitude in height of water column/(half) amplitude of the motion in roll times ABAR.

P5 = pressure (half) amplitude in height of water column/(half) amplitude of the motion in yaw times ABAR.

P6 = pressure (half) amplitude in height of water column/(half) amplitude of the motion in pitch times ABAR.

These definitions are the same as stated in Eqs. (2.20).

The actual pressures at any given node point could be expressed as:

$$P_1 = P1\ \rho g X_1^o\ \bar{a} \cos (PH1 - \sigma t)$$

$$P_2 = P2\ \rho g X_2^o\ \bar{a} \cos (PH2 - \sigma t)$$

$$P_3 = P3\ \rho g X_3^o\ \bar{a} \cos (PH3 - \sigma t)$$

$$P_4 = P4\ \rho g X_4^o\ \bar{a} \cos (PH4 - \sigma t)$$

$$P_5 = P5\ \rho g X_5^o\ \bar{a} \cos (PH5 - \sigma t)$$

$$P_6 = P6\ \rho g X_6^o\ \bar{a} \cos (PH6 - \sigma t)$$

$$P_7 = P7\ \rho g\ (\bar{H}/2) \cos (PH7 - \sigma t)$$

where X_i^o denote the dimensionless half amplitudes of the motion as defined in Eq. (2.1) where

$$X^o_1 = \bar{X}_1^o/\bar{a}$$
$$X^o_2 = \bar{X}_2^o/\bar{a}$$
$$X^o_3 = \bar{X}_3^o/\bar{a}$$
$$X^o_4 = \Theta_4^o$$
$$X^o_5 = \Theta_5^o$$
$$X^o_6 = \Theta_6^o$$

Since the motion of the body is defined by

$$X_i(t) = X^o_i \cos(\delta_i - \sigma t)$$

it is clear the positive phase angles represent a lag of the pressure with respect to the displacement in any given degree of freedom.

The next block of output represents the three components of fluid velocity (in body axes) associated with motion in the six degrees of freedom (1-6), and wave interaction with the fixed hull, (7), corresponding to each node on the complete immersed surface. (Note: if NBA = 1 this information is not computed and the output is suppressed).

The velocity component dimensionless amplitudes are defined, for example, as

VX = velocity (half) amplitude in the x'-direction/
velocity (half) amplitude of the body.

The phase angles are defined with respect to the displacement of the body (positive lag). The x'-component of velocity could be expressed, for example, as

surge (1) $V_x = VX\ X^o_1\ \bar{a}\sigma\ \cos(PX1 - \sigma t)$

heave (2) $V_x = VX\ X^o_2\ \bar{a}\sigma\ \cos(PX2 - \sigma t)$

etc.

The MASS MATRIX is next printed exactly as read-in through data cards. The units are slugs and slugs-ft^2, or kg and kg-m^2.

The SPRING CONSTANT MATRIX is printed next also as it was read in through the six data cards. Note that for a free-floating body all of the values in this array are zero.

The next set of data represents the dimensionless wave load coefficients. The x,y,z subscripts represent body axes so FX, for example, represents the dimensionless excitation force in the x' direction. The definition of the coefficients and phase angles are given on the print-out. The actual wave force and moments can be expressed as a function of time as:

$$F_x = FX\ \rho g \bar{a}^3\ (\bar{H}/2\bar{a}) \cos(\text{PHASE FX} - \sigma t)$$

$$F_y = FY\ \rho g a^3 (\bar{H}/2\bar{a}) \cos(\text{PHASE FY} - \sigma t)$$

$$F_z = FZ\ \rho g a^3 (\bar{H}/2\bar{a}) \cos(\text{PHASE FZ} - \sigma t)$$

$$M_x = MX\ \rho g \bar{a}^4 (\bar{H}/2\bar{a}) \cos(\text{PHASE MX} - \sigma t)$$

$$M_y = MY\ \rho g \bar{a}^4 (\bar{H}/2\bar{a}) \cos(\text{PHASE MY} - \sigma t)$$

$$M_z = MZ\ \rho g a^4 (\bar{H}/2\bar{a}) \cos(\text{PHASE MZ} - \sigma t)$$

Note: the wave crest passes the origin of the coordinate system at t = 0. Thus, a positive phase angle represents a lag with respect to the time the wave crest passes the origin.

The HYDRODYNAMIC ADDED MASS COEFFICIENT MATRIX is next printed followed by the HYDRODYNAMIC DAMPING COEFFICIENT MATRIX.

These parameters are defined through Eqs. (4.9 - 4.13). However, to emphasize their relationship to the velocity and acceleration their definitions will be given here again.

The force (or moment) in the i-direction (in body axes) due to motion in the j-direction is defined as F_{ij} and is given in terms of the added mass and damping coefficients, M_{ij} and N_{ij}, as

$$F_{ij} = -(1.0 \text{ or } \bar{a}) \{\rho \bar{a}^4 M_{ij} \ddot{X}_j + \rho \sigma \bar{a}^4 N_{ij} \dot{X}_j\}$$

where 1.0 is used when F_{ij} represents a force (i = 1,2,3) and $\bar{a}$ is used when F_{ij} denotes a moment (i = 4,5,6). In the above expression

$\ddot{X}_j$ = acceleration in j-direction (Note, $X_j = \bar{X}_j/\bar{a}$ for j = 1,2,3 and $X_j = \theta_j$ for j = 4,5,6).

$\dot{X}_j$ = velocity in j-direction

The next block of output is labeled HASKINDS RELATIONS. Here the excitation forces, moments, phase angles are computed by use of:

(1) the near field pressure distribution

(2) the far field (radiation) potential by use of Haskind's relations

and the damping coefficients are computed by

(1) the near field pressure distribution

(2) the energy radiated at infinity.

The results computed by (1) and (2) are then compared and a percent difference computed.

The use of the Haskind's relations and energy balance represents a self-check on the accuracy of the results computed

by the pressure distribution. The results computed by use of the pressure distribution should be more accurate than those computed from the far field behavior of the potential but the two results should be fairly close. Large percentage differences indicate that there may be some problem and the solution may not be valid. However, if the values of the parameters being compared are very small, large percentage differences should be expected and should cause no significant error in the final results.

Finally the DYNAMIC RESPONSE results are printed. The response amplitude and phase angle in the six degrees of freedom are printed. The amplitudes are defined as:

Surge: Half amplitude of the surge motion/wave (half) amplitude

Heave: Half amplitude of the heave motion/wave (half) amplitude

Sway: Half amplitude of the sway motion/wave (half) amplitude

Roll: Half amplitude of the roll motion in radians x ABAR/wave (half) amplitude.

Yaw: Half amplitude of the yaw motion in radians x ABAR/wave (half) amplitude.

Pitch: Half amplitude of the pitch motion in radians x ABAR/wave (half) amplitude.

The phase angles of the dynamic response are defined with respect to the crest of the incident wave in radians. The crest of the incident wave passes the origin at t=0 so a positive phase angle indicates that the displacement of the body lags the crest.

9. EXAMPLE COMPUTATIONS

In this chapter a simple example calculation is carried out for a rectuangular barge (box) which is 90 x 90 meters in plan with a draft of 40 meters. Results are computed for a series of different wave periods.

Hull Corner Node Points

In Figure 9 is shown the subdivision of the hull; since the immersed surface possesses double symmetry it is necessary to describe only one quarter of it by use of data cards.

The subdivision indicated in Figure 9 is rather coarse. There are 12 panels on the quarter-body and 48 panels all together on the total immersed surface. The quarter-body is described by use of the 19 corner node points so,

NC = 19

NA = 12

NB = 48

for the immersed surface described in Figure 9.

The immersed surface was input with an input coordinate system placed relative to the body as indicated in Figure 9 with the bottom represented by the y" = 0 plane. Since the draft was 40.0 m the inertial coordinate system was placed with origin at the position x" = z" = 0 and y" = 40.0. This is input to the computer program by use of a data statement specifying the parameters as follows:

```
XREF = 0.0
YREF = 40.0
ZREF = 0.0
ANGREF = 0.0
```

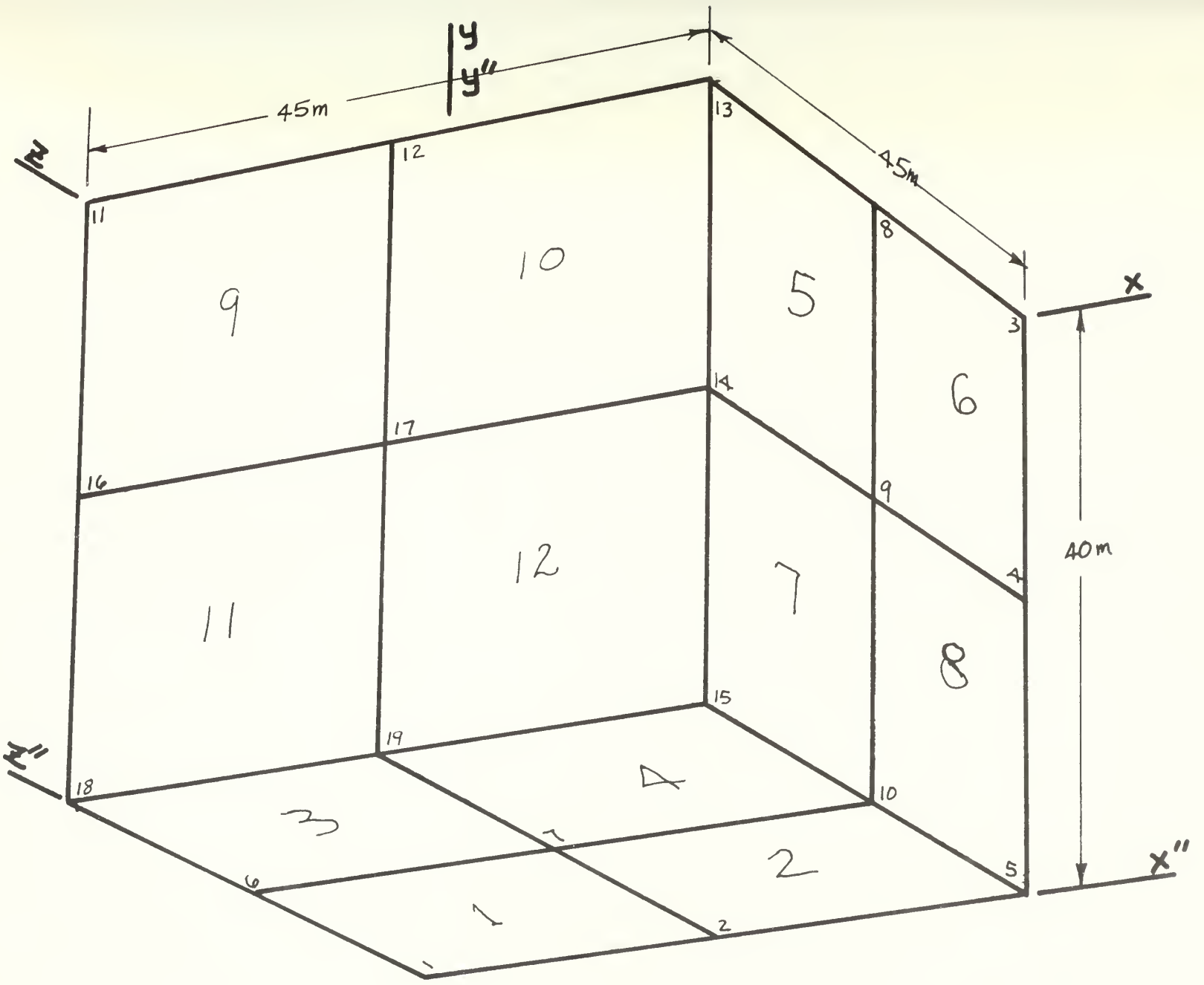

NC = 19

NA = 12

NB = 48

FIGURE 9 FLOATING BARGE 90m x 90m x 40m

The computer "echo check" on the input data is shown in Table 2. The location of the inertial reference frame in the input reference frame is first printed in the table. The rotation angle is zero.

TABLE 2

ROTATION ANGLE= 0.0

XREF= 0.0

YREF= 40.0000

ZREF= 0.0

COORDINATES OF PANEL CORNERS

CORNER NO.	X	Y	Z
1	0.0	-40.000	0.0
2	22.500	-40.000	0.0
3	45.000	0.0	0.0
4	45.000	-20.000	0.0
5	45.000	-40.000	0.0
6	0.000	-40.000	22.500
7	22.500	-40.000	22.500
8	45.000	0.0	22.500
9	45.000	-20.000	22.500
10	45.000	-40.000	22.500
11	0.000	0.0	45.000
12	22.500	0.0	45.000
13	45.000	0.0	45.000
14	45.000	-20.000	45.000
15	45.000	-40.000	45.000
16	0.000	-20.000	45.000
17	22.500	-20.000	45.000
18	0.000	-40.000	45.000
19	22.500	-40.000	45.000

CORRESPONDENCE TABLE

PANEL NO.	NODE 1	NODE 2	NODE 3	NODE 4
1	1	6	7	2
2	2	7	10	5
3	7	6	18	19
4	10	7	19	15
5	8	9	14	13
6	3	4	9	8
7	9	10	15	14
8	4	5	10	9
9	11	12	17	16
10	12	13	14	17
11	16	17	19	18
12	17	14	15	19

The coordinates of the corners of the panels are printed under the heading: COORDINATE OF PANEL CORNERS. A comparison of the numbers listed here can be seen to agree with the location of the corners (in the inertial reference frame) shown in Figure 9.

Next, under the heading CORRESPONDENCE TABLE can be found the information which describes the given panels (numbered 1-12) in terms of the corner node point indices. Under NODE 1, NODE 2, etc. are listed the four corner node points which go to make up a given panel listed in clockwise order when observing from the "water side" of the panel. A comparison of these results with Figure 9 will confirm this.

Table 3 gives the computer print-out of the location of the panel node points, the components of the outward unit normal vectors at the immersed surface (in body axes) and the areas of the panels. The node points are calculated by the computer, as described in Appendix A, and represent the centroids of the panels.

In Table 4 is printed the volume and surface area of the immersed surface as computed on the basis of the information given in Table 3. The volume is computed by three different methods, i.e., by

$$\forall_{(x\text{-proj})} = \sum_{i=1}^{n} \bar{x}_i \, n_{x_i} \, \Delta S_i$$

$$\forall_{(y\text{-proj})} = \sum_{i=1}^{n} \bar{y}_i \, n_{y_i} \, \Delta S_i$$

$$\forall_{(z\text{-proj})} = \sum_{i=1}^{n} \bar{z}_i \, n_{z_i} \, \Delta S_i$$

The volume calculations in this way use all of the information in Table 3 and if the volumes computed by the different methods are equal to, say, 5 or 6 decimal places, it is quite likely that the input data is correct. This represents a simple quick verification of the input data but cannot replace the Calcomp plot for ease and reliability.

The different indices assigned to the different levels of the panel node points are also given in Table 5. It may be seen by looking over the results printed in Table 3 that the node points fall at only three different levels: -10.0, -30.0 and 40.0. As indicated in Table 5, and as can be verified by Figure 9, panel nodes 1-4 are on the bottom and are located at the -40.0 level (LEVEL NO 1), panel nodes 5,6,9,10 are located at the -10.0 level (LEVEL NO 2), and panel nodes 7,8,11,12 are at the -30.0 level (LEVEL NO 3).

The next block of computer print-out gives the WAVE NUMBER and lists the parameters, $a = 2\pi\bar{a}/\bar{L}$, $\nu = a \tanh(ah)$, where $h = \bar{h}/\bar{a}$, water depth, wave period, angle of incidence and the value of NB.

Following this information, the computer print-out contains the pressure distribution and velocity distribution as previously described. After this an "echo check" on the MASS MATRIX and SPRING CONSTANT MATRIX is printed in the same units as input by way of the data cards. This information appears to be straightforward and will not be given here.

TABLE 3

COORDINATES OF CENTROIDS OF PANELS, COMPONENTS OF N AND PANEL AREAS

X	Y	Z	NX	NY	NZ	DS
11.250	-40.000	11.250	0.0	-1.000	0.0	506.249
33.750	-40.000	11.250	0.0	-1.000	0.0	506.249
11.250	-40.000	33.750	0.0	-1.000	0.0	506.249
33.750	-40.000	33.750	0.0	-1.000	0.0	506.249
45.000	-10.000	33.750	1.000	0.0	0.000	450.000
45.000	-10.000	11.250	1.000	0.0	0.000	449.999
45.000	-30.000	33.750	1.000	0.0	0.000	450.000
45.000	-30.000	11.250	1.000	0.0	0.000	449.999
11.250	-10.000	45.000	0.000	0.0	1.000	449.999
33.750	-10.000	45.000	-0.000	0.0	1.000	449.999
11.250	-30.000	45.000	0.000	0.0	1.000	449.999
33.750	-30.000	45.000	-0.000	0.0	1.000	449.999

TABLE 4

VOL.,X-PROJ.=	323999.125
VOL.,Y-PROJ.=	323999.250
VOL.,Z-PROJ.=	323999.063

TOTAL SURFACE AREA=	22499.961
AREA, Y-PROJ.=	-8099.984
AREA, Z-PROJ.=	1799.997

TABLE 5

NODE	LEVEL NO	ELEV
1	1	-40.00
2	1	-40.00
3	1	-40.00
4	1	-40.00
5	2	-10.00
6	2	-10.00
7	3	-30.00
8	3	-30.00
9	2	-10.00
10	2	-10.00
11	3	-30.00
12	3	-30.00

The next block of information on the print-out is the dimensionless excitation force and moment coefficients. For the sample run this is presented in Table 6. It may be noted that the angle of incidence of the wave was zero so naturally Table 6 indicates FZ = MX = MY = 0.0.

Table 7 contains the next three blocks of computer print-out. These three blocks represent the dynamic and hydrostatic force coefficient associated with the motion of the body. In making this example calculation, NSS was set to 1 even though it could have been set to 2 since the body is symmetrical about the x'-y' plane and the angle of incidence was zero. Since NSS = 1 all six degrees of freedom of the body were considered and, accordingly, all of the added mass and damping coefficients were computed. Had NSS been set to 2 only (M_{i1}, M_{i2} and M_{i6}) and (N_{i1}, N_{i2} and N_{i6}) would have been computed. The value of the other coefficients would be meaningless.

It may be noted that the surge and sway added mass and damping coefficients, M_{11} and M_{33}, and N_{11} and N_{33}, are equal. This is, of course, due to the fact that the body is symmetrical in plan view.

It is also interesting to note that the roll, yaw and pitch damping moments, i.e., N_{44}, N_{55} and N_{66}, are quite small. This, in fact, appears to be typical of most cases, and, therefore, must be taken into consideration when interpreting that data. It may be recalled that the computed damping is wave damping only and this tends to be small in the angular modes. In such cases viscous damping may become important and it may be worthwhile to estimate the viscous damping.

TABLE 6

**** WAVE LOAD COEFFICIENTS AND PHASE ANGLES FOR THE CAISSON ****

FX, FY, FZ = AMPLITUDE OF FORCE/RHO*G*ABAR**3(H/2*ABAR)
MX, MY, MZ = AMPLITUDE OF MOMENT/RHO*G*ABAR**4(H/2*ABAR)
PHASE ANGLES = IN RADIANS MEASURED WITH RESPECT TO TIME WAVE CREST IS AT ORIGIN (POSITIVE = LAG)

FX=	2.9564	PHASE FX=	-1.3296
FY=	1.0021	PHASE FY=	-0.4524
FZ=	0.0000	PHASE FZ=	0.5018
MX=	0.0000	PHASE MX=	3.1075
MY=	0.0000	PHASE MY=	2.2377
MZ=	0.0478	PHASE MZ=	-1.2728

TABLE 7

**** HYDRODYNAMIC ADDED MASS COEFFICIENT MATRIX ****

2.7645	-0.0000	-0.0000	-0.0000	-0.0000	0.2076
-0.0000	2.3531	-0.0000	0.0000	0.0000	-0.0000
-0.0000	0.0000	2.7645	-0.2076	0.0000	0.0000
-0.0000	0.0000	-0.2223	0.4534	0.0000	0.0000
-0.0000	0.0000	0.0000	-0.0000	0.6559	-0.0000
0.2224	-0.0000	0.0000	0.0000	-0.0000	0.4534

**** HYDRODYNAMIC DAMPING COEFFICIENT MATRIX ****

1.9416	-0.0000	-0.0000	-0.0000	-0.0000	0.0268
-0.0000	0.4284	0.0000	0.0000	-0.0000	0.0000
-0.0000	0.0000	1.9416	-0.0268	0.0000	0.0000
0.0000	-0.0000	-0.0385	0.0006	0.0000	0.0000
-0.0000	0.0	-0.0000	0.0000	0.0002	0.0000
0.0385	0.0000	-0.0000	0.0000	-0.0000	0.0006

**** BUOYANCY RESTORATION COEFFICIENT MATRIX ****

0.0	0.0	0.0	0.0	0.0	0.0
0.0	4.0000	0.0	0.0000	0.0	0.0
0.0	0.0	0.0	0.0	0.0	0.0
0.0	0.0000	0.0	0.5089	0.0	0.0000
0.0	0.0	0.0	0.0	0.0	0.0
0.0	0.0	0.0	0.0000	0.0	0.5089

TABLE 8

********** HASKINDS RELATIONS **********

	BY PRESS. INTEGRATION		BY HASKINDS REL.		PERCENT DIFF	
FX =	2.9564	FX =	3.1032	4.9638	✓
FY =	1.0021	FY =	1.0609	5.8660	✓
FZ =	0.0000	FZ =	0.0000	6455.8516	
MX =	0.0000	MX =	0.0000	45.6679	
MY =	0.0000	MY =	0.0000	192.0479	
MZ =	0.0478	MZ =	0.0320	33.1688	✓
PFX=	-1.3296	PFX=	-1.3298	0.0202	✓
PFY=	-0.4924	PFY=	-0.4924	0.0045	✓
PFZ=	0.5018	PFZ=	0.4937	1.6092	
PMX=	3.1075	PMX=	3.0717	97.6515	
PMY=	2.2377	PMY=	2.2136	1.0765	
PMZ=	-1.2728	PMZ=	-1.2451	2.1760	✓
N11=	1.9416	N11=	2.0345	4.7875	✓
N22=	0.4284	N22=	0.4532	5.7779	✓
N33=	1.9416	N33=	2.0345	4.7880	✓
N44=	0.0006	N44=	0.0004	29.8528	✓
N55=	0.0002	N55=	0.0001	71.8705	✓
N66=	0.0006	N66=	0.0004	29.8770	✓

The next block of information printed in Table 8 is the Energy and Haskind's relations check on the accuracy of the solution. Here the excitation forces, moments and phase angles as well as the diagonal of the damping matrix is printed. The calculation of these parameters is carried out both through a pressure integration over the immersed surface and using the "far-field" potential through Haskind's relations and the energy balance. The two sets of values and the percent difference between the two results are printed.

It should be kept in mind that in this run FZ = MX = MY = 0 so the percent differences in these cases is meaningless. Generally, even for this very coarse grid the two sets of results agree rather well, at least when the values are not extremely small. For instance, FX and FY differ by only 5 to 6 percent. MZ, however, is rather small and the two results differ by about 33 percent. This is, generally, the case; the moment tends to be rather sensitive to grid size and it requires a finer grid to get accurate moment results.

The values of N_{11}, N_{22} and N_{33} differ by less than 6 percent when computed by the two different methods. However, the damping in pitch, yaw and roll are very small and tend to differ by a sizable amount. The difference is, however, not too important because such small values of the damping coefficient would not affect the response results except at resonance.

The dynamic response of the floating body is given in Table 9. These results indicate that the surge (half-amplitude) is $.5565(\bar{H}/2)$ where $\bar{H}$ denotes the wave height (trough to crest). In this particular run the heave response shows a little dynamic amplification since the dimensionless response is slightly greater than 1.0. The heave half-amplitude is $1.2(\bar{H}/2)$. The pitch half-amplitude is $.0758 \times \bar{H}/(2\bar{a})$, in radians, where $\bar{a}$ = 45.0 m in this example problem.

TABLE 9

DYNAMIC RESPONSE

Surge (X) ** X/ETA =	0.55650	PHASE =	1.51353
Heave (Y) ** Y/ETA =	1.19997	PHASE =	2.22306
Sway (Z) ** Z/ETA =	0.00000	PHASE =	-1.11987
Roll (X) ** X/ETA =	0.00001	PHASE =	-0.71514
Yaw (Y) ** Y/ETA =	0.00000	PHASE =	0.17472
Pitch (Y) ** Y/ETA =	0.04758	PHASE =	-1.61674

10. NUMERICAL RESULTS

The purpose of this chapter is to present some typical numerical results for several simple geometric configurations and to make comparisons with experimental results. It appears that very little experimental data is in fact available for comparison with the computed results but in cases where data is available comparisons are made. In addition, a comparison of the effect of subdivision size on typical results are presented.

Numerical Results for a 90m x 90m x 40 m Free-Floating Box:

Computer calculations have been carried out for the case of the floating box, 90 meters by 90 meters in plan by 40 meters draft, which was discussed in Chapter 10. The hydrodynamic parameters as well as the dynamic response to wave motion are plotted as a function of wave period for two different grid sizes, NB = 48 and 108.

The two different subdivisions of the floating box are shown in Figures 10 and 11 for the NB = 48 and 108 panel layouts. It may be noted that the figures show only one quarter of the box because the box has two planes of symmetry and, accordingly, in the two cases NA = 12 and 27.

Model tests were carried out for the configuration in question at the Vassdrags Og Havnelaboratoriet (Rivers and Harbors Laboratory) in Trondheim, Norway. These results which were reported by Faltinsen and Michelsen (11) are compared with the numerical results presented here.

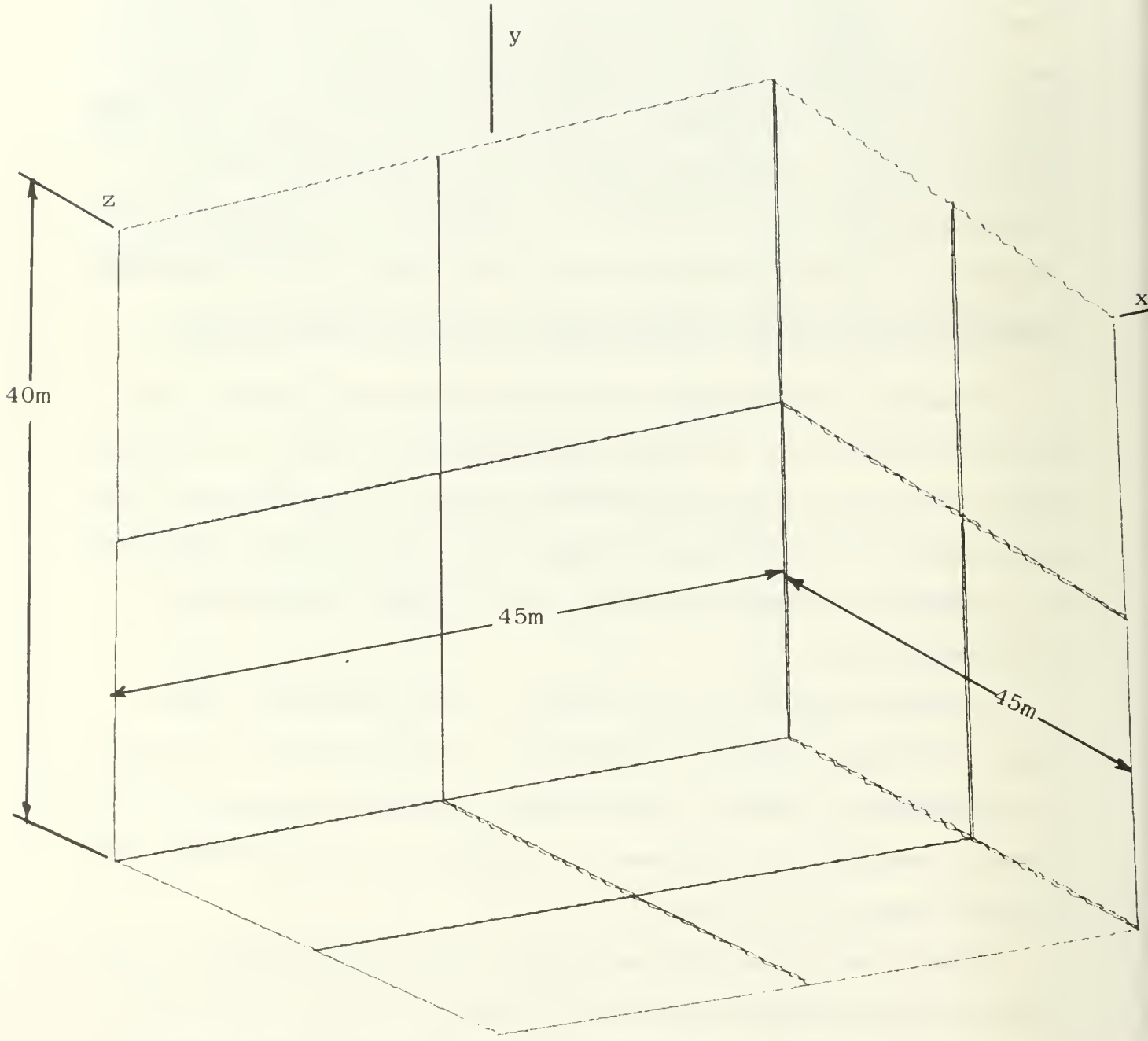

FIGURE 10: FLOATING BOX, 90M x 90M x 40M. NB=48 PANELS

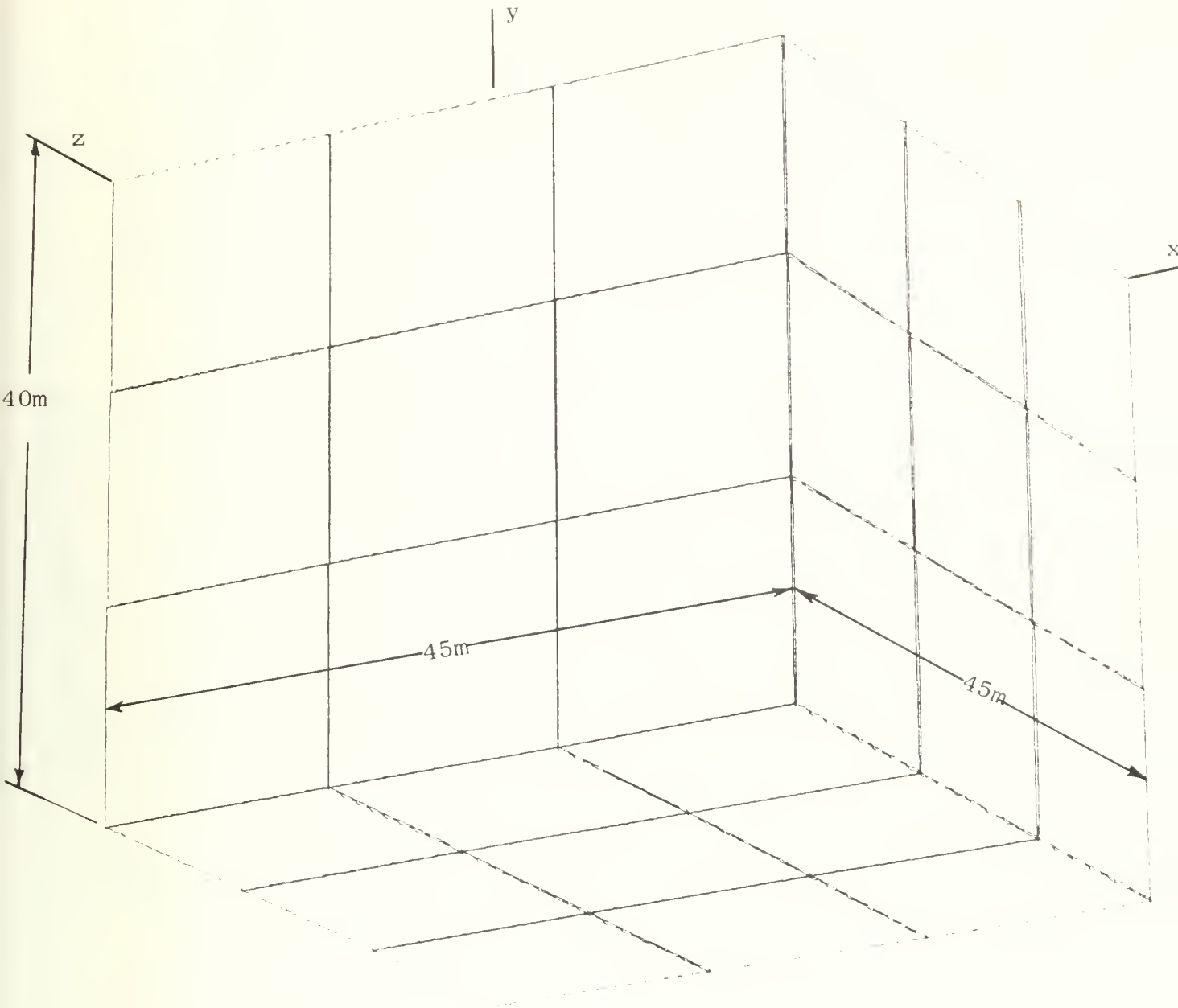

FIGURE 11: FLOATING BOX, 90M x 90M x 40M. NB=108 PANELS

The surge and heave excitation forces are shown in Figures 12 and 13, respectively. The fact that there is very little difference between the two sets of results corresponding to NB = 48 and 108 indicates that the solution tends to converge very rapidly in increasing the number of panels (or decreasing the grid size), at least for the case of the excitation forces. It might be noted that slower convergence should be expected at small periods.

The pitch excitation moment was computed also. However, as it turned out in this particular case, the moment with respect to the body axes (i.e., the centroidal axes was very nearly zero throughout the complete frequency range and the results were, therefore, masked by the "noise" caused by the numerical error.) For all practical purposes the pitch excitation moment was zero.

The surge added mass coefficient is shown in Figure 14, and here again the results corresponding to NB = 48 and 108 indicate that the solution has converged. The experimental results presented for comparison appear to agree rather well with the theory.

The corresponding damping coefficient in surge is shown in Figure 15. These results are typical of most damping results. At high-frequency and low-frequency oscillation, the wave-making damping tends to vanish since no waves are generated at the two extremes. In the intermediate frequency range, however, the wave-making reaches a maximum and the damping coefficient likewise shows a maximum. The experimental results shown on the figure appear to agree fairly well with the theory.

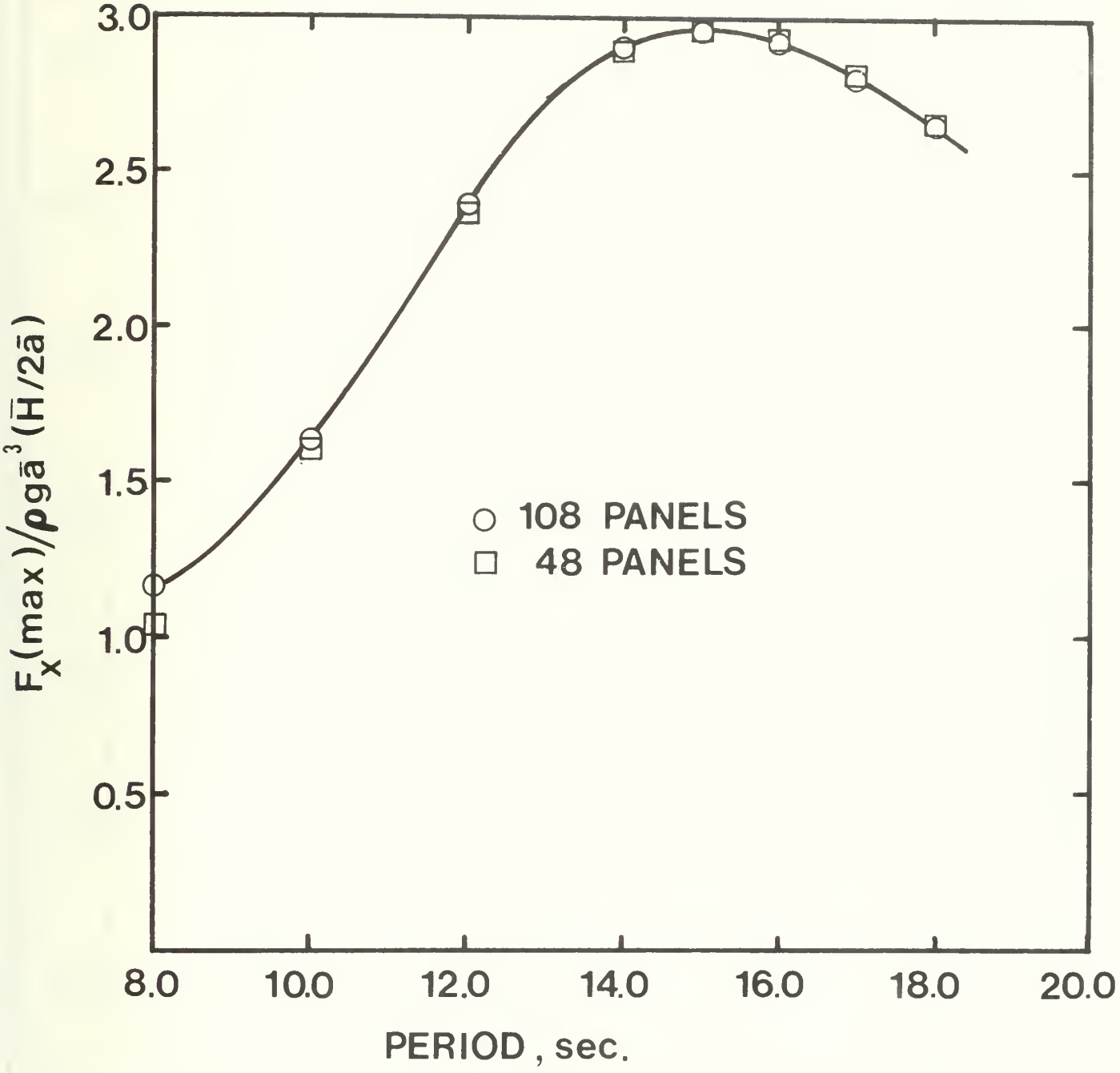

FIGURE 12 HORIZONTAL FORCE COEFFICIENT
(90m x 90m x 40m, Infinite Depth)

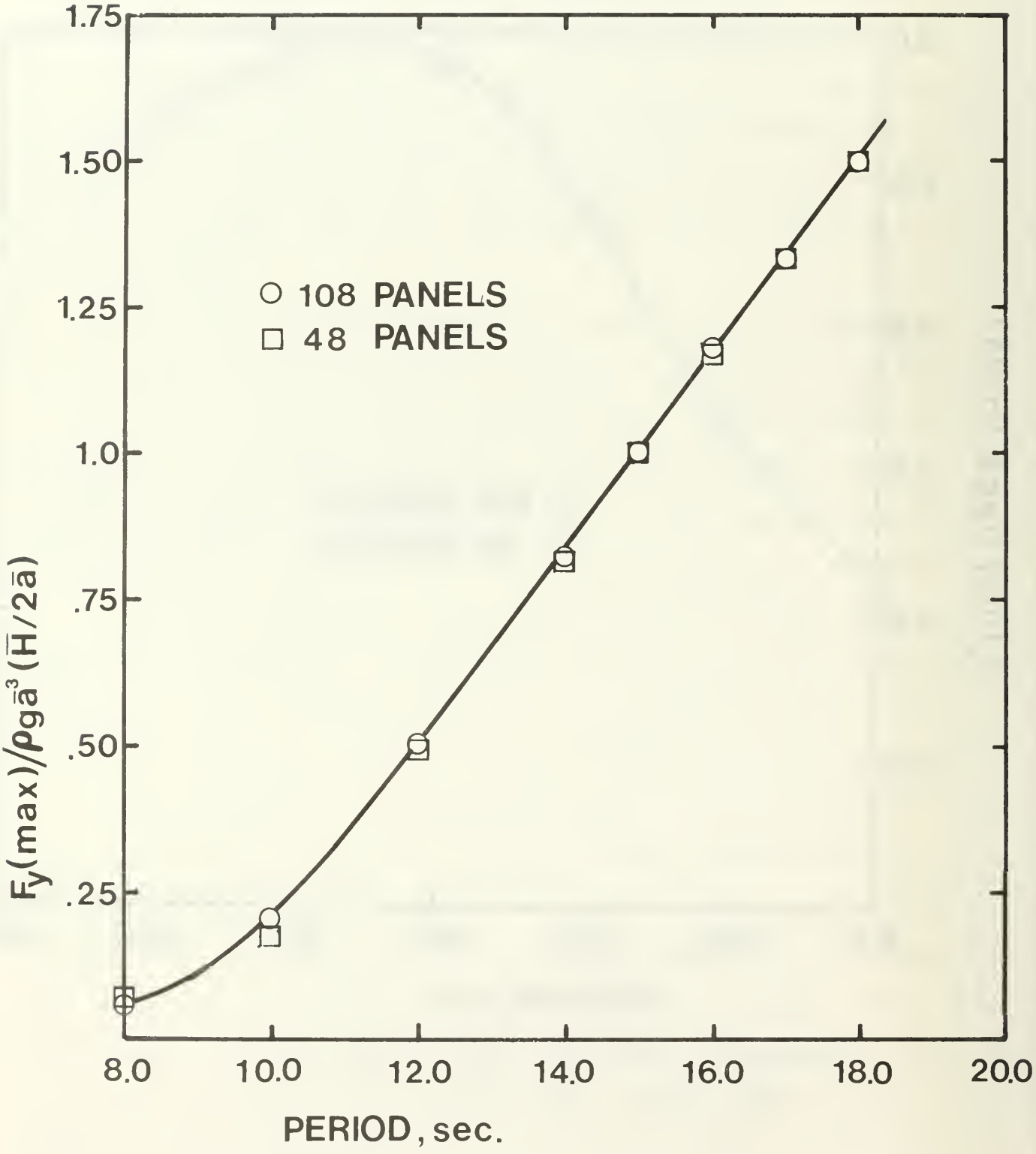

FIGURE 13 VERTICAL FORCE COEFFICIENT
(90m x 90m x 40m, Infinite Depth)

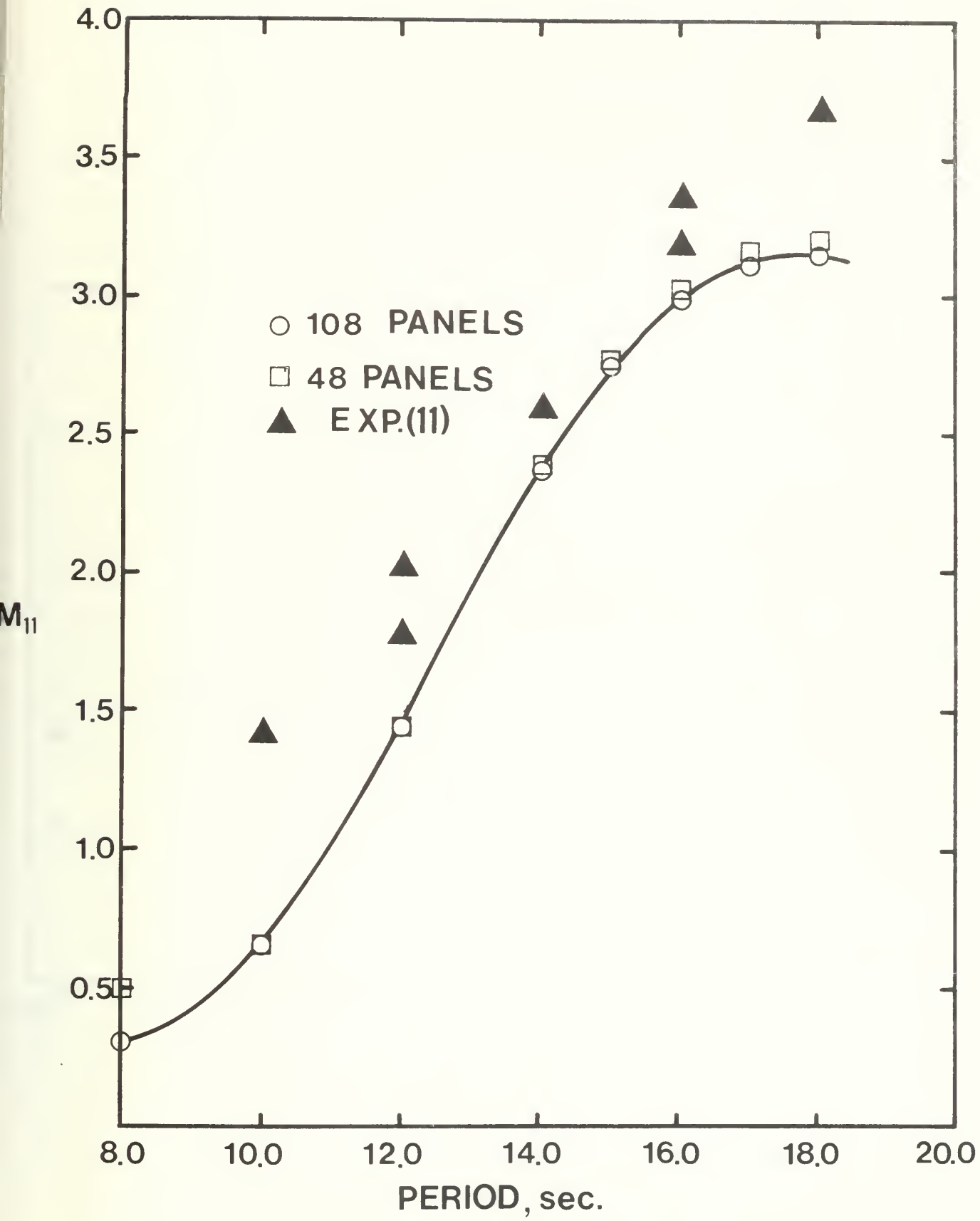

FIGURE 14 SURGE ADDED MASS COEFFICIENTS
(90m x 90m x 40m, Infinite Depth)

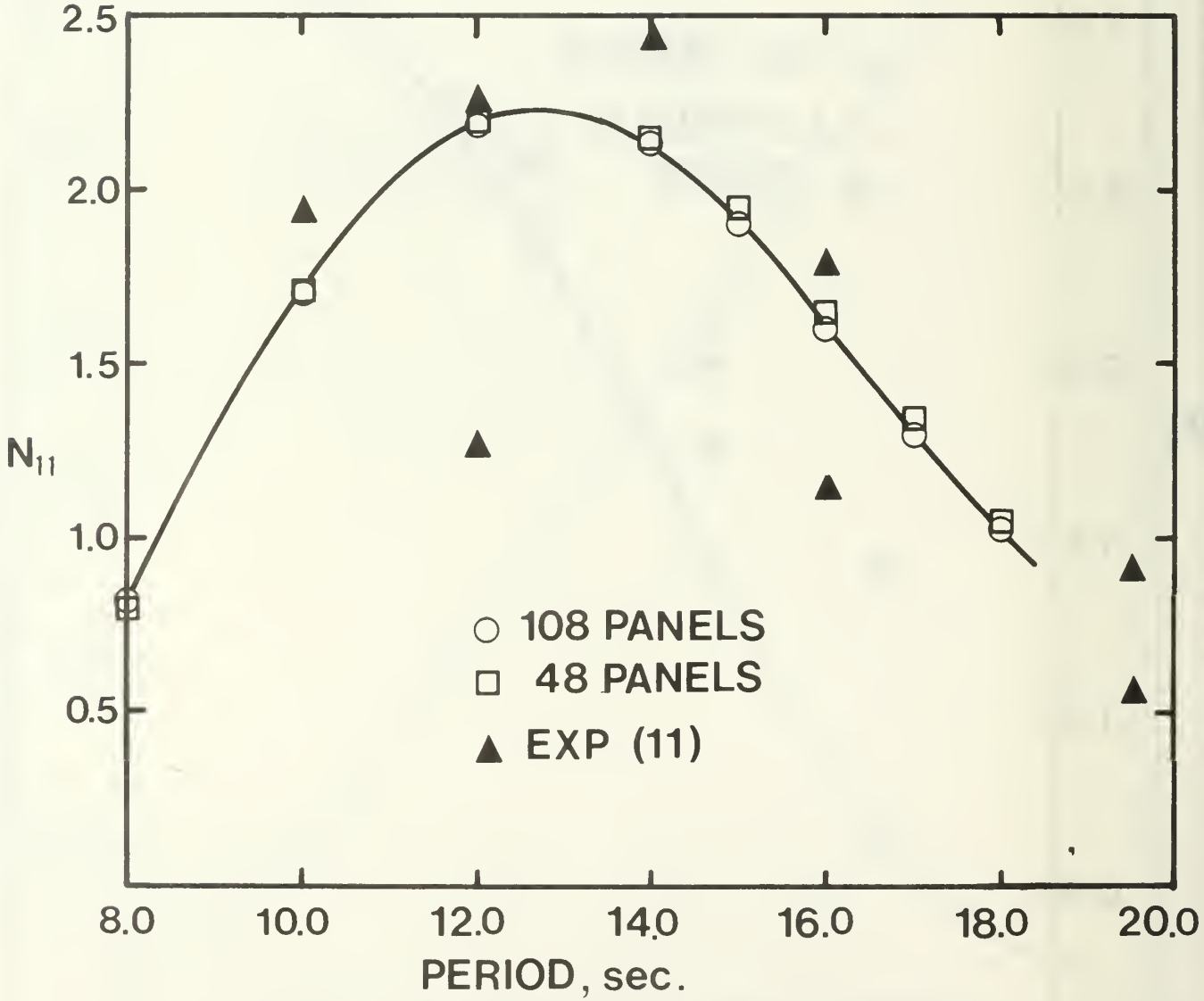

FIGURE 15 SURGE DAMPING COEFFICIENT
(90m x 90m x 40m, Infinite Depth)

The added mass coefficient in heave, M_{22}, is shown in Figure 16 along with experimental values. These results show very little frequency dependence, particularly when compared to the surge damping coefficient, N_{11}. This results from the fact that the surface primarily involved in heave force is the bottom and this surface is fairly distant from the free surface. Thus, free surface effects which are frequency dependent are not pronounced in the case of heave motion whereas they are much more pronounced in the case of surge where surfaces near the free surface are involved.

The computed heave damping coefficient is shown in Figure 17 along with experimental values. It is interesting to note that compared to the surge damping coefficient the heave damping coefficient is rather small. This results from the fact that the bottom surface which acts as the primary wave-maker in heave is rather well removed from the free surface and is, therefore, not too effective in generating waves and resulting damping.

It is also of interest to note that the experimental values of N_{22} fall well above the theoretical results. This difference is attributed to viscous damping and appears to be pronounced in a relative sense because the computed wave-making damping is small.

The added moment of inertia coefficient shown in Figure 18 is essentially independent of frequency (period). This appears to be typical of all results associated with caissons of the type in question. Moreover, the damping coefficient in pitch, N_{66}, which is not plotted, tends to be extremely small. These two

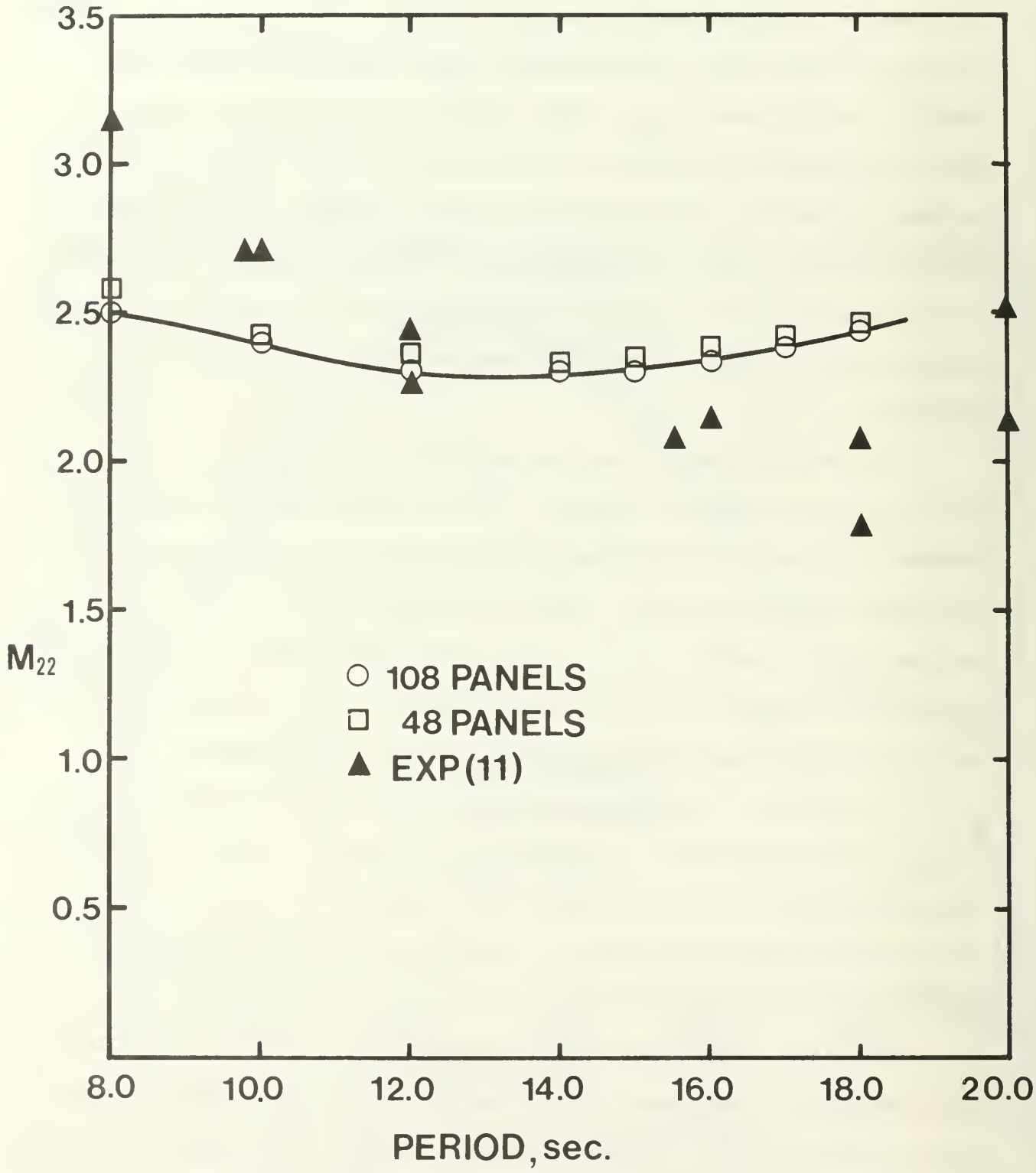

FIGURE 16 HEAVE ADDED MASS COEFFICIENT
(90m x 90m x 40m, Infinite Depth)

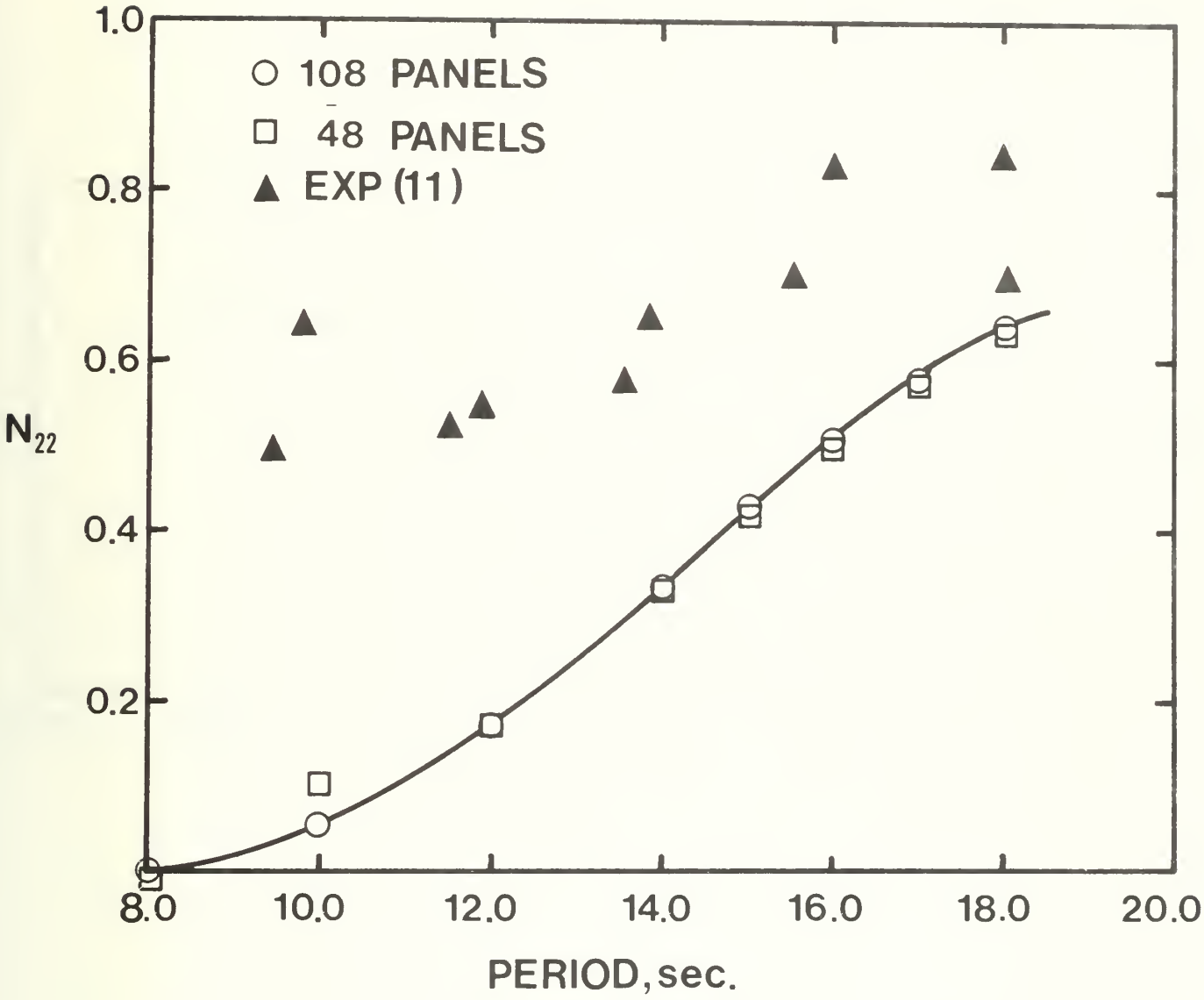

FIGURE 17 HEAVE DAMPING COEFFICIENT
(90m x 90m x 40m, Infinite Depth)

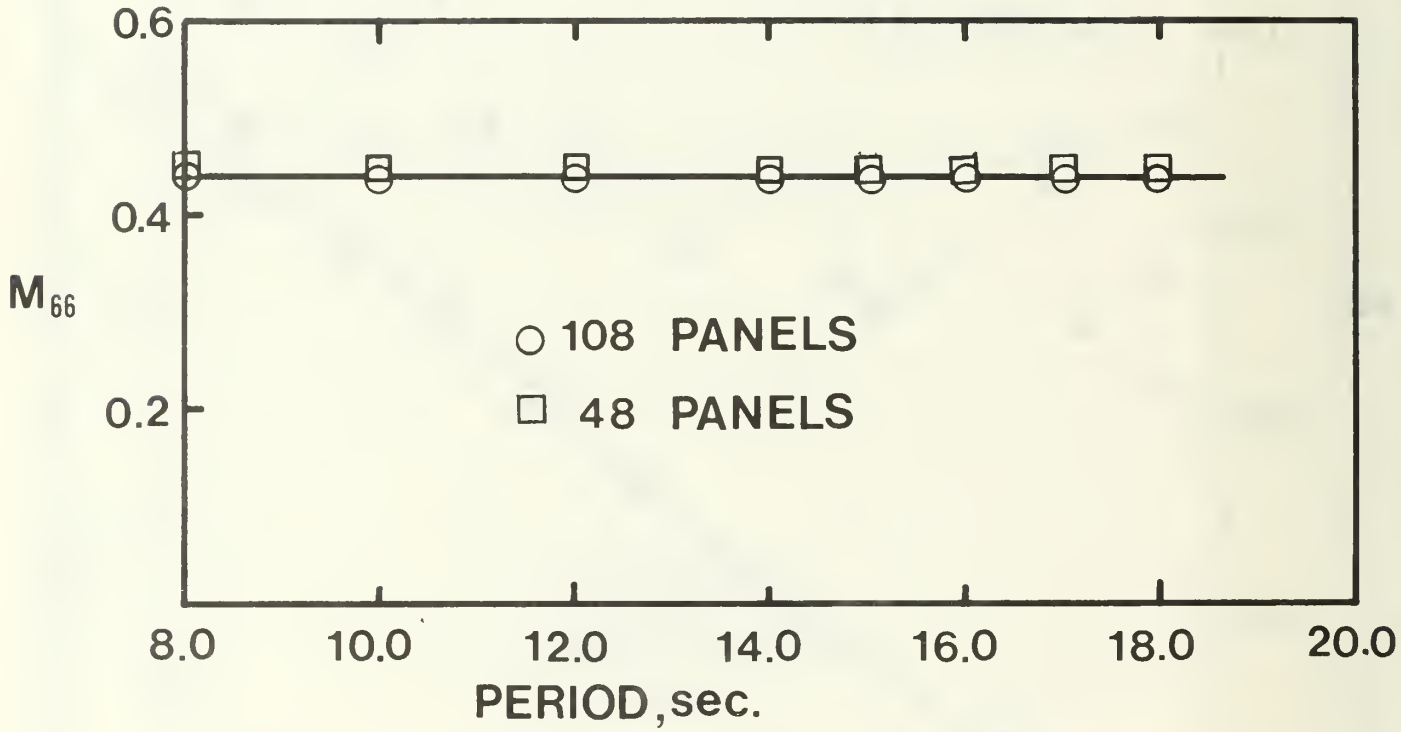

FIGURE 18 PITCH ADDED MOMENT OF INERTIA COEFFICIENT
(90m x 90m x 40m, Infinite Depth)

features result from the fact that frequency dependence and damping is a result of wave production and very little wave generation occurs as a result of pitching motion. This is due to the fact that the bottom surface is far removed from the free surface and the vertical sides do not move in the normal direction very much as a result of pitching motion.

The added mass coefficient in yaw, M_{55}, is shown in Figure 19 along with experimental results. The agreement here appears to be generally good.

Finally, the dynamic response of the box free floating in waves is shown in Figure 20. The pitch response, $\theta_6/(\bar{H}/2\bar{a})$, is extremely small as was expected. The natural frequency in heave occurs at about 16.5 seconds period and, therefore, considerable dynamic amplification occurs. In the case of the heave response several experimental values are shown which tend to agree well with the theory.

Shallow-Draft Barge

The dynamic heave and pitch response has also been computed for comparison with experimental results for a shallow-draft barge. One quarter of the immersed surface of the barge is shown in Figure 21 as it was subdivided for numerical computations. It may be noted that since the draft was rather small the source strength might be expected to show considerable variation in the vertical direction and around the corner. However, in the horizontal direction the source strength should vary rather slowly. Accordingly, the panels were constructed with a rather large aspect ratio as indicated in Figure 21.

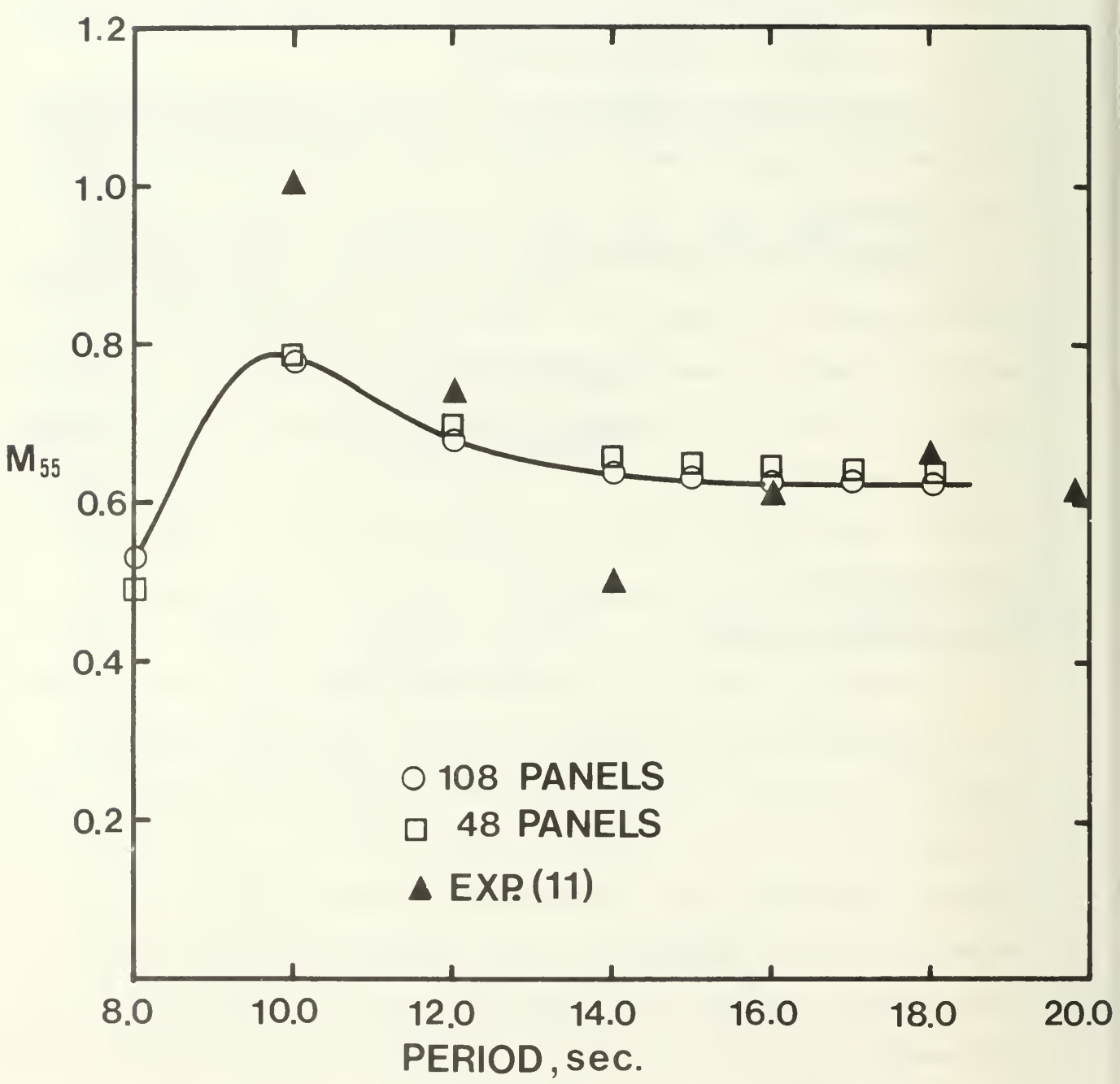

FIGURE 19 YAW ADDED MASS COEFFICIENT
(90m x 90m x 40m, Infinite Depth)

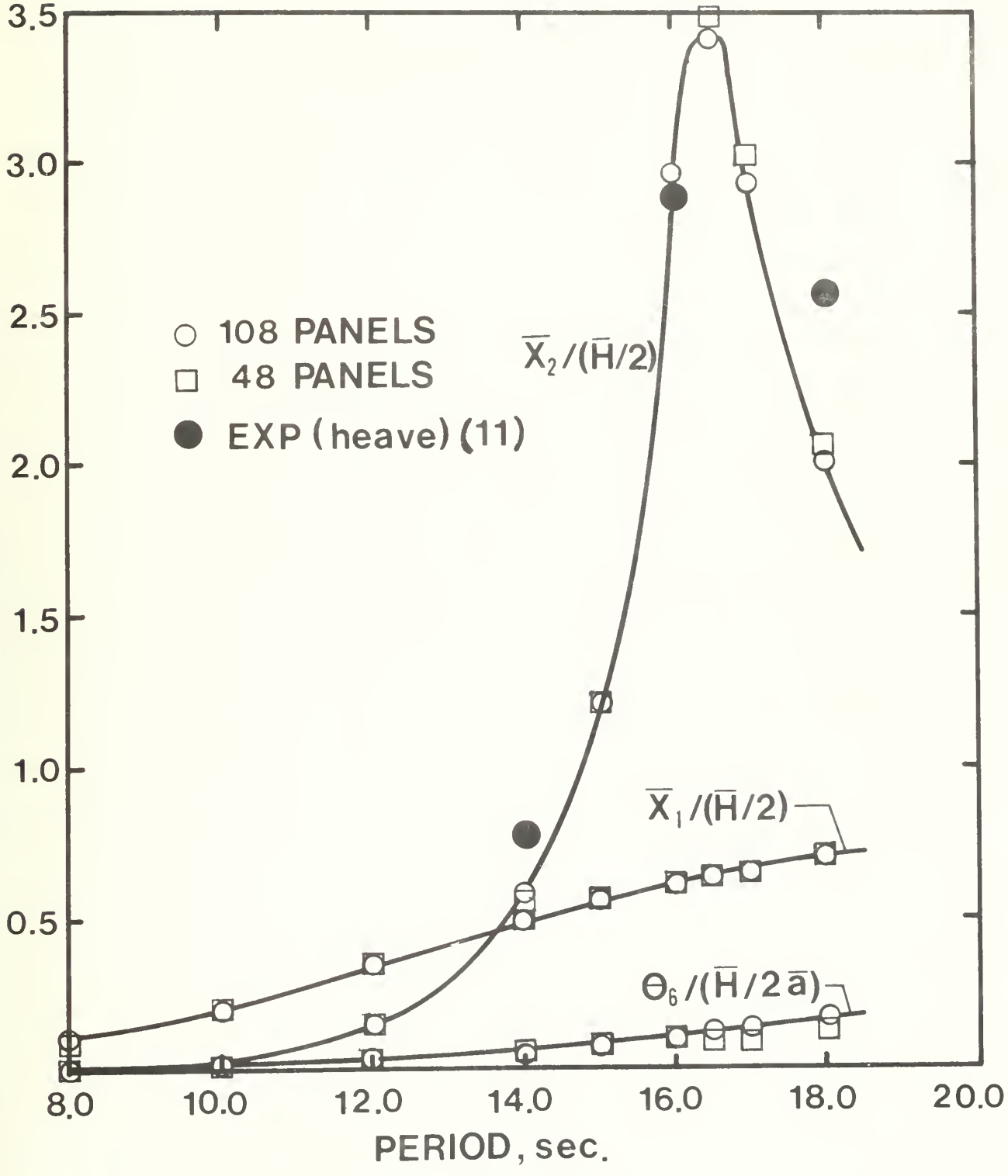

FIGURE 20 SURGE, HEAVE AND PITCH RESPONSE
(90m x 90m x 40m, Infinite Depth)

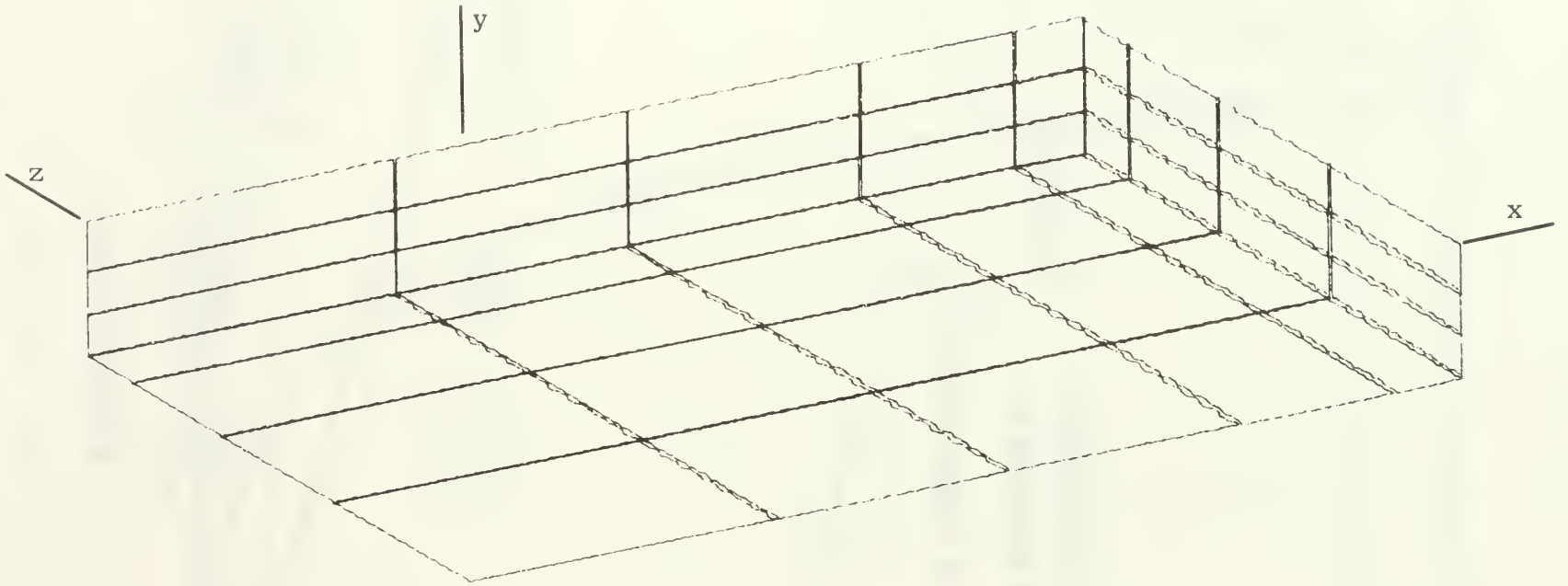

FIG 21 ONE QUARTER OF IMMERSED SURFACE OF SHALLOW DRAFT BARGE SHOWING SUBDIVISIONS

Calculations have been made to compare with the wave channel test results of Kim, Henry and Chou (17) for a shallow draft barge of 1.704 feet beam, by 2.558 feet length, by 0.16 feet draft. The location of the center of gravity and pitch gyradius is shown in Figure 22.

The theoretical heave and pitch response is compared with the experimental values in Figure 22. The results show excellent agreement between the theory and experiment for the case of heave motion. This apparently results from the fact that the wave-making damping in heave for a shallow-draft barge is substantial and, therefore, the heave results are not too sensitive to viscous damping.

The pitch results also show fairly good agreement. While there appears to be some scatter in the pitch results, it appears that near resonance the experimental values of the response fall below the theory. Here again this is attributed to viscous effects which tend to be significant compared to the rather small amount of wave-making damping.

Disc Buoy

As a further example, the dynamic heave and pitch response for a rather shallow-draft disc-buoy is shown in Figure 23. Unlike some of the previous results, the pitch response as well as the heave response shows excellent agreement between the theory and experiment. This is likely due to the fact that the corners on the disc buoy configuration are beveled rather than sharp. This probably reduces some of the separation and resulting viscous damping. Consequently, the experimental results are in good agreement with the calculations.

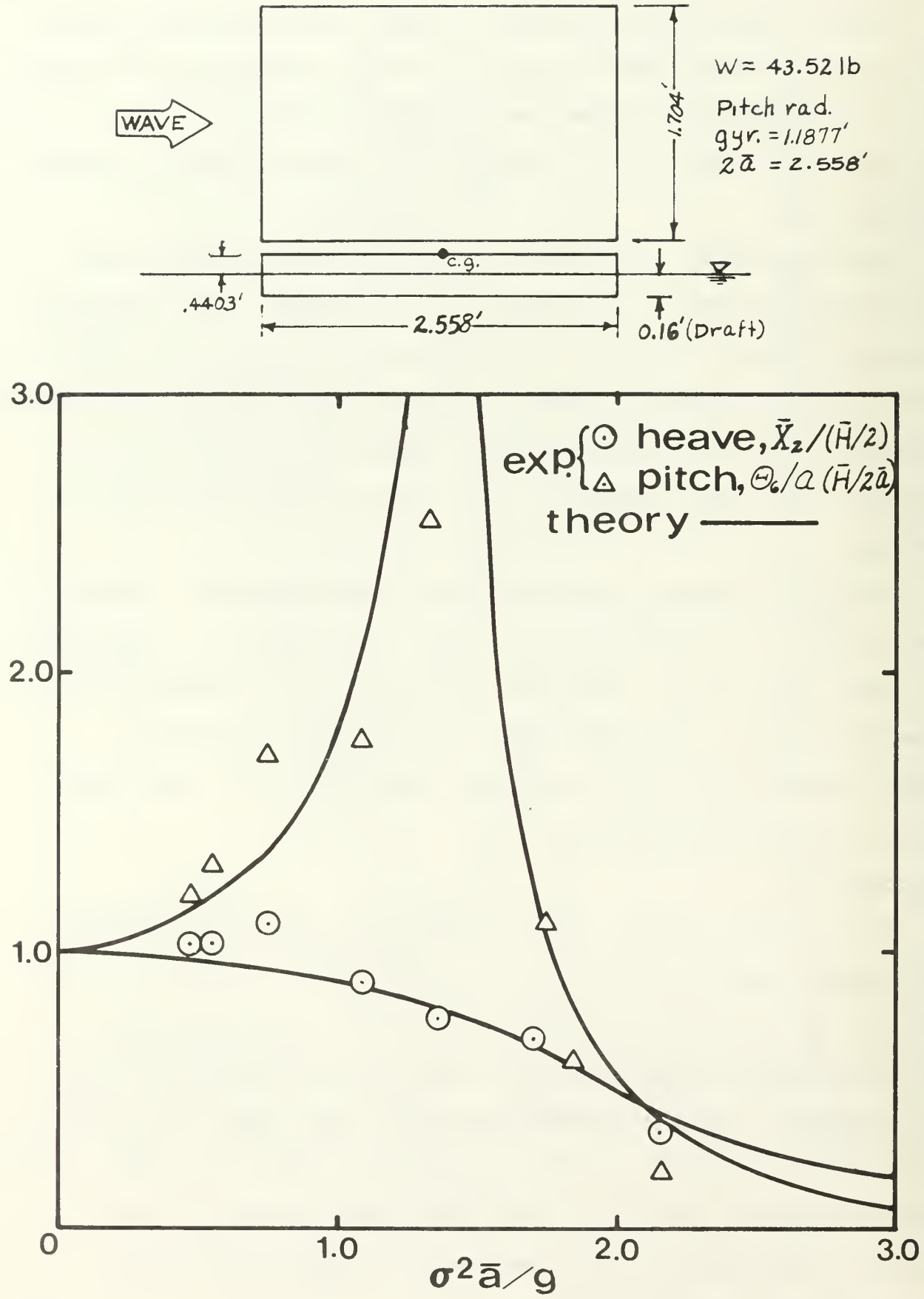

FIGURE 22 HEAVE AND PITCH RESPONSE OF A SHALLOW-DRAFT BARGE, DEEP WATER

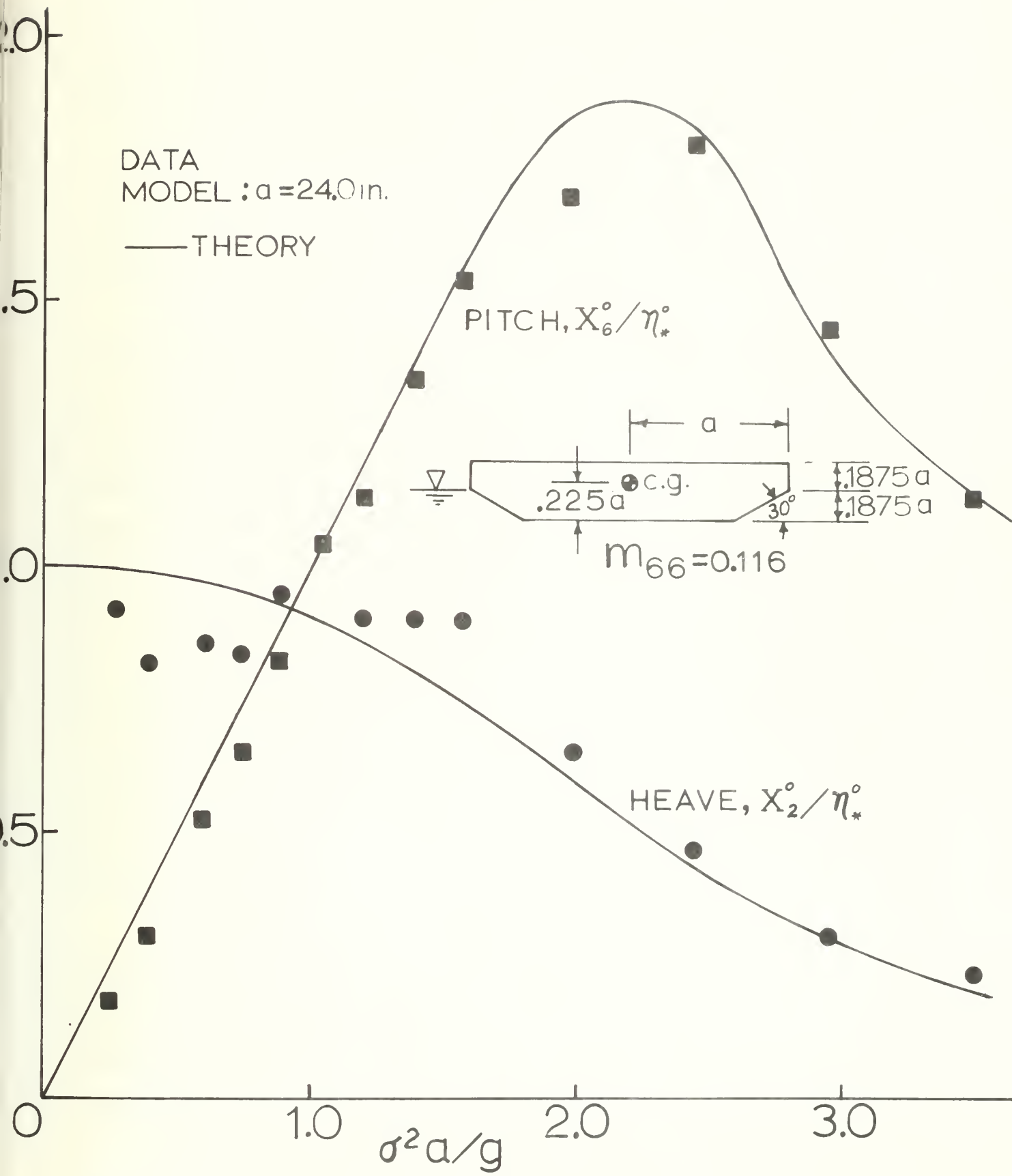

FIGURE 23 HEAVE AND PITCH RESPONSE OF A DISK BUOY IN DEEP WATER

Floating Semi-submerged Sphere

As an example showing the effect of finite depth on a floating body, numerical results are presented for a semi-submerged sphere floating in waves. Figures 24, 25 and 26 show the excitation forces, added mass and damping in heave, and added mass and damping in surge, respectively. In general, the effect of the finite depth tends to be more pronounced at low-frequency than at high-frequency.

Using the results of Figures 24-26 the equations of motion for the free floating sphere give the heave and surge response presented in Figures 27 and 28. The amplitude ratios are shown in Figure 27 and the phase shift angles of the response measured with respect to the phase of the wave crest at the center of the body is shown in Figure 28. In general, there appears to be little effect on the finite depth for the sphere configuration.

Floating Vertical Cylinder

The added mass and damping coefficients for the circular caisson configuration are shown in Figure 29 as a function of the frequency parameter $\sigma^{2-}a/g$ wherein the depth ratio $\bar{h} = \bar{h}/\bar{a}$, represents a parameter. The horizontal force coefficient is shown in Figure 30. These results for the horizontal force coefficient agree well with the theoretical results of Garrett (18).

The dynamic response in surge, heave and pitch is presented in Figures 31, 32 and 33, respectively. In general, the results appear typical of deep water results and little effect of water depth is evident. The pitch response shown in Figure 33 shows

the large dynamic amplification at resonance which tends to be typical of essentially all floating caissons and, here again results from the rather small wave-making damping. This high resonant peak should not be expected in practice, however, due to the fact that viscous effects are undoubtedly considerably larger than the pitch wave-making damping used to compute the results shown in Figure 33.

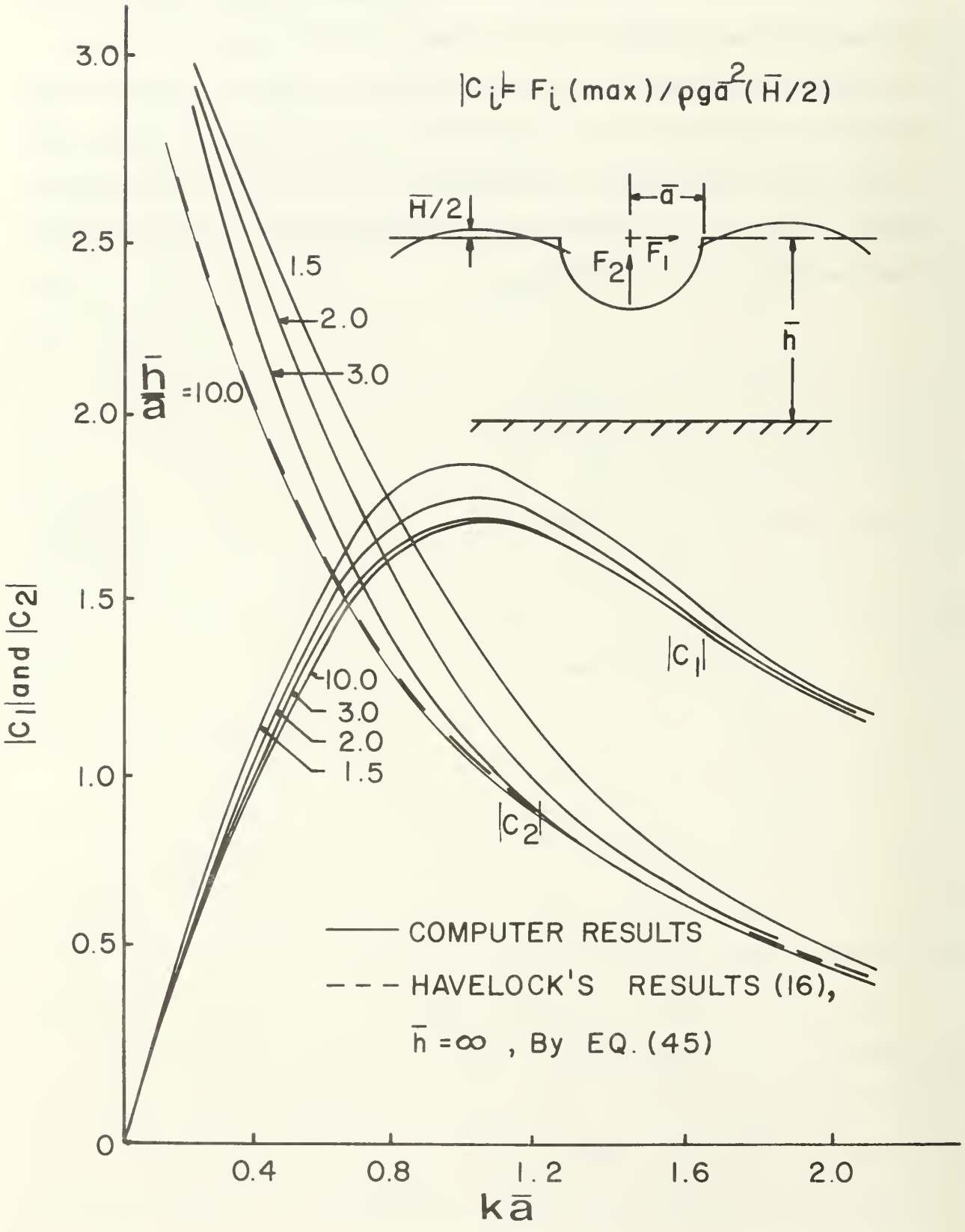

FIGURE 24 WAVE EXCITATION FORCES ON A SEMI-SUBMERGED SPHERE

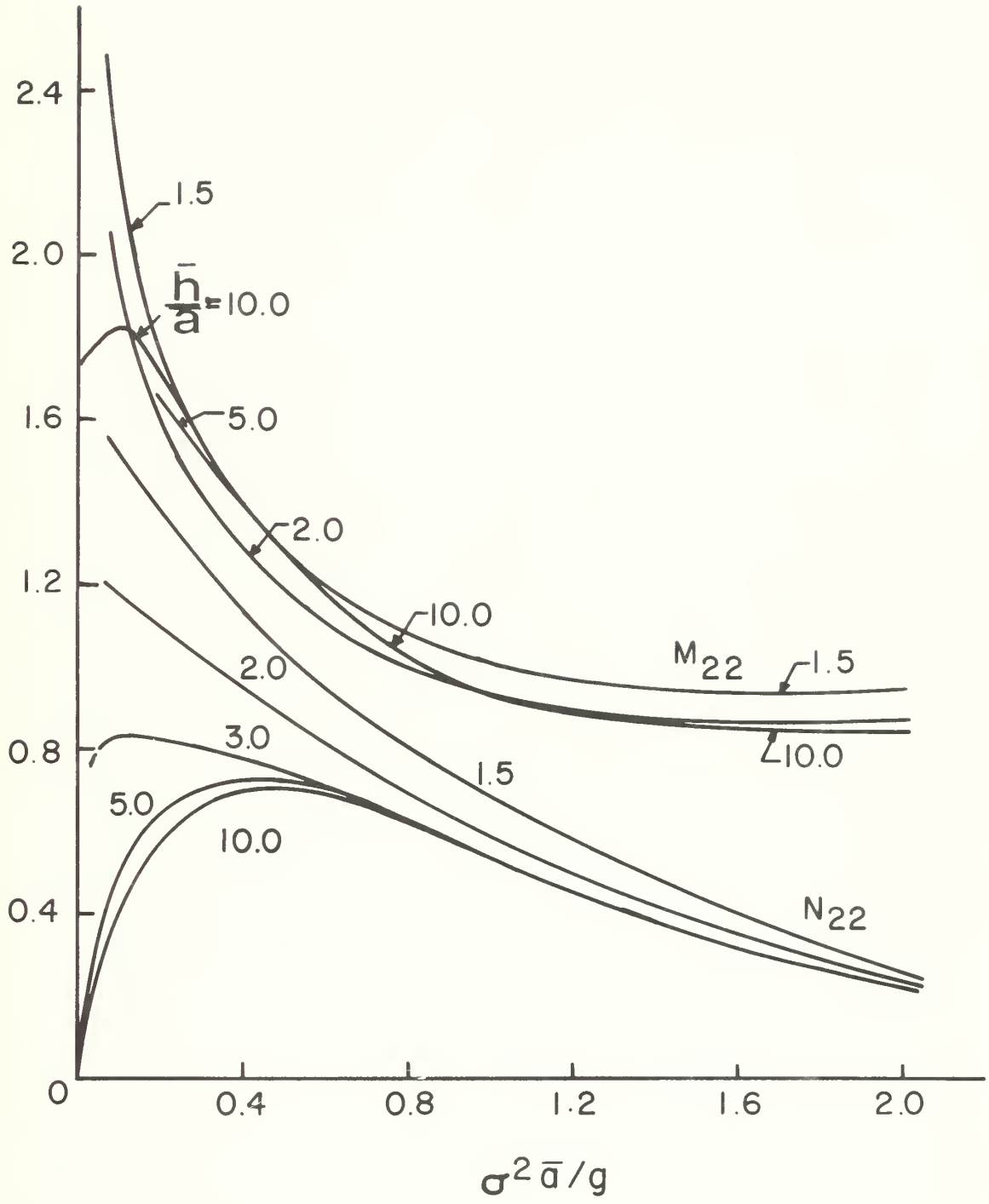

FIGURE 25 ADDED MASS AND DAMPING IN HEAVE FOR A SEMI-SUBMERGED SPHERE.

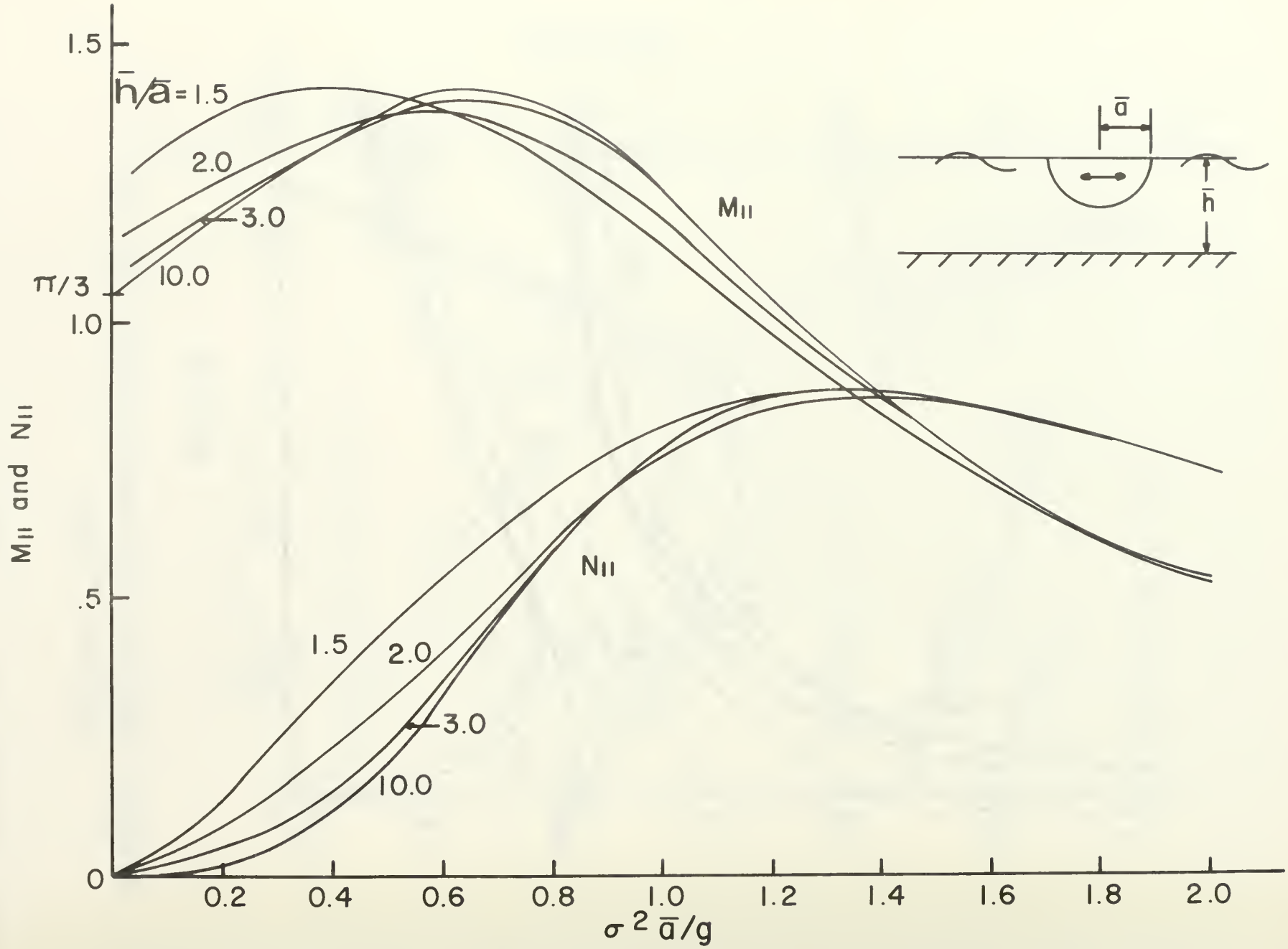

FIGURE 26 ADDED AND DAMPING IN SURGE FOR A SEMI-SUBMERGED SPHERE

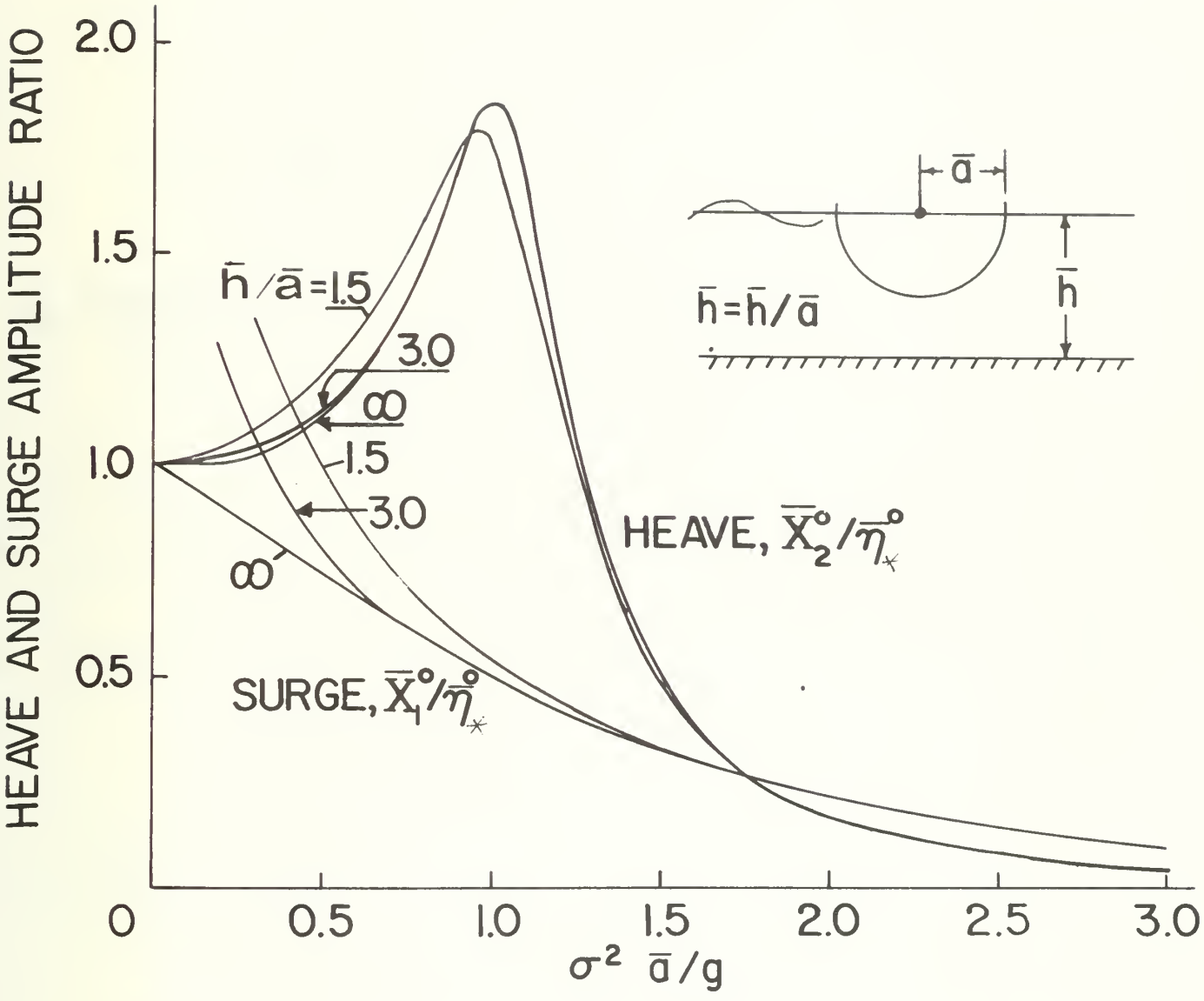

FIGURE 27 HEAVE AND SURGE RESPONSE OF A SEMI-SUBMERGED SPHERE.

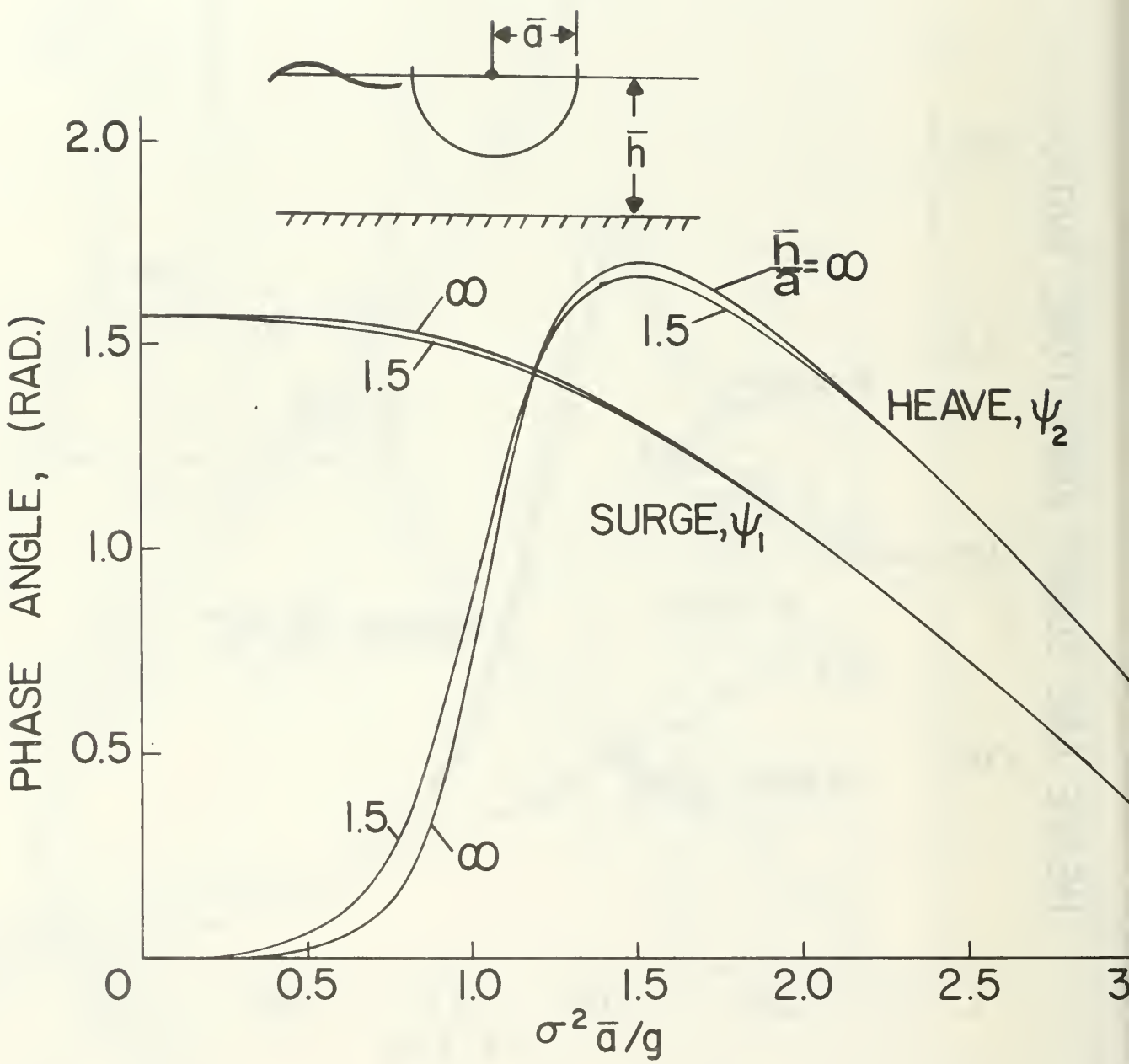

FIGURE 28 PHASE SHIFT ANGLES OF THE HEAVE AND SURGE RESPONSE OF SEMI-SUBMERGER SPHERE.

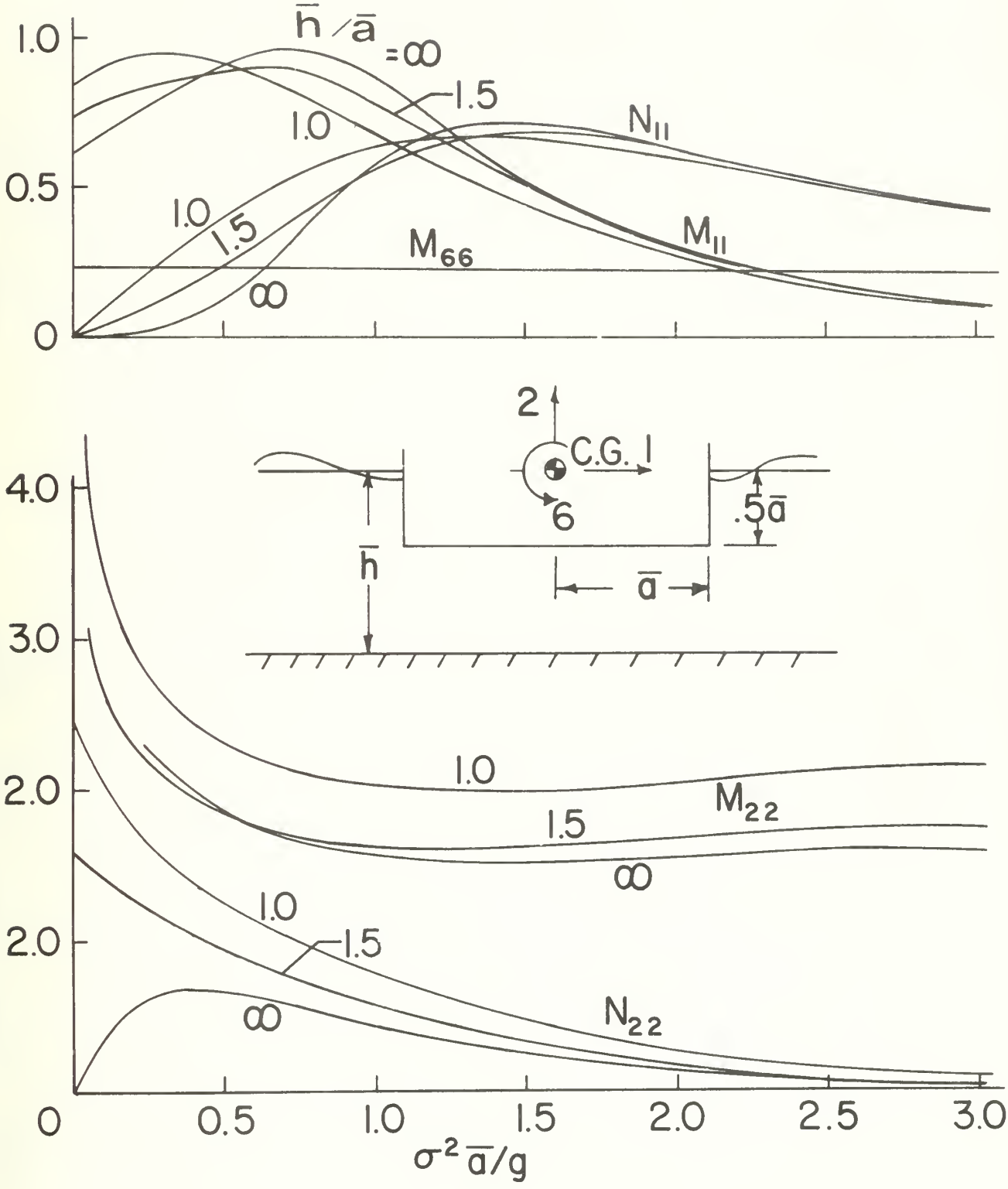

FIGURE 29 ADDED MASS AND DAMPING COEFFICIENTS FOR A FLOATING VERTICAL CIRCULAR CYLINDER.

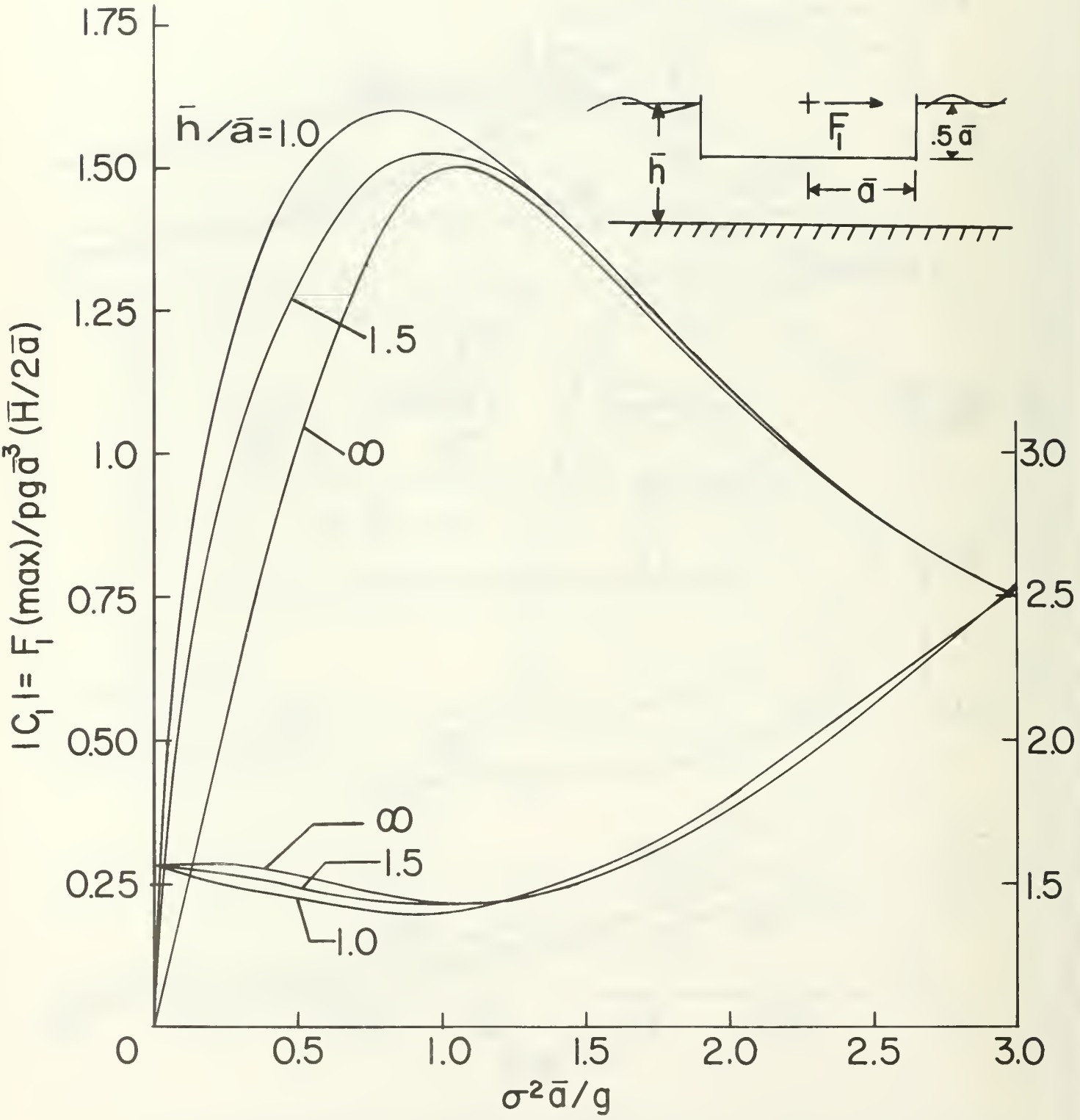

FIGURE 30 HORIZONTAL FORCE COEFFICIENT FOR A FLOATING VERTICAL CIRCULAR CYLINDER.

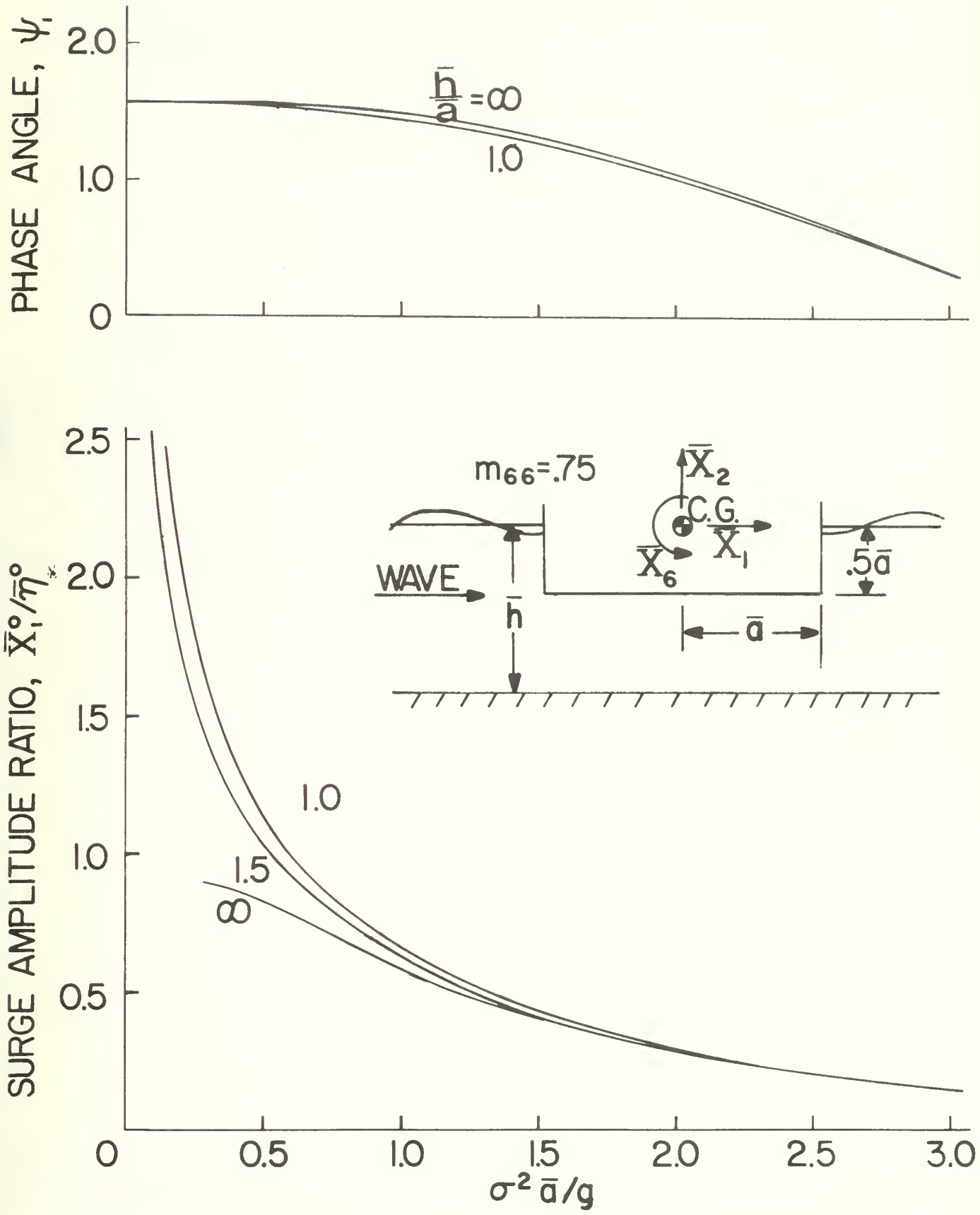

FIGURE 31 SURGE RESPONSE OF A FLOATING VERTICAL CIRCULAR CYLINDER.

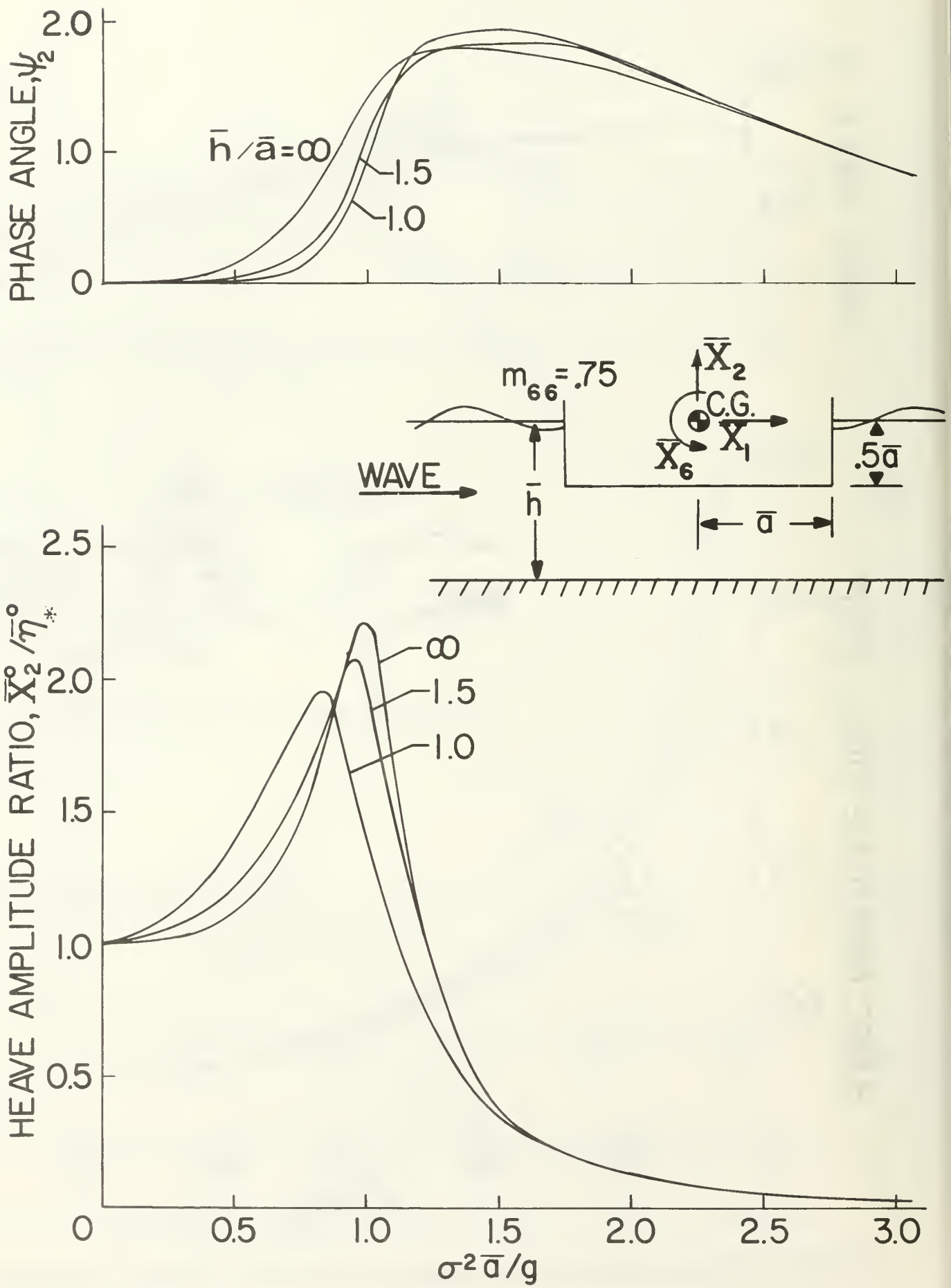

FIGURE 32 HEAVE RESPONSE OF A FLOATING VERTICAL CIRCULAR CYLINDER.

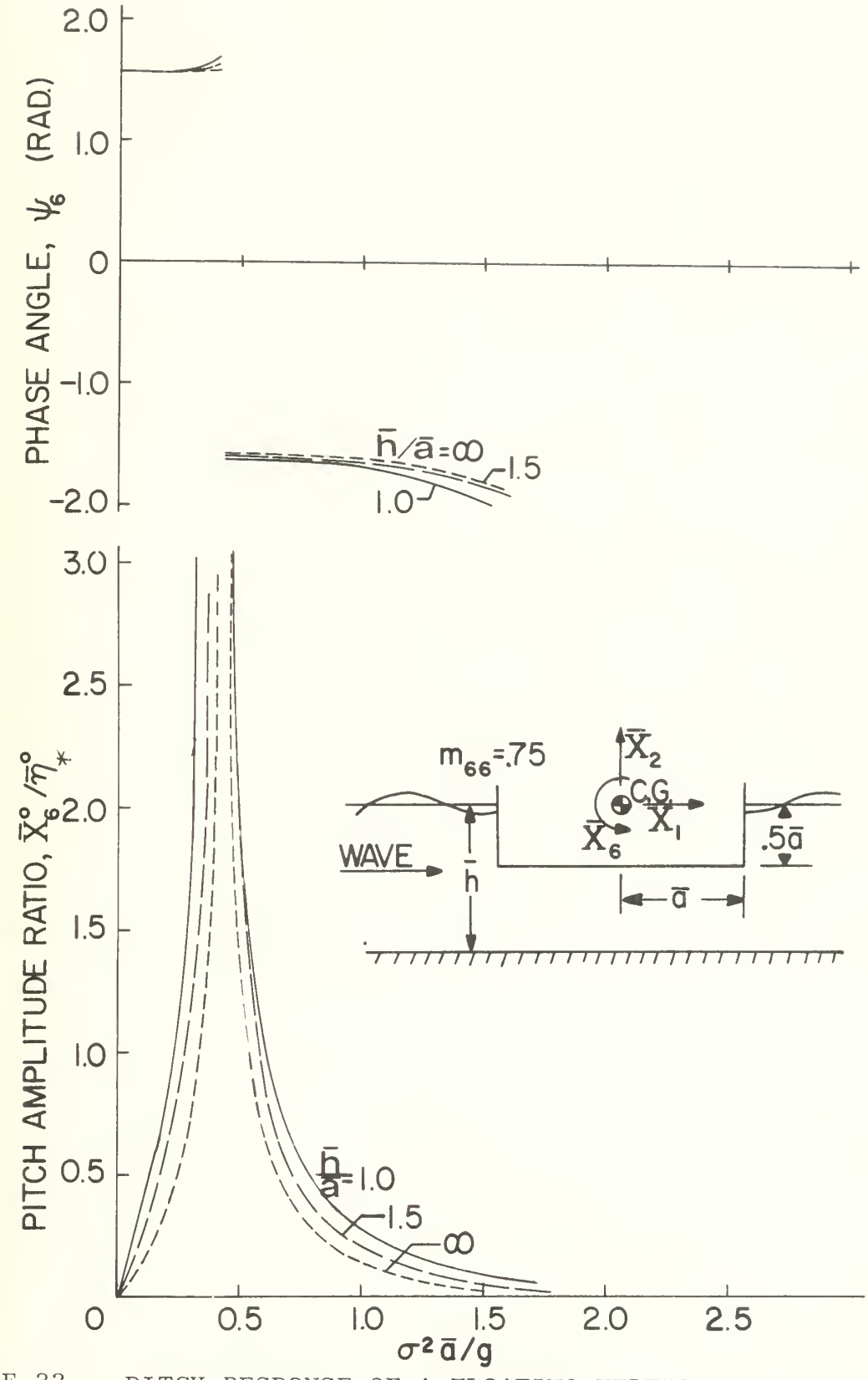

FIGURE 33 PITCH RESPONSE OF A FLOATING VERTICAL CIRCULAR CYLINDER.

APPENDIX A:

DETERMINATION OF THE CENTROIDAL LOCATION, AREA AND UNIT NORMAL VECTOR FOR A PANEL

The computer program is designed to accept the coordinates of the corners of the facets as inputs and, in addition, a set of cards indicating which corners make-up a given panel. A panel is described by the four corner indexes read clockwise moving around the panel in such a way that the panel is always on the right. For example, panel 5, as indicated in Figure 1A, is specified by a data card

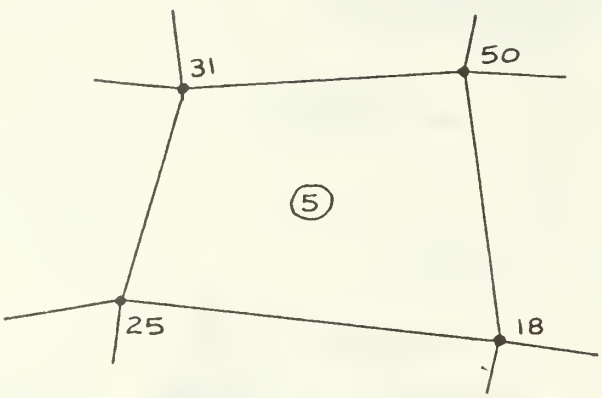

FIGURE 1A

of the following form:

Panel No.	Corner #1	Corner #2	Corner #3	Corner #4
5	25	31	50	18

In working with an individual panel the first corner (25) in the above example is designated as 1, the second corner, moving around the panel keeping the inside of the panel on the right, is labled 2, etc. The panel is re-labled as shown in Figure 2A with indices 1-4.

The area of the panel is computed by first dividing it into two triangles by connecting corner 2 with the diagonal corner 4.

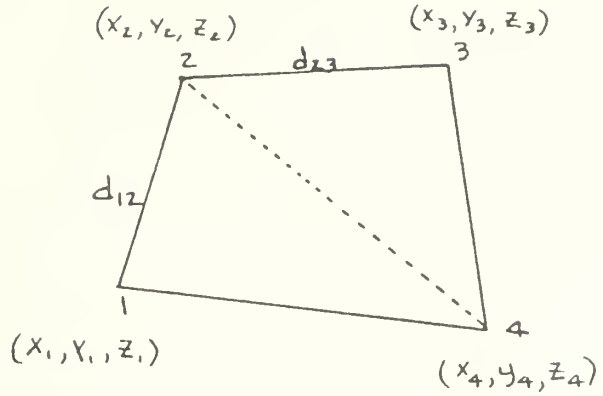

FIGURE 2A

The area of triangle 1-2-4 is then computed by use of a standard formula,

$$\text{Area}(124) = \sqrt{S(S-d_{12})(S-d_{24})(S-d_{41})}$$

where

$$S = \frac{1}{2}(d_{12} + d_{24} + d_{41})$$

and

$$d_{12} = \sqrt{(X_2 - X_1)^2 + (Y_2 - Y_1)^2 + (Z_2 - Z_1)^2}$$

$$d_{24} = \sqrt{(X_4 - X_2)^2 + (Y_4 - Y_2)^2 + (Z_4 - Z_2)^2}$$

$$d_{41} = \sqrt{(X_1 - X_4)^2 + (Y_1 - Y_4)^2 + (Z_1 - Z_4)^2}$$

The centroid of a triangle lies at the average of the coordinates describing its corners as,

$$X_{C_{124}} = \frac{1}{3}(X_1 + X_2 + X_4)$$

$$Y_{C_{124}} = \frac{1}{3}(Y_1 + Y_2 + Y_4)$$

$$Z_{C_{124}} = \frac{1}{3}(Z_1 + Z_2 + Z_4)$$

The area and centroid location of triangle 234 is computed in a similar manner. The total area for the panel is then simply

$$A = A_{124} + A_{234}$$

and coordinates of the centroid of the panel is obtained from

$$X_c = (X_{c_{124}} A_{124} + X_{c_{234}} A_{234}) / (A_{124} + A_{234})$$

$$Y_c = (Y_{c_{124}} A_{124} + Y_{c_{234}} A_{234}) / (A_{124} + A_{234})$$

$$Z_c = (Z_{c_{124}} A_{124} + Y_{c_{234}} A_{234}) / (A_{124} + A_{234})$$

It is also necessary to determine the x,y,z-components of the unit vector normal to the panel and directed <u>outward</u> into the fluid. This is accomplished by defining the vectors, $\vec{\tau}_{13}$ and $\vec{\tau}_{24}$, which extend from point 1 to 3 and from point 2 to 4, respectively, as indicated in Figure 3A. The corners are numbered

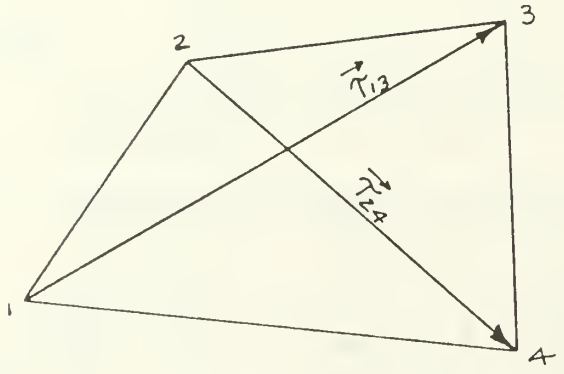

FIGURE 3A

clockwise when viewed from the outside (water side) of the caisson and, therefore, according to the right hand rule the cross product

$$\vec{\tau}_{24} \times \vec{\tau}_{13}$$

represents a vector having direction perpendicular to the plane

1 - 2 - 3 - 4 and pointing outward into the fluid. The unit normal vector is, then, obtained by normalyzing this vector to unit length,

$$\vec{n} = (\vec{r}_{24} \times \vec{r}_{13}) / |\vec{r}_{24} \times \vec{r}_{13}|$$

where $|\vec{n}| = 1$ and $\vec{n} = i\, n_x + j\, n_y + k\, n_z$, the components n_x, n_y and n_z represent the direction cosines.

APPENDIX B:

INTEGRATION OF 1/R AND DERIVATIVES OF 1/R OVER A PANEL

In order to evaluate the elements of the matrices α and β by use of the definitions given in equations (5.3) and (5.7) the necessity arises to evaluate integrals of 1/R and $\partial/\partial x$, $\partial/\partial y$ and $\partial/\partial z$ of 1/R. In this appendix the method of integration is outlined.

In order to carry out the integrations, a local coordinate system is defined in such a way that the panel lies in the x-y plane of the local coordinate system and the unit normal vector is parallel to the z axis. For definiteness the coordinate system is attached to the element in such a way that point 1 is located at the origin and point 4 lies on the x-axis.

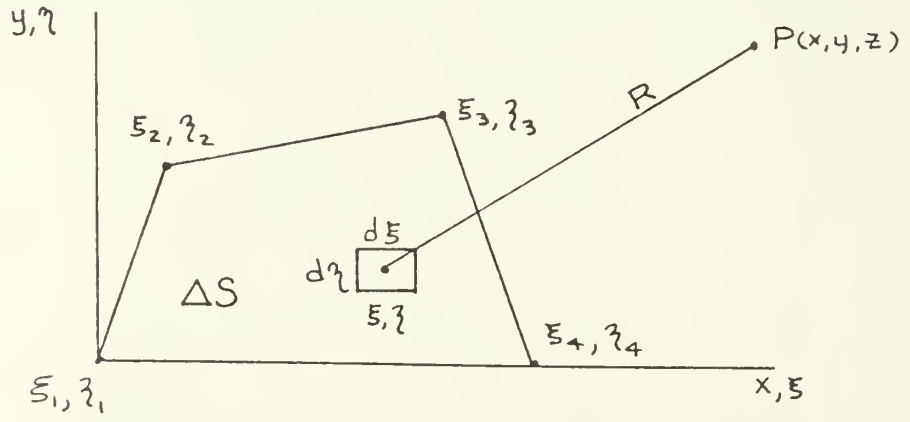

FIGURE 1B

Consider first the integral,

$$\phi = \iint_{\Delta S} \frac{1}{R}\, dS = \iint_{\Delta S} \frac{d\xi\, d\eta}{\sqrt{(x-\xi)^2 + (y-\eta)^2 + (z-\zeta)^2}} \qquad (1B)$$

Following a procedure similar to Hess and Smith(16) for the velocity components, Faltinsen and Michelsen(11) integrated equation (1B with respect to ζ to obtain

$$\phi = -\int_{\xi_1}^{\xi_2} d\xi \ln\left\{ y - \zeta_{12} + \sqrt{(y-\zeta_{12})^2 + (x-\xi)^2 + z^2} \right\}$$

$$-\int_{\xi_2}^{\xi_3} d\xi \ln\left\{ y - \zeta_{23} + \sqrt{(y-\zeta_{23})^2 + (x-\xi)^2 + z^2} \right\} \qquad (2B)$$

$$-\int_{\xi_3}^{\xi_4} d\xi \ln\left\{ y - \zeta_{34} + \sqrt{(y-\zeta_{34})^2 + (x-\xi)^2 + z^2} \right\}$$

$$-\int_{\xi_4}^{\xi_1} d\xi \ln\left\{ y - \zeta_{41} + \sqrt{(y-\zeta_{41})^2 + (x-\xi)^2 + z^2} \right\}$$

where

$$\zeta_{ij} = \zeta_i + \frac{\zeta_j - \zeta_i}{\xi_j - \xi_i}(\xi - \xi_i) \qquad (3B)$$

The integrals in (2B) may be evaluated through numerical integration in most cases.

However, it may be noted that the integrand of the first integral is singular when z = O, ξ = x and y - ζ_{12} < 0. In this case the integral may be replaced by

$$\int_{\xi_1}^{\xi_2} \ln\left[(x-\xi)^2 + z^2\right] d\xi$$

$$-\int_{\xi_1}^{\xi_2} \ln\left\{ -(y-\zeta_{12}) + \sqrt{(y-\zeta_{12})^2 + (x-\xi)^2 + z^2} \right\} d\xi \qquad (4B)$$

The first integral in (4B) can be integrated analytically, the result of which is

$$(x-\xi_1)\ln\left\{(x-\xi_1)^2+z^2\right\}-(x-\xi_2)\ln\left\{(x-\xi_2)^2+z^2\right\} \tag{5B}$$

$$+2z\left[\tan^{-1}\left(\frac{x-\xi_1}{z}\right)-\tan^{-1}\left(\frac{x-\xi_2}{z}\right)\right]+2\left[(x-\xi_2)-(x-\xi_1)\right]$$

The second integral in (4B) has no singularity in the integrand and consequently presents no difficulaties in numerical integration. Difficulties with singularities in the integrand of the other integrals in equation (2B) are handled in a similar manner.

In the evaluation of α_{ij} as defined by equation (4.5) or $\gamma_{x_{ij}}$, $\gamma_{y_{ij}}$ and $\gamma_{z_{ij}}$ as given by equations (4.11) it is necessary to evaluate integrals of the form:

$$\phi_x=\iint_{\Delta S}\frac{(x-\xi)}{R^3}\,dS \tag{6B}$$

$$\phi_y=\iint_{\Delta S}\frac{(y-\eta)}{R^3}\,dS \tag{7B}$$

$$\phi_z=\iint_{\Delta S}\frac{z}{R^3}\,dS \tag{8B}$$

where

$$R=\sqrt{(x-\xi)^2+(y-\eta)^2+z^2}$$

Equations (6B-8B) have been integrated by Hess and Smith[3] the results of which are summarized as:

$$\phi_x = \frac{\zeta_2 - \zeta_1}{d_{12}} \ln\left(\frac{r_1 + r_2 - d_{12}}{r_1 + r_2 + d_{12}}\right) + \frac{\zeta_3 - \zeta_2}{d_{23}} \ln\left(\frac{r_2 + r_3 - d_{23}}{r_2 + r_3 + d_{23}}\right)$$

(9B)

$$+ \frac{\zeta_4 - \zeta_3}{d_{34}} \ln\left(\frac{r_3 + r_4 - d_{34}}{r_3 + r_4 + d_{34}}\right) + \frac{\zeta_1 - \zeta_4}{d_{41}} \ln\left(\frac{r_4 + r_1 - d_{41}}{r_4 + r_1 + d_{41}}\right)$$

$$\phi_y = \frac{\xi_1 - \xi_2}{d_{12}} \ln\left(\frac{r_1 + r_2 - d_{12}}{r_1 + r_2 + d_{12}}\right) + \frac{\xi_2 - \xi_3}{d_{23}} \ln\left(\frac{r_2 + r_3 - d_{23}}{r_2 + r_3 + d_{23}}\right)$$

(10B)

$$+ \frac{\xi_3 - \xi_4}{d_{34}} \ln\left(\frac{r_3 + r_4 - d_{34}}{r_3 + r_4 - d_{34}}\right) + \frac{\xi_4 - \xi_1}{d_{41}} \ln\left(\frac{r_4 + r_1 - d_{41}}{r_4 + r_1 + d_{41}}\right)$$

$$\phi_z = \tan^{-1}\left(\frac{m_{12} e_1 - h_1}{2 r_1}\right) - \tan^{-1}\left(\frac{m_{12} e_2 - h_2}{2 r_2}\right)$$

$$+ \tan^{-1}\left(\frac{m_{23} e_2 - h_2}{2 r_2}\right) - \tan^{-1}\left(\frac{m_{23} e_3 - h_3}{2 r_3}\right)$$

(11B)

$$+ \tan^{-1}\left(\frac{m_{34} e_3 - h_3}{2 r_3}\right) - \tan^{-1}\left(\frac{m_{34} e_4 - h_4}{2 r_4}\right)$$

$$+ \tan^{-1}\left(\frac{m_{41} e_4 - h_4}{2 r_4}\right) - \tan^{-1}\left(\frac{m_{41} e_1 - h_1}{2 r_1}\right)$$

where

$$d_{12} = \sqrt{(\xi_2 - \xi_1)^2 + (\zeta_2 - \zeta_1)^2}$$

$$d_{23} = \sqrt{(\xi_3 - \xi_2)^2 + (\zeta_3 - \zeta_2)^2}$$

$$d_{34} = \sqrt{(\xi_4 - \xi_3)^2 + (\zeta_4 - \zeta_3)^2} \qquad \text{(12B)}$$

$$d_{41} = \sqrt{(\xi_1 - \xi_4)^2 + (\zeta_1 - \zeta_4)^2}$$

in which

$$m_{12} = \frac{\eta_2 - \eta_1}{\xi_2 - \xi_1} \qquad m_{23} = \frac{\eta_3 - \eta_2}{\xi_3 - \xi_2}$$

$$m_{34} = \frac{\eta_4 - \eta_3}{\xi_4 - \xi_3} \qquad m_{41} = \frac{\eta_1 - \eta_4}{\xi_1 - \xi_4} \quad . \tag{13B}$$

and

$$r_k = \sqrt{(x-\xi_k)^2 + (y-\eta_k)^2 + z^2} \quad , \quad k = 1,2,3,4 \tag{14B}$$

$$e_k = z^2 + (x-\xi_k)^2 \quad , \quad k = 1,2,3,4 \tag{15B}$$

$$h_k = (y-\eta_k)(x-\xi_k) \quad , \quad k = 1,2,3,4 \tag{16B}$$

In actually evaluating these expressions ϕ_x and ϕ_y cause no trouble. They become infinite on the edges of the quadrilateral, but in practice they are never evaluated there. The component ϕ_z requires special handling in certain cases. As $z \to 0$, $\phi_z \to 0$ if the point P is approaching a point in the plane outside the boundaries of the quadrilateral. If P approaches a point within the quadrilateral $\phi_z \to 2\pi$ (sgn z) as $z \to 0$. These facts may be verified from equation (11B). In the course of this method of flow calculation it is required to evaluate ϕ_z at points in the plane of the quadrilateral elements. In particular, the centroid of each element is in the plane of that element and within the quadrilateral. At such a point ϕ_z should equal 2π, since the case of interest is that for which $z \to 0$ through positive values, rather than through negative values, i.e., the field point approaches the caisson surface from the exterior flow field rather than from the interior of the caisson.

It may also be required to evaluate induced velocity components at points in the plane of a quadrilateral outside the boundaries of the quadrilateral, for example, at the null points (centroids) of other elements if the body surface has a flat region. Points in the plane of a quadrilateral element should have z = 0, but, because of round-off error, they may have have small values of z with either sign. Thus, for points inside the quadrilateral, equation (11B) may give 2π with either sign. To avoid this error, the absolute value of z is tested before velocities are computed, and if it is less than some small prescribed number, which is nevertheless large compared to the expected round-off error, it is set equal to plus zero and each inverse tangent of equation (11B) is set equal to $\pi/2$ with the sign of the numerator of its argument. This gives $\phi_2 = 0$ for points outside the quadrilateral and $\phi_2 = 2\pi$ for points inside the quadrilateral. Another situation that may cause trouble in the computing machine is when the slope of a side of the quadrilateral is infinite, i.e., when a side is parallel to the y-axis. It is evident from equation (11B) that in this case the two inverse tangents corresponding to that side cancel each other. To avoid difficulties each of the quantities $(\xi_2 - \xi_1)$, $(\xi_3 - \xi_2)$, $(\xi_4 - \xi_3)$, and $(\xi_1 - \xi_4)$ are tested to determine whether they are zero, and if any one of them is zero, the two inverse tangents corresponding to that side are set equal to zero. Finally, it should be mentioned that the inverse tangents in equation (11B) are evaluated in the normal range $-\pi/2$ to $+\pi/2$. It is tempting to combine some of the inverse tangents in this equation using the tangent addition law, but if this is done, great care must be exercised with

regard to the range in which the resulting inverse tangents should be evaluated.

When the distance R is large it is possible to approximate integrals in Eq.(1B) and (6B-8B) by simply multiplying the integrand by the area ΔS. Thus, in order to get some indication of how large R must be in order for this approximation to be valid Figure (1B). The results shown here indicate that in the case of either the induced velocity or the potential contributed by the panels of area ΔS it is necessary that $R \geq 2\sqrt{\Delta S}$ in order for the approximate expression to become valid.

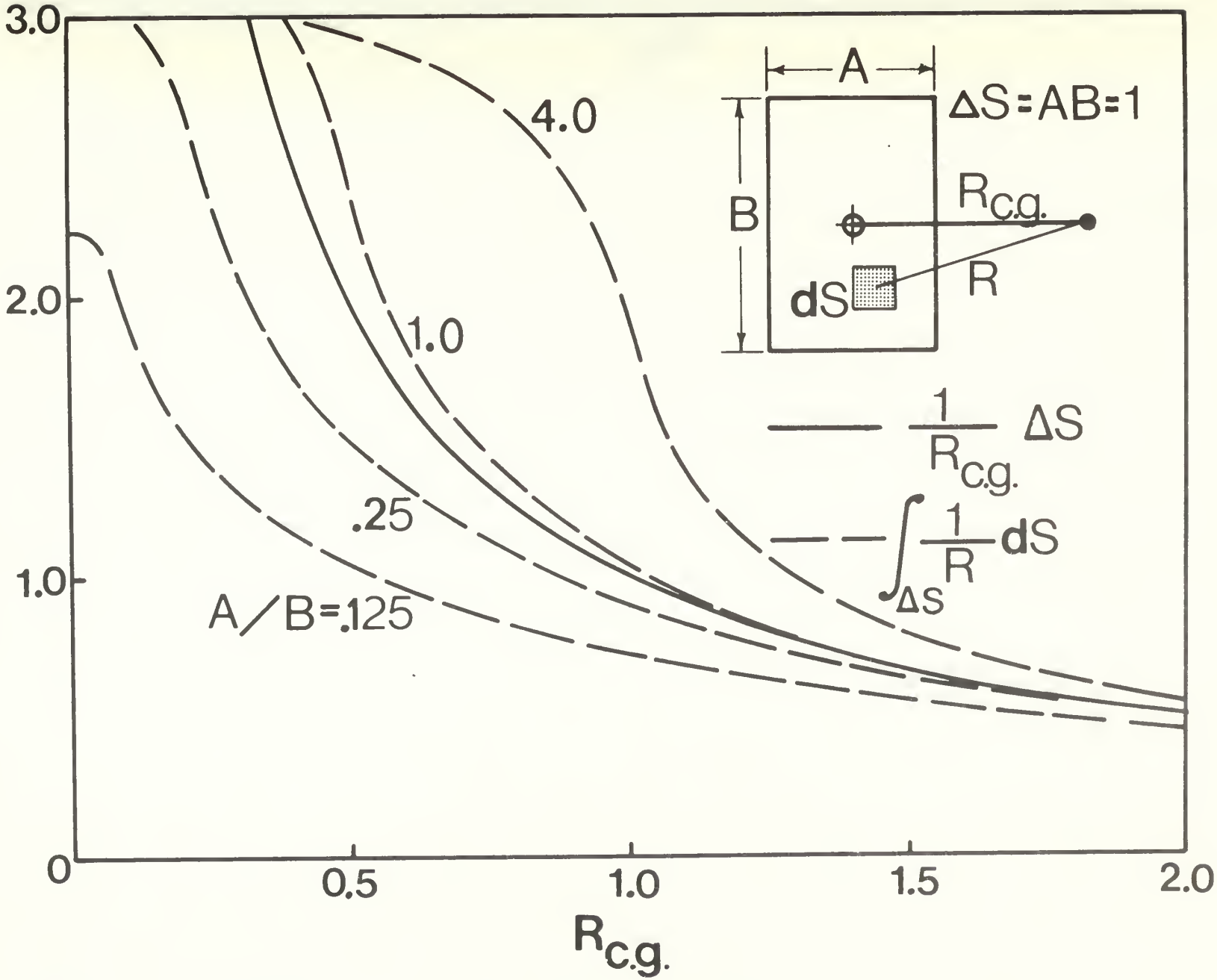

FIGURE LB (a) COMPARISON OF EXACT AND APPROXIMATE ESPRESSIONS FOR INTEGRAL OF 1/R

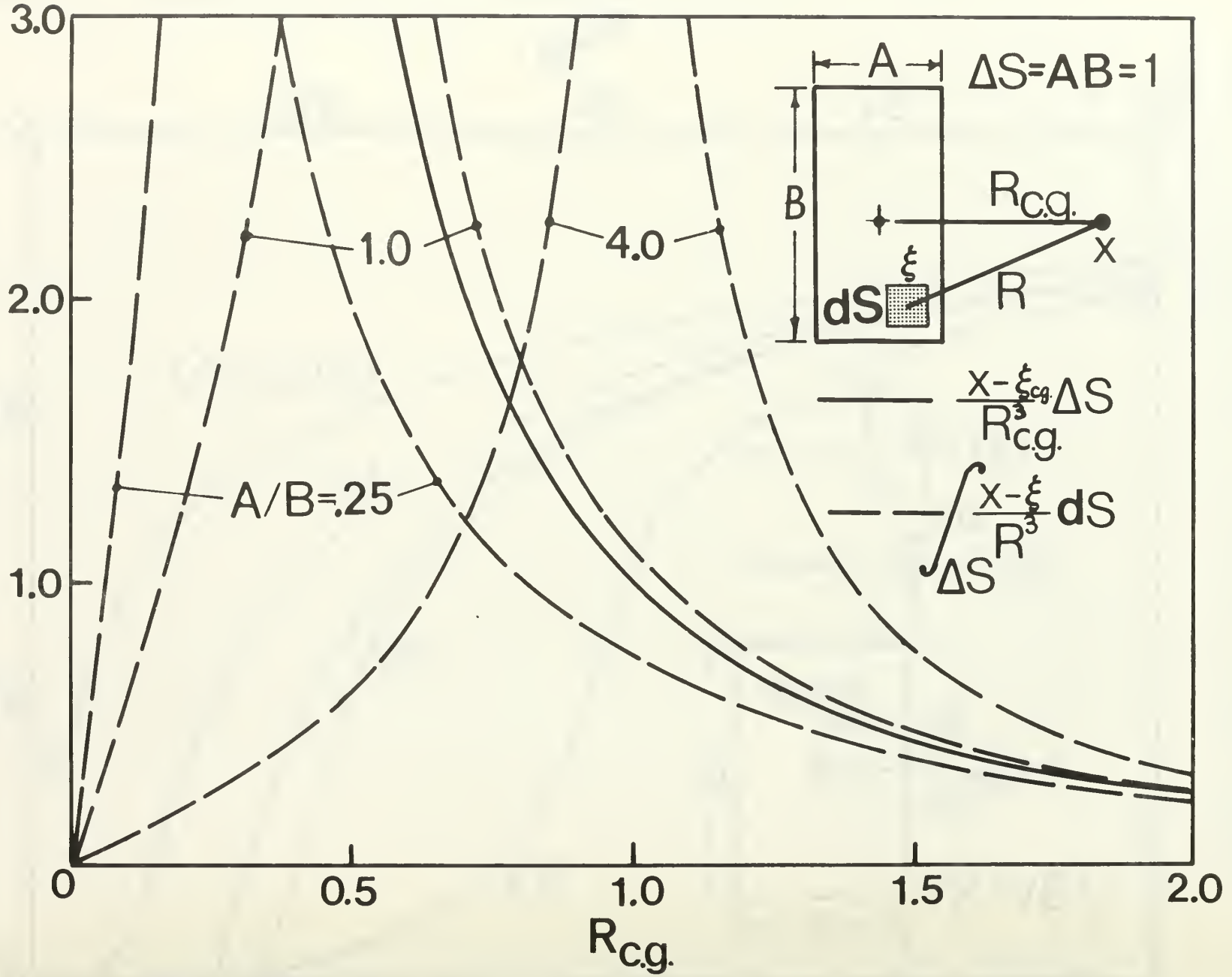

FIGURE 1B (b) COMPARISON OF EXACT AND APPROXIMATE EXPRESSIONS FOR INDUCED VELOCITY

APPENDIX C: ALTERNATE FORM OF THE GREEN'S FUNCTION CONVENIENT FOR NUMERICAL EVALUATION

Except when the point x,y,z lies close to the source located at ξ, ζ, ζ the series form of the Green's function given by Eq.(3.4) is used for computer numerical evaluation. The series appears to converge fairly rapidly and, therefore, the numerical evaluation is quite efficient. However, when the point x,y,z lies close to ξ, ζ, ζ the series form cannot be used because of the singular nature of the Bessel functions $Y_0(ar)$ and $K_0(ar)$ as $r \to 0$. In such cases, i.e., when (ar) becomes less than some arbitrarily small number, the form of the Green's function specified by Eq.(3.3) must be used.

However, Eq.(3.3) may not be evaluated numerically in a direct, straightforward manner because the 1/R term is singular as $R \to 0$ and the integrand of the infinite integral is singular at $\mu = a$. The evaluation of the 1/R term through numerical integration was discussed in Appendix B. In this appendix an efficient method for the numerical evaluation of the infinite integral is discussed.

The integral form of the Green's function is given by

$$G(x,y,z;\xi,\zeta,\zeta) = \frac{1}{R} + \frac{1}{R'} \qquad (1\text{-C})$$

$$+ 2\ \text{P.V.} \int_0^\infty \frac{(\mu+\nu)\, e^{-\mu h} \cosh[\mu(\zeta+h)] \cosh[\mu(y+h)]\, J_0(\mu r)}{\mu \sinh \mu h - \nu \cosh \mu h}\, d\mu$$

$$+ i\, \frac{2\pi (a^2-\nu^2) \cosh[a(\zeta+h)] \cosh[a(y+h)]\, J_0(ar)}{a^2 h - \nu^2 h + \nu}$$

where $$R = \sqrt{(x-\xi)^2 + (y-\eta)^2 + (z-\zeta)^2}$$

$$R' = \sqrt{(x-\xi)^2 + (y+2h+\eta)^2 + (z-\zeta)^2}$$

$$r = \sqrt{(x-\xi)^2 + (z-\zeta)^2}$$

$$\nu = \frac{\sigma^2 \bar{a}}{g} = a \tanh(ah)$$

The integrand of the infinite integral can be simplified by use of the relationships,

$$\sinh(x) \approx \cosh(x) \approx \frac{1}{2} e^x$$

for x larger than about 4.0. Thus, the interval may be broken into two parts. Using, for brevity

$$(\quad) = \frac{(\mu+\nu)\, e^{-\mu h} \cosh[\mu(\eta+h)] \cosh[\mu(y+h)] J_0(\mu r)}{\mu \sinh \mu h - \nu \cosh \mu h} \quad (2\text{-C})$$

Eq.(1-C) may be written as

$$2\, P.V. \int_0^{\infty} (\quad)\, d\mu = 2\, P.V. \int_0^{\mu_1} (\quad)\, d\mu + P.V. \int_{\mu_1}^{\infty} \left(\frac{\mu+\nu}{\mu-\nu}\right) e^{\mu(y+\eta)} J_0(\mu r)\, d\mu \quad (3\text{-C})$$

where $\mu_1 \geq 4.0/h$. The term $(\mu+\nu)/(\mu-\nu)$ may be written

$$\frac{\mu+\nu}{\mu-\nu} = \frac{2\nu}{\mu-\nu} + 1$$

so that the infinite integral becomes

$$2\, P.V. \int_0^{\infty} (\quad)\, d\mu = 2\, P.V. \int_0^{\mu_1} (\quad)\, d\mu + P.V. \int_{\mu_1}^{\infty} e^{\mu(y+\eta)} J_0(\mu r)\, d\mu + P.V. \int_{\mu_1}^{\infty} \frac{2\nu}{\mu-\nu} e^{\mu(y+\eta)} J_0(\mu r)\, d\mu \quad (4\text{-C})$$

This may be further rearranged by use of the relationship given for example, by Gradsheteyn and Ryzhik (21).

$$\frac{1}{R''} = \int_0^\infty e^{\mu(y+\zeta)} J_0(\mu r)\, d\mu \qquad (5\text{-C})$$

where R'' represents an image source with respect to the free surface

$$R'' = \sqrt{(x-\xi)^2 + (y+\zeta)^2 + (z-\gamma)^2} \qquad (6\text{-C})$$

The infinite integral may now be written,

$$2\,P.V.\int_0^\infty (\quad)\, d\mu = \frac{1}{R''} + 2\,P.V.\int_0^{u_1} (\quad)\, d\mu$$

$$-\int_0^{u_1} e^{\mu(y+\zeta)} J_0(\mu r)\, d\mu + P.V.\int_{u_1}^\infty \frac{2\nu}{\mu-\nu} e^{\mu(y+\zeta)} J_0(\mu r)\, d\mu \qquad (7\text{-C})$$

The remaining infinite integral can now be expressed in terms of a finite integral by use of the relationship (See Abramowitz and Stegun(22)).

$$J_0(\mu r) = \frac{1}{\pi}\int_0^\pi e^{i\mu r\cos\theta}\, d\theta \qquad (8\text{-C})$$

Using Eq.(8-C), the last term may, therefore, be written as

$$P.V.\int_{u_1}^\infty \frac{2\nu}{\mu-\nu} e^{\mu(y+\zeta)} J_0(\mu r)\, d\mu = \frac{2\nu}{\pi}\int_{u_1}^\infty\int_0^\pi \frac{e^{\mu(y+\zeta+ir\cos\theta)}}{\mu-\nu}\, d\mu\, d\theta \qquad (9\text{-C})$$

Now, let $t = \mu-\nu$ and $dt = d\mu$ in Eq.(9-C):

$$P.V.\int_{u_1}^\infty \frac{2\nu}{\mu-\nu} e^{\mu(y+\zeta)} J_0(\mu r)\, d\mu = \frac{2\nu}{\pi}\int_0^\pi\int_{t=u_1-\nu}^\infty \frac{e^{(y+\zeta+ir\cos\theta)t}\, e^{\nu(y+\zeta+ir\cos\theta)}}{t}\, dt\, d\theta \qquad (10\text{-C})$$

or, simplifying further by use of the substitution $S = t/(u_1-\nu)$

$$P.V.\int_{u_1}^\infty \frac{2\nu}{\mu-\nu} e^{\mu(y+\zeta)} J_0(\mu r)\, d\mu$$

$$= \frac{2\nu}{\pi}\int_{S=1}^\infty\int_0^\pi \frac{e^{(y+\zeta+ir\cos\theta)(u_1-\nu)S}}{S}\, e^{\nu(y+\zeta+ir\cos\theta)}\, ds\, d\theta \qquad (11\text{-C})$$

The exponential integral as defined by Abramowitz and Stegun is

$$E_1(z) = \int_z^\infty \frac{e^{-t}}{t}\,dt = \int_1^\infty \frac{e^{-zt}}{t}\,dt \qquad (12\text{-C})$$

so, the above result may be written as

$$P.V.\int_{u_1}^\infty \frac{2\nu}{u-\nu}\, e^{u(y+\zeta)}\, J_0(ur)\, du \qquad (13\text{-C})$$
$$= \frac{2\nu}{\pi}\int_0^\pi e^{\nu(y+\zeta+ir\cos\theta)}\, E_1[-(y+\zeta)+ir\cos\theta)(u_1-\nu)]\, d\theta$$

With this, the complete expression for G may be written

$$G = \frac{1}{R} + \frac{1}{R'} + \frac{1}{R''} + 2\,P.V.\int_0^{u_1} \frac{(u+\nu)e^{-uh}\cosh[u(\zeta+h)]\cosh[u(y+h)]}{\cosh uh\,(u\tanh uh - \nu)} J_0(ur)\,du \qquad (14\text{-C})$$

$$-\int_0^{u_1} e^{u(y+\zeta)}\, J_0(ur)\,du + \frac{2\nu}{\pi}\int_0^\pi e^{\nu(y+\zeta+ir\cos\theta)}\, E_1[-(y+\zeta+ir\cos\theta)(u_1-\nu)]\,d\theta$$

$$+ i\,\frac{2\pi(a^2-\nu^2)\cosh[a(\zeta+h)]\cosh[a(y+h)]\,J_0(ar)}{a^2h - \nu^2h + \nu}$$

This form of the Green's function involves no infinite integrals and, therefore, can be evaluated numerically fairly efficiently.

The integrand of the first integral is, however, singular when μ = a so a special procedure must be followed in evaluation of that integral. Let

$$f(u) = \frac{2(u+\nu)e^{-uh}\cosh[u(\zeta+h)]\cosh[u(y+h)]\,J_0(ur)}{\cosh(uh)} \qquad (15\text{-C})$$

The integral in question can be written

$$P.V.\int_0^{u_1} \frac{f(u)\,du}{u\tanh uh - \nu} = \int_0^{2a} \frac{f(u)-f(a)}{u\tanh uh - \nu}\,du + f(a)\int_0^{2a} \frac{du}{u\tanh uh - \nu}$$
$$+ \int_{2a}^{u_1} \frac{f(u)\,du}{u\tanh uh - \nu}$$

The first and third integrals in Eq.(16-C) are not singular and will cause no difficulty in numerical integration provided the integrand is not evaluated exactly at the midpoint where $\mu = a$. The integration procedure used, therefore, is the "3/8 rule" which evaluates the integrand at end points and two intermediate points. Using an odd number of subdivisions then the integrand is never evaluated at $\mu = a$.

The second integral in Eq.(16-C) is singular and a special procedure must be followed. The integral may first be written as

$$\int_0^{2a} \frac{du}{u \tanh uh - v} \equiv \int_0^{2u_0} \frac{du}{u \tanh u - u_0 \tanh u_0} \qquad (17\text{-}C)$$

where

$$u_0 = ah$$

which indicates clearly the singular nature of the integrand at $u = u_0$. The interval may be broken into three parts as

$$\int_0^{2u_0} \frac{du}{u \tanh u - u_0 \tanh u_0} \equiv \int_0^{u_0-\epsilon} \frac{du}{u \tanh u - u_0 \tanh u_0} \qquad (18\text{-}C)$$
$$+ \int_{u_0-\epsilon}^{u_0+\epsilon} \frac{du}{u \tanh u - u_0 \tanh u_0} + \int_{u_0+\epsilon}^{2u_0} \frac{du}{u \tanh u - u_0 \tanh u_0}$$

and the first and last integral integrated in a straightforward manner by numerical integration. The second integral is evaluated by first expanding the denominator in a Taylor series about and then dividing 1.0 by this series. The result of this is

$$\int_{u_0-\epsilon}^{u_0+\epsilon} \frac{du}{u \tanh u - u_0 \tanh u_0} = \int_{u_0-\epsilon}^{u_0+\epsilon} \left[\frac{1}{a_1(u-u_0)} - \frac{a_2}{a_1^2} + \frac{1}{a_1}\left(\frac{a_2^2}{a_1^2} - \frac{a_3}{a_1}\right)(u-u_0)\cdots \right] du$$

$$= \int_{-\epsilon}^{\epsilon} \left[\frac{1}{a_1 \lambda} - \frac{a_2}{a_1^2} + \frac{1}{a_1}\left(\frac{a_2^2}{a_1^2} - \frac{a_3}{a_1} \right)\lambda + \cdots \right] d\lambda \qquad (19\text{-C})$$

$$= -\frac{a_2}{a_1^2}(2\epsilon) + O(\epsilon^3)$$

where

$$a_1 = \tanh(ah) + ah\,\mathrm{sech}^2(ah)$$

$$a_2 = \mathrm{sech}^2(ah)\left(1 - ah\,\tanh(ah)\right)$$

$$a_3 = \frac{1}{3}\mathrm{sech}^2(ah)\left\{2ah\left(1 - \mathrm{sech}^2(ah)\right) - 3\tanh(ah) - ah\,\mathrm{sech}^2(ah)\right\}$$

$$\vdots$$

Thus, the complete integral, Eq.(17-C) may be written

$$\int_0^{2a} \frac{du}{u\,\tanh \mu h - \nu} = \int_0^{u_0-\epsilon} \frac{du}{u\,\tanh u - u_0\,\tanh u_0} \qquad (20\text{-C})$$

$$+ \int_{u_0+\epsilon}^{2u_0} \frac{du}{u\,\tanh u - u_0\,\tanh u_0} - 2\epsilon\,\frac{\mathrm{sech}^2(ah)\left(1 - ah\,\tanh ah\right)}{\left(\tanh(ah) + ah\,\mathrm{sech}^2(ah)\right)^2}$$

where ϵ denotes some small value between 0 and ah. In the numerical evaluation, ϵ has been set to 0.10.

The final form of the Green's function in the form appropriate for numerical evaluation may now be written as

$$G = \frac{1}{R} + \frac{1}{R'} + \frac{1}{R''} + \int_0^{2a} \frac{f(u) - f(a)}{u\,\tanh \mu h - \nu}\,du + \int_{2a}^{u_1} \frac{f(u)\,du}{u\,\tanh \mu h - \nu}$$

$$+ f(a)\int_0^{ah-\epsilon} \frac{du}{u\,\tanh u - ah\,\tanh(ah)} + f(a)\int_{ah+\epsilon}^{2ah} \frac{du}{u\,\tanh u - ah\,\tanh(ah)} \qquad (21\text{-C})$$

$$- 2\epsilon\,\frac{\mathrm{sech}^2(ah)\left(1 - ah\,\tanh(ah)\right) f(a)}{\left(\tanh(ah) + ah\,\mathrm{sech}^2(ah)\right)^2}$$

$$-\int_0^{u_1} e^{\mu(y+\zeta)}\, J_0(\mu r)\, d\mu$$

$$+\frac{2\nu}{\pi}\int_0^{\pi} e^{\nu(y+\zeta+ir\cos\theta)}\, E_1[-(y+\zeta+ir\cos\theta)(u_1-\nu)]\, d\theta$$

$$+i\,\frac{2\pi(a^2-\nu^2)\cosh[a(\zeta+h)]\cosh[a(y+h)]\,J_0(ar)}{a^2h-\nu^2h+\nu}$$

where

$$f(\mu)=\frac{2(\mu+\nu)e^{-\mu h}\cosh[\mu(\zeta+h)]\cosh[\mu(y+h)]\,J_0(\mu r)}{\cosh\mu h}$$

The derivatives of $G(x,y,z;\xi,\eta,\zeta)$ follow from Eq.(21-C)as:

$$\frac{\partial G}{\partial x}=-\frac{1}{R^3}(x-\xi)-\frac{1}{R'^3}(x-\xi)-\frac{1}{R''^3}(x-\xi)$$

$$-(x-\xi)\int_0^{2a}\frac{f'(u)-f'(a)}{u\tanh uh-\nu}\,d\mu-(x-\xi)\int_{2a}^{u_1}\frac{f'(u)\,du}{u\tanh uh-\nu}$$

$$-(x-\xi)f'(a)\int_0^{ah-\epsilon}\frac{du}{u\tanh u-ah\tanh ah}-(x-\xi)f'(a)\int_{ah+\epsilon}^{2ah}\frac{du}{u\tanh u-ah\tanh ah}$$

$$+2\epsilon\,\frac{\operatorname{sech}^2 ah\,(1-ah\tanh ah)}{(\tanh ah+ah\operatorname{sech}^2 ah)^2}\,f'(a)\,(x-\xi) \qquad (22\text{-C})$$

$$+(x-\xi)\int_0^{u_1}\mu\, e^{\mu(y+\zeta)}\,\frac{J_1(\mu r)}{r}\,d\mu$$

$$+i\,\frac{2\nu}{\pi}\,\frac{(x-\xi)}{r}\int_0^{\pi}\cos\theta\Big\{\nu e^{\nu(y+\zeta+ir\cos\theta)}\,E_1[-(y+\zeta+ir\cos\theta)(u_1-\nu)]$$

$$-\frac{e^{(y+\zeta+ir\cos\theta)u_1}}{(y+\zeta+ir\cos\theta)}\Big\}\,d\theta$$

$$-i\,\frac{2\pi a(a^2-\nu^2)}{(a^2h-\nu^2h+\nu)}\cosh[a(\zeta+h)]\cosh[a(y+h)]\,\frac{J_1(ar)}{r}\,(x-\xi)$$

where

$$f'(\mu) = \frac{2\mu(\mu+\nu)e^{-\mu h}\cosh[\mu(z+h)]\cosh[\mu(y+h)]}{\cosh(\mu h)} \quad \frac{J_1(\mu r)}{r}$$

$$\frac{\partial G}{\partial y} = -\frac{1}{R^3}(y-z) - \frac{1}{R'^3}(y+2h+z) - \frac{1}{R''^3}(y+z)$$

$$+\int_0^{2a} \frac{f_y(\mu) - f_y(a)}{\mu \tanh \mu h - \nu}\, d\mu + \int_{2a}^{u_1} \frac{f_y(\mu)\, d\mu}{\mu \tanh \mu h - \nu}$$

$$+ f_y(a)\int_0^{ah-\epsilon} \frac{d\mu}{\mu \tanh \mu - ah \tanh ah} + f_y(a)\int_{ah+\epsilon}^{2ah} \frac{d\mu}{\mu \tanh \mu - ah \tanh(ah)}$$

$$- 2\epsilon \frac{\operatorname{sech}^2 ah\,(1 - ah \tanh ah)}{(\tanh ah + ah \operatorname{sech}^2 ah)^2} f_y(a) \qquad (23\text{-c})$$

$$-\int_0^{u_1} \mu\, e^{\mu(y+z)}\, J_0(\mu r)\, d\mu$$

$$+ \frac{2\nu}{\pi}\int_0^{\pi} \left[\nu\, e^{\nu(y+z+ir\cos\theta)}\, E_1[-(y+z+ir\cos\theta)(u_1-\nu)] \right.$$

$$\left. - \frac{e^{(y+z+ir\cos\theta)u_1}}{(y+z+ir\cos\theta)} \right] d\theta$$

$$+ i\, \frac{2\pi a(a^2-\nu^2)\cosh[a(h+z)]\sinh[a(h+y)]}{a^2 h - \nu^2 h + \nu}\, J_0(ar)$$

where

$$f_y(\mu) = \frac{2\mu(\mu+\nu)e^{-\mu h}\cosh[\mu(z+h)]\sinh[\mu(y+h)]}{\cosh(\mu h)}\, J_0(\mu r)$$

and finally,

$$\frac{\partial G}{\partial z} = -\frac{1}{R^3}(z-\zeta) - \frac{1}{R'^3}(z-\zeta) - \frac{1}{R''^3}(z-\zeta)$$

$$-(z-\zeta)\int_0^{2a} \frac{f'(u) - f'(a)}{u\tanh uh - \nu}\,du - (z-\zeta)\int_{2a}^{u_1} \frac{f'(u)\,du}{u\tanh uh - \nu}$$

$$-(z-\zeta)f'(a)\int_0^{ah-\epsilon} \frac{du}{u\tanh u - ah\tanh ah} - (z-\zeta)f'(a)\int_{ah+\epsilon}^{2ah} \frac{du}{u\tanh u - ah\tanh ah}$$

$$+2\epsilon\frac{\operatorname{sech}^2 ah\,(1-ah\tanh ah)}{(\tanh ah + ah\operatorname{sech}^2 ah)^2} f'(a)(z-\zeta) \qquad (24\text{-c})$$

$$+(z-\zeta)\int_0^{u_1} u\, e^{u(y+\zeta)}\frac{J_1(ur)}{r}$$

$$+i\frac{2\nu}{\pi}\frac{(z-\zeta)}{r}\int_0^{\pi}\cos\theta\left\{\nu e^{\nu(y+\zeta+ir\cos\theta)} E_1[-(y+\zeta+ir\cos\theta)(u_1-\nu)]\right.$$

$$\left. - \frac{e^{(y+\zeta+ir\cos\theta)u_1}}{(y+\zeta+ir\cos\theta)}\right\} d\theta$$

$$-i\frac{2\pi a(a^2-\nu^2)}{(a^2h-\nu^2h+\nu)}\cosh[a(\zeta+h)]\cosh[a(y+h)]\frac{J_1(ar)}{r}(z-\zeta)$$

REFERENCES

1. MacCamy, R. C. and Fuchs, R. A., "Wave Forces on Piles: A Diffraction Theory," Beach Erosion Board, Technical Memorandum No. 69, 1954.

2. Havelock, T., "Waves Due to a Floating Sphere Making Periodic Heaving Oscillations," Proc. Royal Society, London, Vol. 231, Series A, England, pp. 1-7, 1955.

3. Newman, J. N., "The Exciting Forces on Fixed Bodies In Water," Journal of Ship Research, Vol. 6, pp. 10-17, 1962.

4. Kim, W. D., "On the Harmonic Oscillations of a Rigid Body on a Free Surface," Journal of Fluid Mechanics, Vol. 21, pp. 427-451, 1965.

5. Kim, W. D., "On a Free Floating Ship in Waves," Journal of Ship Research, pp. 182-200, Sept. 1966.

6. Garrison, C. J. and Seetharama Rao, V., "Wave Interaction with Large Submerged Objects," Journal of the Waterways, Harbors and Coastal Engineering Division, Proc. ASCE, Vol. 97, No. WW2, pp. 259-277, May 1971.

7. Garrison, C. J. and Chow, P. Y., "Wave Forces on Submerged Bodies," Journal of the Waterways, Harbors and Coastal Engineering Division, Proc. ASCE, Vol. 98, No. WW3, pp. 375-392. Aug. 1972.

8. Chakrabarti, S. K. and Tam, W. A., "Gross and Local Wave Loads on a Large Vertical Cylinder - Theory and Experiment," Paper No. OTC1818, Offshore Technology Conference, Houston, Texas, 1973.

9. Hogben, N. and Standing, R. G., "Experience in Computing Wave Loads on Large Bodies," Paper No. OTC2189, Offshore Technology Conference, Houston, Texas, 1975.

10. Garrison, C. J., Torum, A., Iversen, C., Leivseth, S. and Ebbesmeyer, C. C., 1974, "Wave Forces on Large Volume Structures --A Comparison Between Theory and Model Tests," Paper OTC2137, Offshore Technology Conference, Houston, Texas.

11. Faltinsen, O.M. and Michelsen, F.C. 1974, "Motion of Large Structures in Waves at Zero Froude Number," The Dynamics of Marine Vehicles and Structures in Waves, Paper No. 11, The Institution of Mechanical Engineers.

12. Garrison, C. J. 1975, "Hydrodynamics of Large Objects in the Sea, Part II - Motion of Free-Floating Bodies," Journal of Hydronautics, Vol. 9, April, pp. 58-63.

13. Wehausen, J.V. and Laitone, E.V., 1960, "Surface Waves," Encyclopedia of Physics, Vol. 9, Springer-Verlag, Berlin, pp. 446-778.

14. Haskinds, J. D., "The Exciting Forces and Wetting of Ships in Waves"(in Russian), Tsvestra Akademic Nauk SSSR, Otdelenie Teknicheskikh Hauk, No. 7, pp. 65-78, (English Translation: David Taylor Model Basin Translation, No. 30, March 1962, Washington, D. C.)

15. Seetharamá Rao, V., and Garrison, C. J., "Interaction of a Train of Regular Waves with a Rigid Submerged Ellipsoid," Sea Grant Publication No. TAMU-SG-71-209, Coastal and Ocean Engineering Division, Texas A&M University, 1971.

16. Hess, J. L. and Smith, O.M.A., 1962, "Calculation of Non-Lifting Potential Flow About Arbitrary Three-Dimensional Bodies," Rept. No. E. S. 40622, (Douglas Aircraft Division, Long Beach, CA) Also, Journal of Ship Research, 1964, Vol. 8.

17. Kim, C. H., Henry, C. J., and Chou, F., "Hydrodynamic Characteristics of Prismatic Barges,"Offshore Technology Conference, Paper No. 1417, 1971.

18. Garrett, C. J. R., "Wave Forces on a Circular Dock," Journal of Fluid Mechanics, Vol. 46, Pt. 1, pp. 129-139, 1971.

19. Hoffman, D., Geller, E. S., and Niederman, C. S., "Mathematical Simulation and Model Tests in the Design of Data Buoys," SNAME, presented at the Annual Meeting, New York, N.Y., Nov. 15-17, 1973.

20. Garrison, C. J. and Stacey, R., "Wave Loads on North Sea Gravity Platforms: A Comparison of Theory and Experiment," Offshore Technology Conference, Paper No. OTC2794, May 1977.

21. Gradsheteyn, I.S. and Ryzhik, I.M., "Tables of Integrals, Series and Products," 1965, Academic Press, New York and London.

22. Abramowitz, M. and Stegun, I.A., "Handbook of Mathematical Functions," 1964 (National Bureau of Standards Mathematical Series, 55, Washington, D.C.).

INITIAL DISTRIBUTION LIST

1.	Mr. W. G. Sherwood Program Manager Ocean Thermal Energy Conversion Program Division of Solar Energy Department of Energy/ERDA 20 Massachusetts Avenue, NW Washington, D.C. 20545	15
2.	Mr. R. L. Waid Lockheed Missiles & Space Co. ORG 57-02; Bldg. 150 P.O. Box 504 Sunnyvale, California 94086	1
3.	Mr. R. J. Scott Gibbs & Cox, Inc. 2341 Jefferson Davis Highway Arlington, Virginia 22202	1
4.	Mr. N. S. Basar M. Rosenblatt & Son, Inc. 350 Broadway New York, New York 10013	1
5.	Mr. J. R. Vadus (OEX3) Office of Ocean Engineering NOAA 6010 Executive Blvd. Rockville, Maryland 20852	2
6.	Mr. W. Trzaskoma Gilbert Associates Suite 1201 1828 "L" Street, NW Washington, D.C. 20036	2
7.	Dr. E. A. Silva, Code PC-21 Naval Facilities Engineering Command 200 Stovall Street Alexandria, Virginia 20360	4
8.	Professor John Nath Department of Civil Engineering Oregon State University Corvallis, Oregon 97330	1
9.	Professor Robert Hudspeth Department of Civil Engineering Oregon State University Corvallis, Oregon 97330	1

10. Department of Mechanical Engineering
Naval Postgraduate School
Monterey, California 93940 — 2

11. C. J. Garrison
Department of Mechanical Engineering
Naval Postgraduate School
Monterey, California 93940 — 20

12. Library
Naval Postgraduate School
Monterey, California 93940 — 2

13. Professor Tok Yamomoto
Department of Civil Engineering
Oregon State University
Corvallis, Oregon 97330 — 1

14. Professor Charles Sollitt
Department of Civil Engineering
Oregon State University
Corvallis, Oregon 97330 — 1

15. Mr. Min-Chu Chen
Department of Civil Engineering
Oregon State University
Corvallis, Oregon 97330 — 1

16. Professor R. E. Nece
Department of Civil Engineering
University of Washington
Seattle, Washington 98105 — 1

17. Professor R. G. Dean
Departmentof Civil Engineering
University of Delaware
Newark, Delaware 19711 — 1

18. Professor T. Dalrymple
Department of Civil Engineering
University of Delaware
Newark, Delaware 19711 — 1

19. Research Administration (Code 012)
Naval Postgraduate School
Monterey, California 93940 — 1

20. Dr. C.M. Lee
DTNSRDC
Bethesda, Maryland 20034 — 1

21. Professor John B. Herbich
Dept. of Civil Engr
Texas A&M University
College Station, Texas — 1